Evaluation of the effects of urbanization and climate change on aquifer thermal regimes

Doctoral dissertation

EVALUATION OF THE EFFECTS OF URBANIZATION AND CLIMATE CHANGE ON AQUIFER THERMAL REGIMES

Hewawasam Gamage Luminda Niroshana Gunawardhana

TOHOKU UNIVERSITY

JAPAN

MARCH 2010

ACKNOWLEDGEMENTS

I would like to express my profound gratitude and appreciation to my advisor Associate Professor So Kazama for his continuous suggestions, comments and kind encouragements. The outstanding lessons from him that I was guided at the every stage of my study will stand before me throughout my professional carrier in future.

My earnest and sincerest gratitude is also addressed to committee members of my dissertation Prof. Hitoshi Tanaka and Associate Professor Li Yu-You for their valuable comments and precious time for the successful completion of this study. I extended my appreciations to Professor Masaki Sawamoto, Prof. Akira Mano, Prof. Fumihiko Imamura, Associate Professor Koshimura Shunichi, Associate Professor Umeda Mukoto, Assistant Professor Udo Keiko, Assistant Professor Goto Kazuhisa and Assistant Professor Asaoka Yoshihiro for their valuable suggestions during examinations in each semester.

Sincere appreciations are due to Dr. Priyantha Ranjan, who helped me since the beginning of my research and also the family life in Sendai. My study would not be completed without the enormous supports for the field observations from Dr. Seiki Kawagoe. Also I am extremely thankful to Miss. Mariko Izumi in Environmental Protection Division, Sendai city office for making the kind arrangements for my field observations.

I would like to extend my gratitude to Ms. Machiko Sasaki and the administrative staff of the Graduate School of Environmental Studies, for their assistance in innumerable tasks. Also I am thankful to my friends and colleges, who helped me directly and indirectly. For those I could not name them all, and for this purpose let me appreciate them.

I also would like to express my sincere thanks to Tohoku University and to the scholarship donor, Ministry of Education, Culture, Sports, Science and Technology, Government of Japan, for providing financial support during entire period of study.

I offer my deepest respect and gratitude to my dear parents, sister, beloved wife and son for their patience, unconditional love and support without complaining.

Finally, I wish to express my deepest gratitude to my beloved teacher, my former academic supervisor in Asian Institute of Technology, Dr. Nowarat Coowanitwong, who sadly passed away on 18th of March 2009. I presumed she has been beside me and trying to make me strong from the heaven as knowing success of her students always make her happy. She will always be remembered as a devoted teacher with ideal of love, strength and high spirit.

ABSTRACT

The main objective of this research is to estimate the climate change impacts on aquifer thermal regime. In recent studies, there have been several attempts to determine the combined effects of urbanization and past global warming on average deviations from steady state thermal profiles. However, no previous study has considered the future effects of global warming as an equally important cause for local subsurface temperature change.

Continuous field measurements of groundwater temperature and aquifer water level fluctuations were made to understand the significant factors that influence the aquifer thermal regimes. In deep aquifer depths, tidal effect is determined as the dominant force of governing the groundwater flow and temperature distribution. A significant correlation between tide and water levels in inland aquifer (0.74 at the nearest observation well to the coast) was found suggesting reasonably good relationship between tide and water levels in the Sendai plain. In general, the magnitudes of seasonal temperature change and amplitude of water level fluctuation were subjected to attenuation as the distance from the coast increased. Based on these observations, new analytical solution was developed to incorporate the advection effect of sea water for temperature distribution in the coastal aquifers. Moreover, a set of type-curves were developed in such a way that the curves account for the advection effect of groundwater flow and can be applied under different aquifer and tidal conditions to estimate the resulting temperature distribution. The proposed method will be important in evaluating the long-term effects of urbanization and climate change on coastal eco-systems where limited observation wells are available.

In the shallow subsurface layers, urbanization and climate change effects are identified as the dominant causes of influencing the temperature distribution. The magnitude of aquifer temperature change at the ground surface, as evaluated from subsurface temperatures at five observation wells, spans 0.9–1.3ºC. Estimated groundwater recharge rates from T–D profiles (105–215 mm/year) were further verified against estimates from three other techniques (the water budget method, Darcy's method and the WLF method), which produced the groundwater recharge estimates in a consistent range (105–210 mm/year). When a global warming rate of 0.004ºC/year was selected based on meteorological records from rural areas in the region, the urbanization effect was estimated to account for about 75% of the aquifer temperature change (0.7–1.0ºC) in the Sendai plain suggesting that urbanization effect has been dominated the causes of influencing subsurface temperature in 20th century. Considering the higher degree of uncertainty inherent in recharge estimation using T–D profiles and other techniques, we developed a set of type-curves by combining water budget technique and heat transport model that can be used to test the accuracy of the recharge estimates in general applications.

For the purpose of estimating potential global climate changes at the local scale, output from five general circulation models (GCMs) were spatially downscaled to the Sendai plain. The transfer function method was used to develop the empirical relationship between large scale GCMs and local scale climate. Furthermore, the potential changes in the precipitation and temperature from each model scenario were applied to the water budget technique to estimate the possible recharge variations in the future. When all model scenarios are considered groundwater recharge predictions will vary in a range of 96-182 mm/year in 2080. The groundwater temperature at 8 m depth from the ground surface (the representative depth for the comparison) could possibly increase within the range of 1.5–4.0 °C by 2080 compared to the observations in 2007. According to the latest findings from Intergovernmental Panel on Climate Change (IPCC) in their Fourth Assessment Report (AR4), predicted potential range of aquifer temperature change will be significant for the ecological balance of the ecosystem in the Sendai plain. Findings of this research will inform the policy makers for building resilient decisions for the mitigation measures.

Furthermore, a relationship between level of urbanization and ground surface air temperature change was developed by considering the aquifer temperature as a common parameter. According to that, by reducing 20% of urbanizing level in the Sendai area (from 100% to 80%), it will be able to lower the surface air temperature by 0.4 °C, which is approximately equal to the magnitude of climate change effect to increase the surface air temperature in 20th century in Japan. Therefore, given the increasing certainty that climate change is accelerating, developed methodology through this study will guide the decision makers for making more resilient decisions to cope with its adverse impacts.

TABLE OF CONTENTS

LIST OF FIGURES

Chapter 6: Future predictions of climate change impacts

LIST OF TABLES

CHAPTER 1

INTRODUCTION

1.1 General background

In many countries, groundwater is vital to the livelihood of the people, since it provides water for domestic, agricultural and industrial use. Some of the largest cities in the world (e.g. Jakarta, Dhaka, and Mexico City) depend on groundwater for almost all their water needs (Sampat, 2001). Apart from its social and economical value in providing a wide range of benefits/services to people, groundwater also plays an important role in ecosystem management (Alley et al., 2007). Groundwater sustains the flow of streams and rivers and is a source of fresh water to balance the temperature and nutrients in ponds, wetlands, and other aquifer ecosystems. In such cases, the hydrology of the aquifer and the health of the ecosystems are closely connected (Eaton and Scheller, 1996; Jones et al., 2006). Importantly, this relationship can be disrupted by human-induced loss of groundwater quantity and quality due to excessive groundwater pumping (Taniguchi, 1995), variation of groundwater recharge due to land use change (Allison et al., 1990) and less precipitation (low recharge) or high intensity rain fall (more run-off, less recharge) due to climate change (Chen, 2002; Eckhardt and Uibrich, 2003).

From an ecological point of view, the metabolic rates of organisms and the overall productivity of ecosystems are directly regulated to temperature (Lee and Bell, 1999; Oie and Olsen, 1993; Oltra and Todolf, 1997). Changes in groundwater temperatures will alter fundamental ecological processes and the geographic distribution of aquatic species in groundwater-dominated wetlands, estuaries and ponds. Both ground surface temperature change and variations in groundwater flow patterns will alter the aquifer thermal regime (Fig. 1), because heat in the subsurface layer is transported not only by conduction, but also by convection through the groundwater (Suzuki, 1960; Stallman, 1963). The urbanization and climate change are two dominant forces that significantly alter the aquifer thermal regimes (Taniguchi, 2007; Reiter, 2006; Bense and Beltrami, 2007). Already at this moment, many urbanizing and pre-urbanized cities in the world exhibit strong disturbances of natural temperature distribution, especially in shallow aquifer depths (Taniguchi et al., 2005; Taniguchi, 2006). Over the 20^{th} century, especially during the second half, rapid development and expansion of urban cities dominated the causes of influencing the climate at ground surface, hydrology, and associate temperature distribution in the subsurface layer. The urban heat island effect, which is actually the sum of microclimatic changes in the urban environment, does have a significant effect on

ground surface temperatures on a local scale (Ferguson and Woobbury, 2004). The land-use changes, such as deforestations and reforestations substantially alter the groundwater recharge patterns as well as natural energy balance at the ground surface (Battin et al., 2007). Moreover, climate projections, such as intergovernmental panel on climate change fourth assessment report (IPCC AR4) warn the potential of substantial changes in future climate, in particular, surface air temperature and precipitation that may exert additional pressure besides the impact of urbanization on aquifer temperature change.

Therefore, proper understanding of urbanization and climate change effects on the aquifer thermal regime will be useful in terms of planning coastal ecosystem management programs.

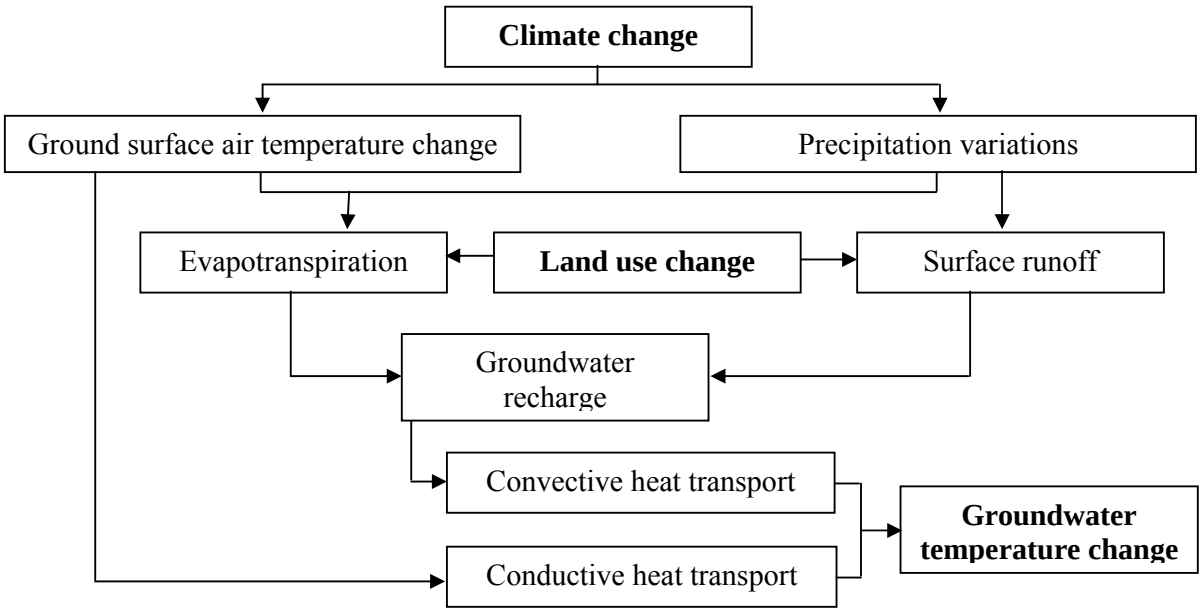

Fig. 1.1 Interrelation-ship of anthropogenic effects on groundwater temperature change

1.2 Important of the study

Since the groundwater temperature directly connects with the health of the ecosystems (Lee and Bell, 1999; Oie and Olsen, 1993; Oltra and Todolf, 1997), the studies on the potential changes of aquifer temperature under the local effects of urbanization and global scale changes of climate have become necessary. Due to its low thermal diffusivity and small rate of groundwater flow, signatures of the past global warming and urbanization effects have been preserved in the subsurface thermal regime as a deviation from the steady state conditions (Pollack and Huang, 1998; Huang et al., 2000). In an urban environment, urban heat island effect is a critical phenomenon for ground surface temperature change (Ferguson and Woobbury, 2004) and therefore, in some of areas, it is

difficult to discriminate the effects between global climate change and heat loss from buildings in terms of possible causes altering the temperature profiles (Taniguchi, 2006). However, impact predictions of urbanization and climate change in future essentially require proper understanding of their individual effects in past and present for altering the natural state of temperature distribution in the subsurface layer. Therefore, a careful and integrated assessment is necessary to distinguish the influence of each force, and require multitude of methods for verifying the accuracy of the estimations.

The Sendai plain in Japan has warmed by 0.02 ^{o}C/year (2 ^{o}C per 100 years) during the 20th century. Other areas in the same prefecture, such as Fukushima and Yamagata also show similar magnitude of air temperature change (1.7 and 1.8 ^{o}C per 100 years, respectively). The climate models with very high confident predicts another 1.8-4.0 ^{o}C increase at the global scale by the end of 21st century (Alley et al., 2007). Higher air temperatures are likely to increase subsurface water temperatures (Taniguchi, 1994), which could be harmful to aquatic ecology in groundwater dominated ecosystems. Planners and decision makers at the policy level rely heavily on estimated impacts and their significance in planning counter measures. Therefore, integrated assessment of urbanization and climate change is timely important to guide the decision makers in environment management programs.

1.3 Objectives and scope of the study

The main objective of this study is to estimate the past urbanization effects and future climate change impacts on aquifer thermal regime. It aims to propose a methodology, which is applicable under diverse climatic and site characteristics with limited hydrological and climatic data. In order to estimate the past urbanization and global warming effects that have experienced at the local scale in the Sendai plain, the study expects to conduct a series of preliminary analysis based on the physical observations of the study area (i.e., land-use type, soil conditions, temperature-depth measurements, and water level records at different aquifer depths) and the climatic variations in the past (i.e., surface air temperature and precipitation changes). Moreover, several conventional methods of groundwater recharge estimation are intended to incorporate for the purpose of verifying the calibrated parameters through the preliminary analysis. Finally, in order to predict the potential climate change impacts, a set of General Circulation Models (GCMs) output are planed to downscale for a site specific assessment of aquifer temperature change in the Sendai plain.

CHAPTER 2

LITERATURE REVIEW

2.1 Pioneering works and potential of heat as a groundwater tracer

Although there was early recognition of groundwater as water quality parameter, in recent studies, groundwater temperature has been widely used as a tracer to estimate the groundwater recharge and discharge rates (Taniguchi, 1993; Ferguson et al., 2003). This is because; heat in the subsurface layer is transported not only by the conduction, but also by the convection through groundwater flow. Suzuki (1960) and Stallman (1963) were among the first to identify the true potential of using temperature-depth profiles measured in the subsurface to estimate flow velocity and aquifer hydraulic conductivity.

Owing to the generally low thermal diffusivity of rock and small groundwater flow rate, temperature fluctuations at the Earth's surface take several hundred years to penetrate the upper few hundred meters of the subsurface. Therefore, signatures of the past ground surface temperature change and groundwater flow have been preserved in shallow subsurface layer, which is noticeable as the aquifer temperature apart from general geothermal gradient. In homogeneous rock and in the absence of changes at the ground surface and significant water movements, the temperature in the subsurface increases linearly with depth, at a rate which is governed by the magnitude of the terrestrial heat flow and the thermal conductivity of the aquifer. In general, two zones in the subsurface, the surficial zone and the geothermal zone can be identified. The seasonal change in surface air temperature predominantly influences the temperature distribution in the surficial zone. However, the amplitude of temperature oscillation attenuates with depth (Stallman, 1965), and in general, it does not have a significant effect at depths below 15–20m (Taniguchi, 1994). Within the geothermal zone, the temperature profiles are not subject to seasonal variations. Groundwater flow perturbs the geothermal gradient by infiltration of relatively cool water in recharge areas and upward flow of relatively warm water in discharge areas, causing concave profiles in recharge areas and convex profile in discharge areas (Fig. 2.1). Therefore, the curvature of the observed temperature-depth profile can be used to estimate the representative groundwater recharge or discharge rate of the surrounding area.

Inversions by the general geothermal gradient can be caused by both transient GST change and groundwater recharge or discharge. With the presence of cooling (Pollack and Huang, 1998) or warming trend (Huang et al., 2000) at the ground surface, curvature of the T–D profile is altered accordingly and will be difficult to discriminate the individual

effects of groundwater flow and diffusion of transient GST change. Nevertheless, the assumption of strictly vertical groundwater flow must be considered with the proper evidences as horizontal flow may have significant influence on subsurface temperature distribution, in which case the resulting estimates of velocity will be incorrect.

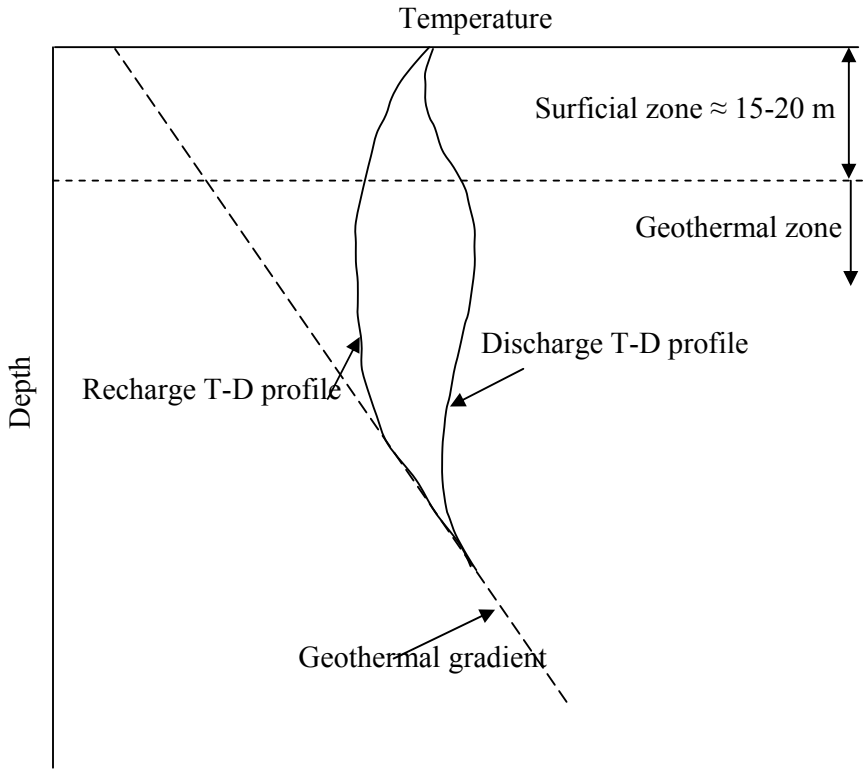

Fig. 2.1 Schematic temperature profiles for recharge and discharge water flows

2.2 Studies on factors altering general geothermal gradient

Ground surface temperature change and variations of groundwater flow patterns are assigned as the main factors influencing the natural state of temperature distribution in the subsurface layer. Global climate change may impose threats at the macro-scale by varying the local precipitation patterns and warming ground surface air temperature, which intern impact the aquifer thermal regime. Urbanization at the local scale alters the land-use types, which indefinite affects for ground surface temperature change and groundwater recharge. The increased rate of surface and subsurface temperature in cities is thus caused by these combined effects. However, in coastal aquifers, a tidal effect additionally adds to the list of the factors regulating the subsurface temperature distribution. The periodic rise and fall of the tide water stage in the ocean produces sinusoidal groundwater level fluctuations in adjacent inland aquifers. The seawater and groundwater are generally two different

temperatures, and therefore, the degree to which waters mix in the transition zone decides the pattern of temperature distribution. Under these circumstances, a careful and well detailed study is necessary to understand the dominant causes influencing the heat transport in the particular depths of the subsurface layer.

2.2.1 Urbanization and deforestation effects

Groundwater flow and ground surface temperature change can alter the natural state of subsurface temperature distribution through convective and conductive heat transport. The man made changes at the ground surface, such as deforestation (Nitoui and Beltrami, 2005) and urbanization (Ferguson and Woodbury, 2004), result directly in evapotranspiration and albedo changes and affects subsurface temperature through alternation in groundwater recharge and ground surface temperature.

The urban heat island effect on subsurface temperatures has been studied in several studies (Taniguchi et al., 1999; Ferguson and Woodbury, 2004; Taniguchi, 2006, 2007). Taniguchi (2006) suggested a link between population density and the magnitude of the temperature perturbation in the subsurface in the Bangkok area. This relationship was then used to explain a relationship between the distance from the city centre and the magnitude of the perturbation. In a more recent study, Taniguchi (2007) examined subsurface temperatures in several urban areas in Asia and found a link between surface air temperatures and the average deviation from steady state heat flow in the subsurface. Increases in soil temperatures of more than 5 ^{0}C have been found in urban areas than rural surroundings (Reiter, 2006; Bense and Beltrami, 2007). Moreover, numerical simulation of heat transport by Ferguson and Woodbury (2004) found similar magnitude of temperature change (4.0 to over 5.0 ^{0}C) in subsurface layer largely attributed to heat loss from buildings. Most interestingly, this research noticed that during 100 years of time after the buildings are constructed, more than 70% from total temperature change is occurred in first 50 years (approximately 2.5 ^{0}C from total of 3.5 ^{0}C). During the next 50 years, the temperature is expected to rise less than 1.0 ^{0}C.

In a forest ecosystem, only 5–20% of the short-wave solar radiation incident on the forest canopy reaches the land surface (Beltrami, 2001a). Therefore any removal of trees (i.e. albedo decrease) results in a substantial increase in solar radiation reaching the land surface. If the energy balance at the ground surface is concerned, decrease in evapotranspiration due to deforestation is not compensated by an increase in surface albedo, the ground gains energy increasing its surface temperature (Lean et al., 1996). Observations show that the removal of vegetation results in a significant increase of

surface temperature of up to 7-8 Celsius (Bense and Beltrami, 2007; Bond-Lamberty et al., 2005; Taniguchi et al., 1999).

Changing land-use and land-management practices can also alter the hydrology of the aquifer. Ranjan et al. (2005) determined that in the arid areas, agricultural lands have less evapotranspiration and provide higher recharge whereas the forest with higher evapotranspiration provides less recharge. Groundwater recharge in urban areas with sealed surfaces is less than in areas of strong vegetation. Allison et al. (1990) observed groundwater levels that were steadily increasing at 0.1 m/year following the clearing of native vegetation in southern Australia. Therefore, land-use change may cause significant impact not only on ground surface temperature but also natural groundwater recharge that indeed alter the temperature distribution in the subsurface layer.

2.2.2 Climate change effects

Climate change imposes threat on aquifer thermal regime by warming surface air temperature and altering groundwater recharge. Groundwater flow in shallow aquifers is part of the hydrological cycle and is affected by climate variability and change through recharge processes (Chen et al., 2002). Owing to a lack of data and the very slow reaction of groundwater systems to changing recharge conditions, impacts of climate change on groundwater are poorly understood. Groundwater resources are related to climate change through hydrologic processes, such as precipitation and evapotranspiration, and through interaction with surface water. With increased evapotranspiration as a result of higher air temperature and decreased precipitation, the impact of climate change will result in declining groundwater recharge (Eckhardt and Ulbrich, 2003; Brouyere et al., 2004) and alter the associate temperature distribution in the subsurface. For example, in the Ogallala Aquifer region, projected natural groundwater recharge decreases more than 20% in all simulations with warming of 2.5°C or greater (Rosenberg et al., 1999).

Increased precipitation variability may decrease groundwater recharge in humid areas because more frequent heavy precipitation events may result in the infiltration capacity of the soil being exceeded more often. In semi-arid and arid areas, however, increased precipitation variability may increase groundwater recharge, because only high-intensity rainfalls are able to infiltrate fast enough before evaporating, and alluvial aquifers are recharged mainly by inundations due to floods (Bates et al., 2008). According to Domenico and Palciauskas (1973), the curvature of the temperature-depth profile depends on the magnitude of groundwater recharge. Therefore, potential variations of groundwater recharge under changing climate may have significant impact on aquifer thermal regime.

Among the various influential, such as snow cover, land-use type etc., surface air temperature is the dominant force on ground surface temperature (Mann and Schmidt, 2003). Several studies found that, on the long scale, surface air temperature change primarily governs the ground surface temperature change (Baker and Ruschy, 1993; Putnam and Chapman, 1996; Majorowicz and Skinner, 1997) and has been considered a direct relationship in many studies (Ferguson et al., 2003; Ferguson and Woodbury, 2005; Taniguchi et al., 1999a). In recent years there has been increasing concern regarding the trends of global climate change (Salathe and Mote, 2007). The collection of global climate simulations performed for the Intergovernmental Panel on Climate Change (IPCC) Fourth Assessment Report (AR4) (Alley et al., 2007) provide an excellent standardized set of scenarios for climate impact studies. According to IPCC AR4 (Fig 2.2), the best estimates of projected globally averaged surface air temperature change at 2090–2099 relative to 1980–1999 span 1.8 ^{0}C (for B1 scenario with the likely range of 1.1 ^{0}C to 2.9 ^{0}C) to 4 ^{0}C (for A1F1 scenario with the likely range of 2.4 ^{0}C to 6.4 ^{0}C), warning the fears of substantial changes in aquatic ecology.

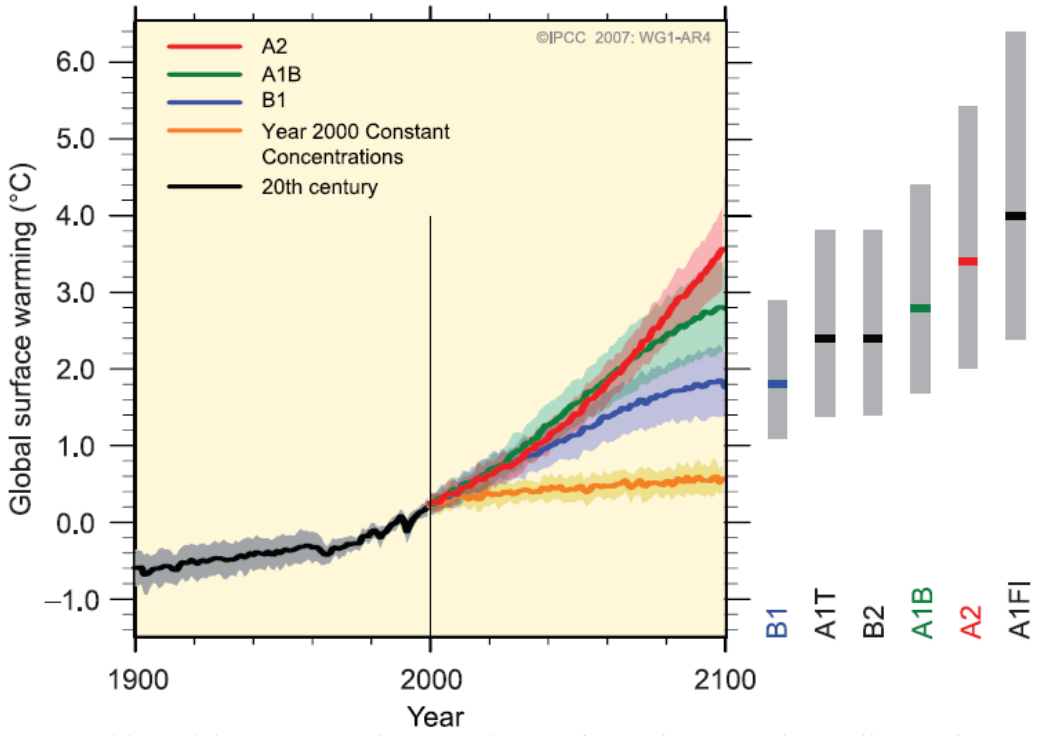

Fig. 2.2 Multi-model averages and assessed range for surface warming (Alley et al., 2007)

The direct impact of surface air temperature rise might be increased or decreased depend on the magnitude of groundwater recharge change and also, affect in different magnitudes on aquifer temperature at different depths. However, IPCC AR4 concluded

that approximately 20–30% of plant and animal species assessed so far are likely to be at increased risk of extinction if increases in global average temperature exceed 1.5–2.5 °C. Therefore, in accordance with the IPCC AR4 projections of future global warming, climate change may adversely change the groundwater temperature which in turn affect for the fundamental ecological processes and the geographic distribution of aquatic species (Jones et al., 2006; Eaton and Scheller, 1996).

2.2.3 Tidal effects

Fresh groundwater comes in contact with saline groundwater at the seaward margins of coastal aquifers. The freshwater and saltwater within coastal aquifers are separated by a transition zone within which there is mixing between freshwater and saltwater (Fig. 2.3).

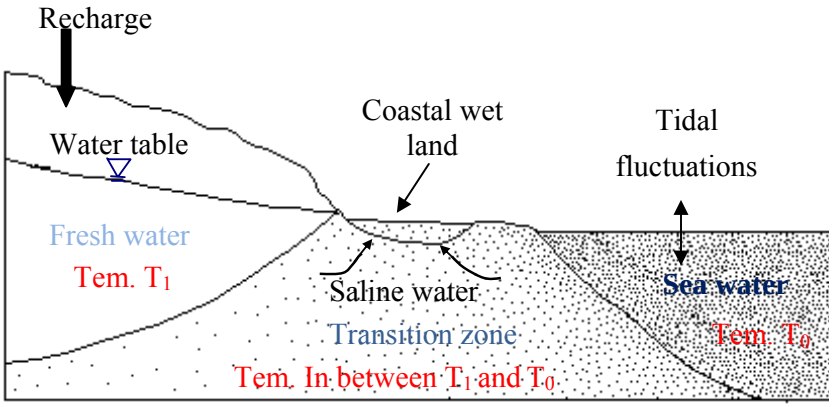

Fig. 2.3 Schematic representation of transition zone (Gunawardhana and Kazama, 2009)

Kim et al. (2006) estimated the tidal effects on variations of fresh-saltwater interface and groundwater flow on Jeju Island, Korea. The periodic rise and fall of the tide water stage in the ocean produces sinusoidal groundwater level fluctuations in adjacent inland aquifers. Taniguchi (2002) observed both diurnal and semi-diurnal fluctuations of submarine groundwater discharge due to changes in hydraulic gradient between the groundwater and seawater in Osaka bay, Japan. Seawater intrusion or salt water flow to the inland in a fresh water aquifer is not only a major constraint in groundwater utilization, but also alters the aquifer thermal regime. This is because, seawater and groundwater are generally two different temperatures, and therefore, the degree to which waters mix in the transition zone decides the pattern of temperature distribution. Diurnal, seasonal and the long term changes of water level and water temperature at two zones (fresh water zone and seawater zone) might significantly alter the thermal regime in the transition zone. In previous studies, the effect of the seawater intrusion on the aquifer thermal regime has not been identified. Therefore, proper understanding of the physical process of temperature

change in groundwater aquifers under the tidal effect will be important in estimating the adverse effects of urbanization and climate change on coastal ecosystems.

2.3 Past studies to model aquifer temperature distribution

With the pioneering works by Suzuki (1960) and Stallman (1963), groundwater temperature has been used as a tracer to estimate flow velocity and aquifer permeability. Stallman (1963) proposed a solution for subsurface temperature change under the steady state conditions by considering only the vertical conduction and horizontal groundwater flow. Bredehoft and Papadopulos (1965) presented a curve matching method for temperature data in wells to solve the analytical solution for one-dimensional steady state groundwater flow and heat transfer. Taniguchi et al. (2003) applied this method in Western Australia to estimate the groundwater discharge rates in a coastal aquifer. Another analytical solution for two-dimensional temperature distribution, but for steady state groundwater flow was found by Domenico and Palciauskas (1973). Taniguchi et al. (1989) and Sakura (1993) applied this method to identify regional and local groundwater flow systems.

Analytical solutions for transient groundwater flow and heat transport are relatively small. Vertical steady state water flow with sinusoidal change in the surface temperature was estimated by Stallman (1965). Based on this finding, Taniguchi (1993) developed a type curve fitting method to estimate vertical groundwater fluxes using transient temperature-depth profiles in relatively shallow aquifers. In addition, solutions for the transient heat flow have been developed considering constant horizontal water flow that is shallow enough for interaction with the surface (Cartwright 1971, Cartwright 1974, Ziagos and Blackwell 1981 and Ziagos and Blackwell 1986). Moreover, Carslaw and Jaeger (1959) obtained an analytical solution for temperature using a one-dimensional heat conduction-advection equation under the condition of a linear increase in surface air temperature. Since then, several studies approximated the ground surface warming rate in their study areas due to combined effects global warming and urban heat island effects as a linear trend and applied Carslaw and Jaeger (1959) model to simulate subsurface temperature distributions (Taniguchi et al. 1999a, and Uchida and Hayashi 2005).

However, the assumption of spatially uniform groundwater flow may not be appropriate in coastal aquifers, where significant water level fluctuations are caused by tides. In previous studies, the effects of the seawater, that is obviously different from the fresh groundwater temperature, have not been taken in to account. Therefore, a new analytical solution will be developed to incorporate the advection effect of seawater for temperature distribution in coastal aquifers.

CHAPTER 3

STUDY AREA AND DATA COLLECTIONS

3.1 Geology, land-use types and historical development of the Sendai plain

Sendai city located in Tohoku prefecture, Japan, experienced rapid development after the destruction of the Second World War, and became the economic center of the region. The Sendai plain extends about 40 km with a width of 10 km and is bounded by a mountain region (elevation 1000-1500 m) in the west. On the east side of the mountain region is an area with steep hills (elevation 50–300 m) followed by a low land area forming the plain. The Nanakita and Natori rivers (Fig. 3.1b) emerge from the peripheral mountain regions and flow toward the sea. The Sendai plain is an alluvial formation and serves as the main aquifer of the catchment. The maximum depth of the aquifer ranges between 60–80 m and is shallow compared with other plains, such as the Kanto Plain (more than 2000 m) near the Tokyo Metropolitan area. The permeability of the soil below the main aquifer is significantly (approximately 10^4 times) less than the permeability of the main aquifer (Uchida and Hayashi, 2005). Therefore, it is reasonable to assume that the main aquifer is unconfined and bounded by an impermeable layer below that. The geological formation in the Sendai plain is not complex. Clay, silt and sand formations dominate in the shallow subsurface layer (0~15m in Fig. 3.1c) and below that it consist of thick gravel formation (15~55m).

There are five water level observation stations located within the area (Fig. 3.1b), which are used to measure the groundwater level and land subsidence. Among them, W1, W2, W4 and W5 have three sub–wells (SWs) each, directed to different aquifer depths (Table 3.1). Water level records at different aquifer depths (with different screen intervals) represent the actual hydraulic head at that particular depth and are important in determining how the horizontal and vertical water flows behave in the area.

Some significant differences in land use types exist at the local scale surrounding the wells (Fig. 3.2). When selecting the representative land use types, the predominant category in the 10,000 m^2 surrounding the well was chosen. Wells W2, W3 and W4 are located in paddy field areas and have similar surface characteristics and land use histories. Well W1 is located in a residential area that is partially covered with home gardens and vegetation. However, the unpaved area surrounding W1 is significantly smaller than in the areas surrounding W2, W3 and W4. Well W5 is located at the city center, which is more urbanized than all other well locations. All well locations are situated within seven kilometers of the city center and the Sendai meteorological station.

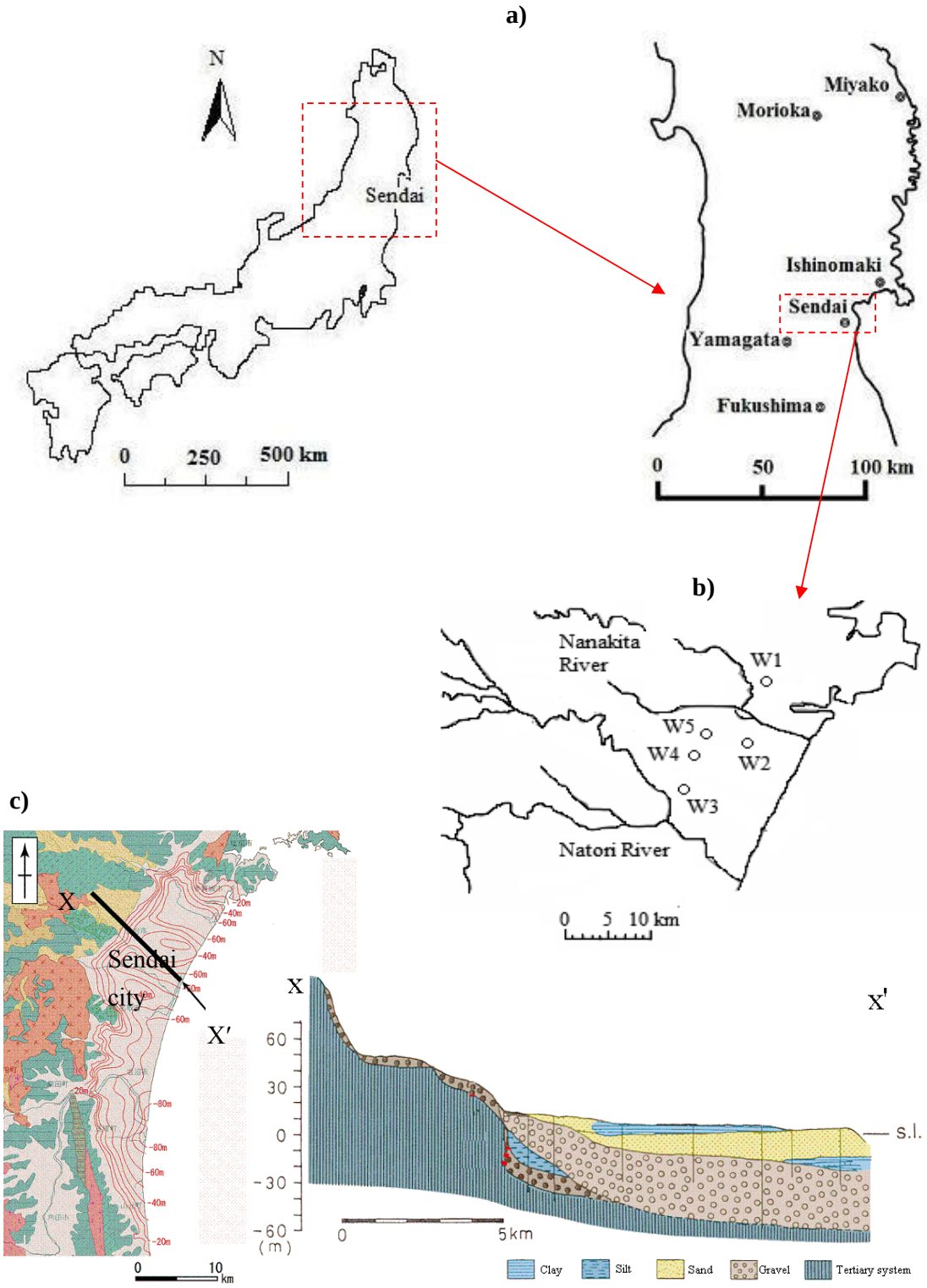

Fig. 3.1 a) Study area, b) locations of observation wells, and c) geological cross-section

(Source: Water Environmental Map No 1, Sendai Plain 2004. Geological Survey of Japan AIST.)

Table 3.1 Well depths and screen intervals

Well No.		Depth (m)	Screen interval (m)	Well No.		Depth (m)	Screen interval (m)
W1	SW 1	7	2.5~5.5	W4	SW 1	11	6.8~9.3
	SW 2	26	16.0~20.0		SW 2	23	13.8~17.8
	SW 3	60	45.0~51.0		SW 3	54	35.0~41.0
W2	SW 1	5	2.0~3.0	W5	SW 1	6	1.0~3.7
	SW 2	16	8.0~12.0		SW 2	45	23.0~34.0
	SW 3	50	37.0~44.0		SW 3	100	72.2~83.2
W3		50	23.0~47.6				

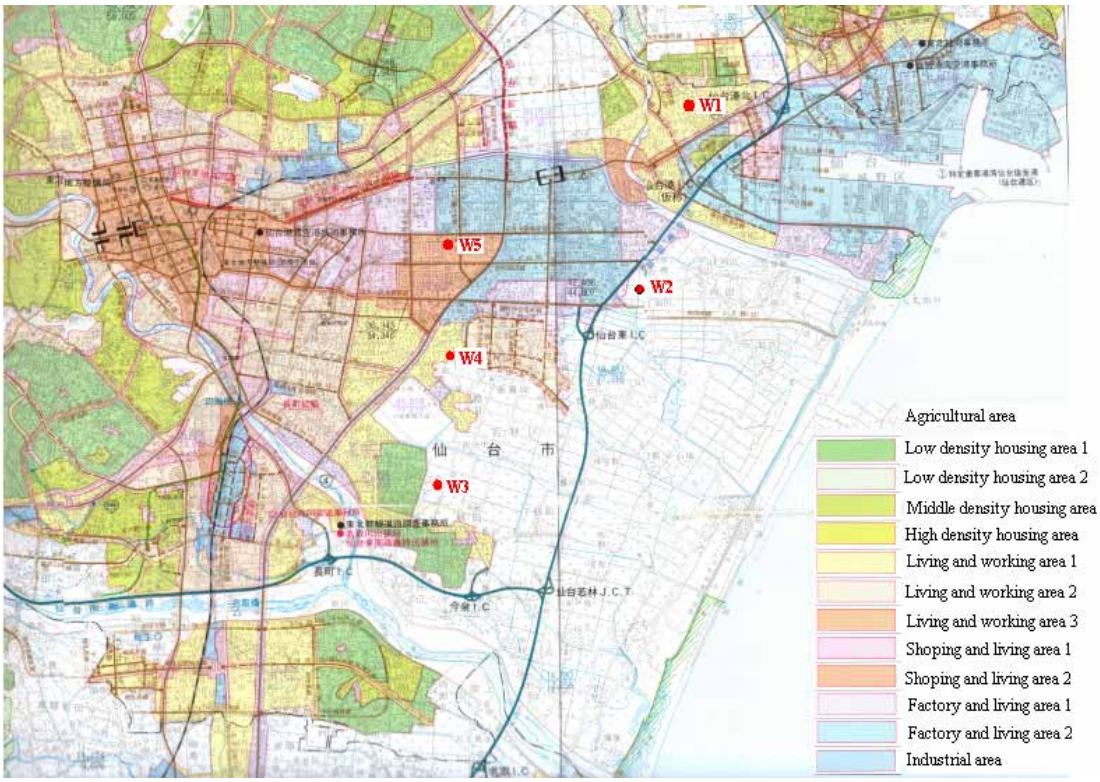

Fig. 3.2 Land-use map in the Sendai plain

3.2 Groundwater temperature observations

Continuous 1-hr temperature measurements were observed in all wells and sub wells, except at W5, from May, 2007 to February, 2008 using Tidbit temperature loggers (Fig. 3.3). Moreover, Groundwater temperature was measured at W1, W2, W3 and W4 at one-meter intervals (Fig. 3.4). Groundwater temperatures presented on Water Environmental Map No. 1, Geological Survey of Japan, were used to obtain W5 data.

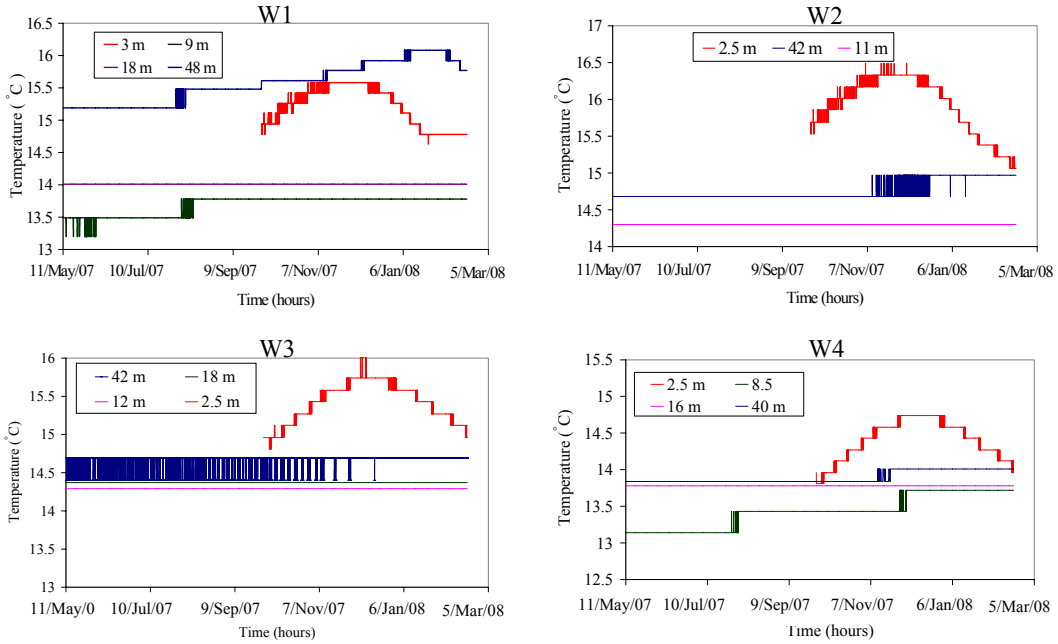

Fig. 3.3 Continuous 1-hr temperature measurements at different aquifer depths

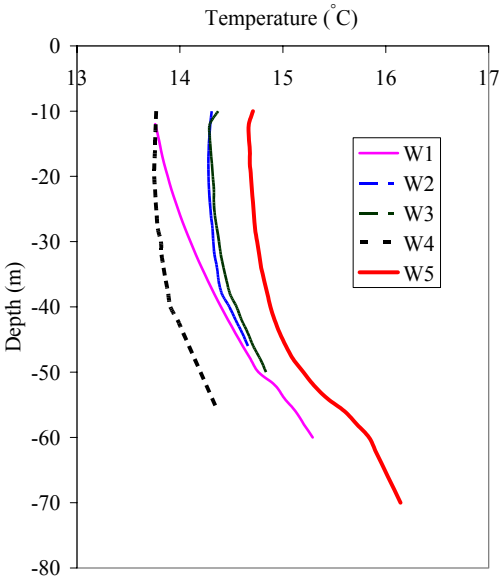

Fig. 3.4 Instant temperature records at 1 m depth intervals

According to the observations in Fig. 3.3, significant temperature fluctuations were noted just below the water table (about 3 m from the ground surface), possibly because of the seasonal change of ground surface air temperatures. These fluctuations failed to continue to deeper aquifer depths, where they diminish around 15 m depths. However,

groundwater temperatures in the bottom parts of the observation wells (40-50 m) considerably changed during the observation time, and it is noted that the magnitude of change in groundwater temperature decreased as the distance from coast increased. These behaviors will be discussed and explained with the effects of potential influences in Chapter 4.

Background temperature in the aquifer is higher than the annual average air temperature, giving an upward heat flow from the interior of the earth. Under steady state heat conduction, this produces a linear geothermal gradient within homogeneous depth intervals. However, in all wells, there is clear evidence of a temperature profile inversion from the general geothermal gradient (Fig. 3.4). The magnitude of ground surface warming, which was calculated as the difference between the observed subsurface temperature profile and the extrapolated steady state linear curve to the ground surface, ranges from spans 0.9–1.3ºC. The depth of departure from the general geothermal gradient is different in each well, which may indicate local variations in the magnitude of surface warming and groundwater recharge. Starting from the bottom of the temperature-depth (T–D) profile of each well, the first point that deviated from the general geothermal gradient by 0.1ºC was designated as the representative depth of departure from steady state heat conduction (Taniguchi, 2006). Well W5 shows the greatest depth of departure (60±1 m), followed by W1 (52±1 m). Wells W2, W3 and W4 exhibit similar depths of departure (38±1 m, 40±1 m and 42±1 m, respectively), reflecting their similar site conditions. These observations may confirm the combined effects of global climate change and different magnitudes of local urbanization have experienced in the Sendai plain. Therefore, Carslaw and Jaeger (1959) model will be applied to simulate the urbanization and climate change impacts on temperature distribution and discuss with details in Chapter 5.

3.3 Groundwater level variations

1-hr water level records measured by the Sendai city office were used for the analysis. Sub wells with different screen intervals (Table 3.1) give reasonable indication of the real groundwater head at a certain depth. The midpoints of the screens were used as the representative depths.

Groundwater level changes in first (the shallowest) and second (medium depth) sub-wells at all the well points are more sensitive to the recharge water from precipitation (Fig. 3.5) and no periodic of water level fluctuations were observed. On the other hand, groundwater level fluctuations in the deepest sub-wells show strong periodicity at all the well points. Regional groundwater flows and/or the inland direction tidal water flow may

cause such fluctuations. In Chapter 4, we will relate the water level changes with the tidal fluctuations by analyzing their auto-correlation and cross-correlation functions. Further discussions will be maid considering the all potential influences to vary the groundwater level in deep aquifer depths.

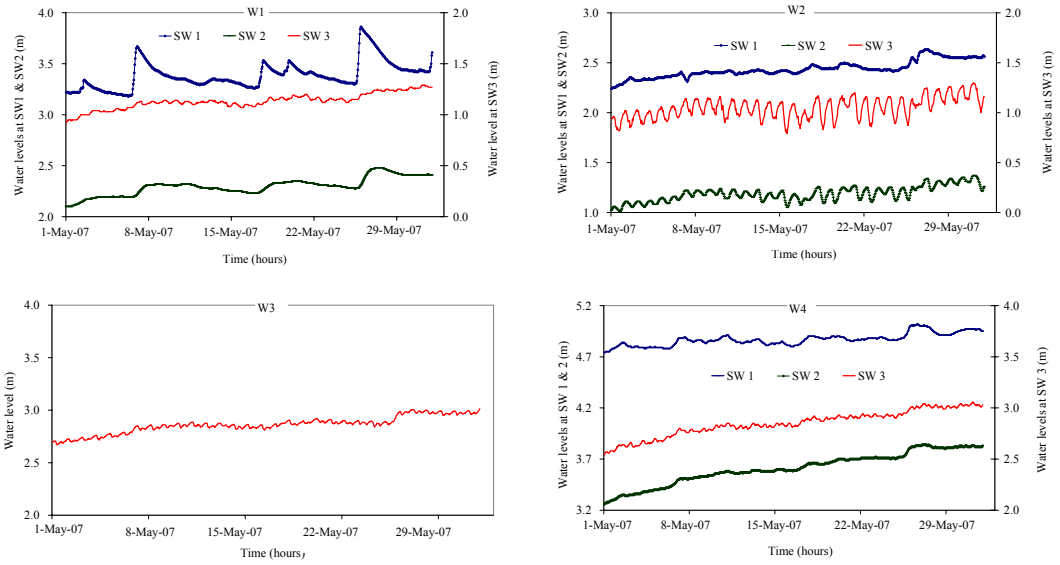

Fig. 3.5 Groundwater level variations at different aquifer depths

3.4 Historical and seasonal trends of climatic parameters in the region

Sendai metrological station observes temperature and precipitation since 1927 (Fig. 3.6).

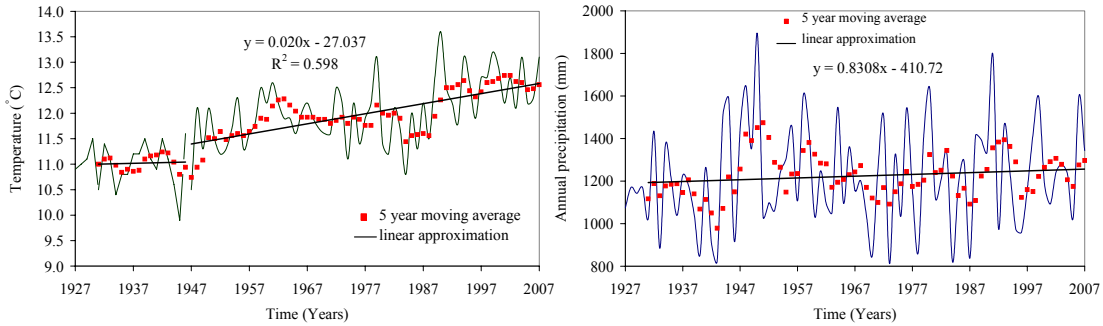

Fig. 3.6 Temperature and precipitation trends in past

According to the temperature records, surface air temperature indicates no significant trends until the middle of the 19th century. However, the annual mean temperature in the Sendai area has increased by about 1.8ºC from 1947 to 2007 with a rate of 0.02ºC/year (Fig. 3.6a). In contrast to temperature, annual precipitation in the Sendai plain shows no strong trend over the last 80 years.

In the Sendai plain, large seasonal variations of air temperature and precipitation commonly occur during four seasons. According to Fig. 3.7, which depicts five year average monthly mean temperature, approximately 22 °C temperature difference was observed during winter and summer seasons. Sendai's rainy season usually begins in late June to early July, which according to monthly average, peaks in July (Fig. 3.7).

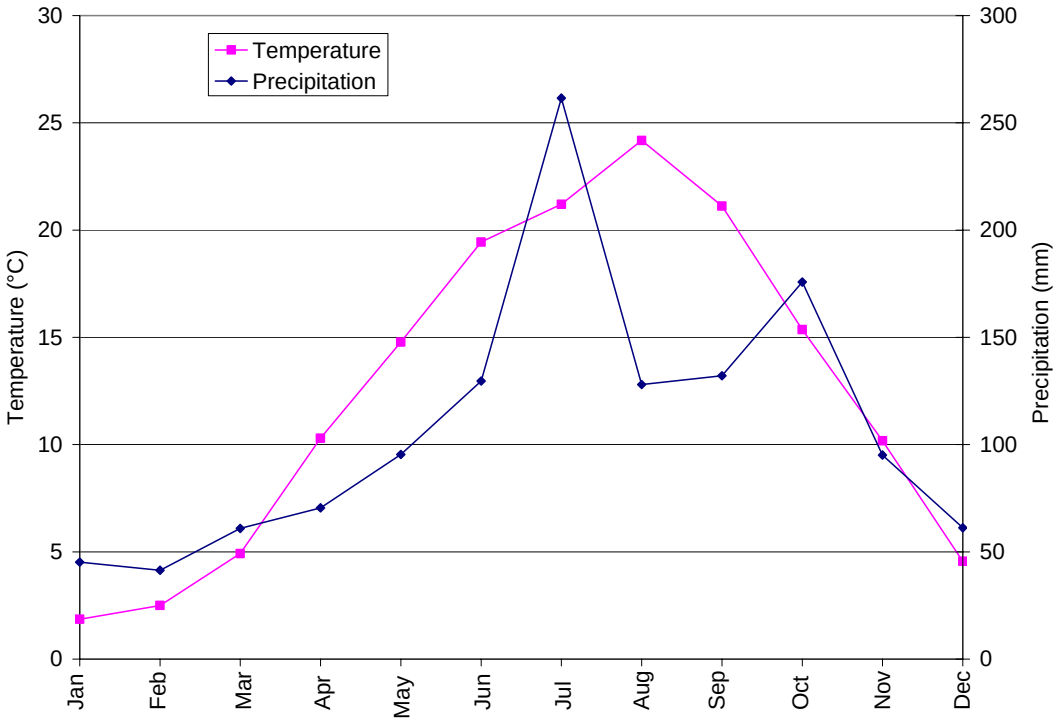

Fig. 3.7 Seasonal variations of five year averaged (2003-2007) surface air temperature and precipitation in the Sendai plain.

Seasonal variations of ground surface temperature largely influence the thermal regime in shallow aquifer depths. As an example, Taniguchi (1994) observed maximum of 5.3 °C aquifer temperature change at 2 m depth from ground surface with respect to seasonal air temperature change in the Nara basin, Japan. The effect of seasonal temperature variations significantly decay as the depth from ground surface increases. In the same study by Taniguchi (1994), seasonal temperature change was insignificant below depths of 15-20 m. However, long-term warming trend in the Sendai plain (0.02ºC/year) may have altered the deep aquifer depths, which is noticeable in terms of the deviations from steady state temperature-depth profiles. Therefore, it is timely important to examine the impacts of above changes in the ground surface to govern the temperature distribution in the sub-surface layer, which we will discuss consecutively in the following chapters.

CHAPTER 4

TIDAL EFFECT ON AQUIFER TEMPERATURE CHANGE

Understanding the physical process of temperature change in groundwater aquifers is important in estimating the adverse effects of urbanization and climate change on coastal ecosystems. Seawater intrusion or salt water flow to the inland in a fresh water aquifer is not only a major constraint in groundwater utilization, but also alters the aquifer thermal regime. This is because, seawater and groundwater are generally two different temperatures, and therefore, the degree to which waters mix in the transition zone decides the pattern of temperature distribution.

Continuous and long-term temperature measurements at different aquifer depths are important to understanding the seasonal heat flux change in the costal aquifers. Moreover, the combined analysis of water level and temperature records in different aquifer depths at several locations might help in understanding the significant factors, which include seasonal changes of atmosphere temperature, hydraulic head and/or the sea water temperature which alters the temperature at a particular depth. Therefore, this chapter will (1) investigate the correlation of groundwater level variations in the costal aquifers with the tidal fluctuations, (2) develop a heat transport model that can incorporate the effects of non-uniform seawater flow and (3) compose a set of curves to estimate the temperature distribution in coastal aquifers under different site and tidal characteristics.

The periodic rise and fall of the tide water stage in the ocean produces sinusoidal groundwater level fluctuations in adjacent inland aquifers. Therefore, the assumption of spatially uniform groundwater flow may not be appropriate in coastal aquifers. In previous studies, the effects of the seawater, that is obviously different from the fresh groundwater temperature, have not been taken in to account. Therefore, a new analytical solution was developed to incorporate the advection effect of seawater for temperature distribution in coastal aquifers.

4.1 Analytical model development

4.1.1 *Symbols*

T : Temperature
V : Horizontal water flux
t : Time
x : Horizontal distance from the coast

K_{ws} : Thermal conductivity of the saturated porous medium
C_w : Specific heat capacity of water
C_s : Specific heat capacity of solid
ρ_w : Density of water
ρ_s : Density of solid
θ : Porosity
T_0 : groundwater temperature at the coastal line
T_L : groundwater temperature at the inland distance L from the coast
β : Temperature decay coefficient
h : groundwater table height
K : Hydraulic conductivity
D : Aquifer depth
τ : Tidal period
A : Tidal amplitude

4.1.2 *Governing equation for the temperature distribution under tidal effect*

The governing equation for the unsteady, non-uniform heat transport in three-dimensional system is,

$$\nabla\left(K_{ws}\nabla T\right)-\nabla\left(C_w\rho_w VT\right)=\frac{\partial\left[\theta C_w\rho_w+\left(1-\theta\right)C_s\rho_s\right]T}{\partial t} \tag{4.1}$$

Assuming the aquifer is homogeneous, one-dimensional heat transport becomes,

$$K_{ws}\frac{\partial^2 T_{x,t}}{\partial x^2}-C_w\rho_w\left[T_{x,t}\frac{\partial V_{x,t}}{\partial x}+V_{x,t}\frac{\partial T_{x,t}}{\partial x}\right]=\frac{\partial\left[\theta C_w\rho_w+\left(1-\theta\right)C_s\rho_s\right]T_{x,t}}{\partial t} \tag{4.2}$$

If we assume steady state water flow and heat transport (in which the condition such as velocity, pressure, etc. may differ from point to point but do not change with time), Eq. (4.2) becomes (Domenico and Palciauskas, 1973 and Mansure and Reiter, 1979),

$$K_{ws}\frac{\partial^2 T_x}{\partial x^2}-C_w\rho_w\left[T_x\frac{\partial V_x}{\partial x}+V_x\frac{\partial T_x}{\partial x}\right]=0 \tag{4.3}$$

The assumption of uniform water flow is not valid in the coastal aquifers, because the effect of tidal water flow exponentially decays as the distance from the coast is increased (Jacob 1950). As in Suzuki (1960), Stallman (1965) and Bredefoeft and Papadopulos

(1965), an exponential relationship for inland temperature change would also be applicable. Therefore, groundwater temperature variation can be defined as,

$$T_x = C_1 + C_2 \exp(Bx) \tag{4.4}$$

where, B, C_1 and C_2 can be determined with the appropriate boundary conditions.

4.1.3 *Governing equation for the groundwater flow and local water table height due to tidal effect.*

When it is assumed that the porous medium is homogeneous and isotropic with hydraulic conductivity and porosity, and the flow velocity is essentially horizontal, Darcy's law gives,

$$V_{x,t} = -K\,\partial h_{x,t}/\partial x \tag{4.5}$$

Continuity equation,

$$\partial h_{x,t}/\partial t = (-1/\theta)\partial(h_{x,t}V_{x,t})/\partial x \tag{4.6}$$

When Eqs. (4.5) and (4.6) are applied in the Boussinesq's equation,

$$\frac{\partial h_{x,t}}{\partial t} = \frac{K}{\theta}\frac{\partial}{\partial x}\left(h_{x,t}\frac{\partial h_{x,t}}{\partial x}\right) \tag{4.7}$$

When the tidal amplitude is small compared with the aquifer depth and beach is practically vertical, Eq. (4.7) can be simplified as

$$\frac{\partial h_{x,t}}{\partial t} = \frac{KD}{\theta}\frac{\partial^2 h_{x,t}}{\partial x^2} \tag{4.8}$$

Jacob (1950) proposed a solution for Eq. (4.8) as

$$h_{(x,t)} = A\cos[(2\pi t/\tau) - ax]\exp(-ax) \tag{4.9}$$

where, $a = (\theta\pi/\tau KD)^{0.5}$ (4.10)

Furthermore, Nielsen (1990) considered following boundary conditions,

$$\frac{\partial h_{x,t}}{\partial t} = \frac{\partial h_{x,t}}{\partial x} = 0 \quad \text{at } x = \infty \tag{4.11}$$

$$h_{0,t} = h_{tide} = D + A\cos\omega t \tag{4.12}$$

and derived an expression for the time average local water table height considering the effect of the tidal flow as,

$$h_x = D + \left(A^2/4D\right)\left[1 - \exp(-2ax)\right] \tag{4.13}$$

Nielsen (1990) successfully represented the observed water levels in 11 observation wells near to the coast using Eq. (4.13). Here, we used the Eq. (4.4) and (4.13) with appropriate derivatives in Eq. (4.3) to obtain solutions for the C_1, C_2 and B based on spatially varying water head due to tidal effect. Three basic assumptions were made to simplify the mathematics of the solution.

1. Water movement due to tidal effects is essentially parallel with the x axis
2. Short term temperature fluctuations at the boundaries are negligible.
3. Heat characteristics of the porous medium and water are homogeneous and constant with temperature.

When applying the derivation of Eq. (4.13) in Eq. (4.5),

$$V_x = \left(-KA^2/4D\right)2a\exp(-2ax) \tag{4.14}$$

Taking the appropriate derivatives of the Eq. (4.14) and Eq. (4.4), and substituting in Eq. (4.3),

$$K_{ws}B^2C_2\exp(Bx) = \frac{C_w\rho_w KA^2 2a}{4D}\left\{\left[\left(C_1 + C_2\exp(Bx)\right)\left(2a\exp(-2ax)\right)\right] - \left[BC_2\exp(-2ax)\exp(Bx)\right]\right\} \tag{4.15}$$

Considering coastal and inland boundary conditions as,

$T_x = T_0$ at $x = 0$ (coastal line) (4.16)

$T_x = T_L$ at $x = L$ (an inland distance) (4.17)

We then applied two boundary conditions (Eqs. (4.16) and (4.17)) in Eqs. (4.4) and (4.15) to find the unknown parameters as,

$$C_1 = T_0 - \left[\frac{T_0 - T_L}{1 - \exp(BL)}\right] \tag{4.18}$$

$$C_2 = \left[\frac{T_0 - T_L}{1 - \exp(BL)}\right] \tag{4.19}$$

$$\frac{T_0 - T_L}{T_0} = \frac{2a[\exp(-2aL) - \exp(BL)]}{2a\exp(-2aL) + \left(\frac{B\exp(BL)}{\exp(BL) - 1}\right)(1 - \exp(-2aL))} \tag{4.20}$$

Introducing new parameter as $\beta = BL$, final solution was obtained as,

$$\frac{T_0 - T_L}{T_0} = \frac{2a[\exp(-2aL) - \exp(\beta)]}{2a\exp(-2aL) + \left(\frac{\beta}{L}\right)\left(\frac{\exp(\beta)}{\exp(\beta) - 1}\right)(1 - \exp(-2aL))} \tag{4.21}$$

The magnitude of β determines the degree to which temperature is distributed within the boundaries in a particular distance. When the β value is negatively small, the temperature distribution within the boundaries gentler than when the β value is negatively high, which rapidly draws the temperature down near the coast (Fig.4.1).

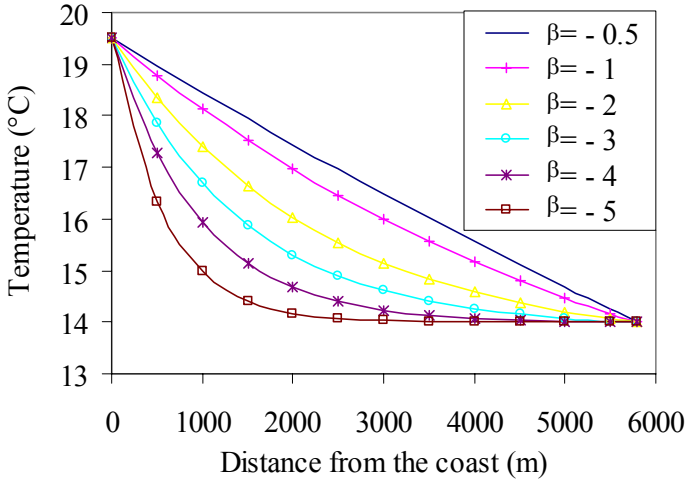

Fig. 4.1 Change in temperature distribution with β value

Therefore, accurate estimation of the β value is important from an ecological point of view for a proper evaluation of urbanization and climate change effects on coastal ecosystems. When the appropriate water level records are available, the value of *a* can be determined easily by observing the slope of the curve ln (amplitude at *x*) versus *x*. According to Eq. (4.9), damping and phase lag both grow with *ax*. Therefore, the calculated value of *a* from

the amplitude records can be further verified from the phase lags in each observation well. When the observed temperature records of T_0 and T_L are available and the appropriate value for a is calculated, they can be substituted into Eq. (4.21) to find the value for β.

4.2 Time series analysis of tides and water levels in observation wells

Groundwater level changes in first (the shallowest) and second (medium depth) sub-wells at all the well points are more sensitive to the recharge water from precipitation (Fig. 3.4) and no periodic of water level fluctuations were observed. On the other hand, groundwater level fluctuations in the deepest sub-wells show strong periodicity at all the well points. Diurnal fluctuations of water levels are shown (Fig.4.2), and the amplitude of water level fluctuation decays as the distance of the well from the coast increases.

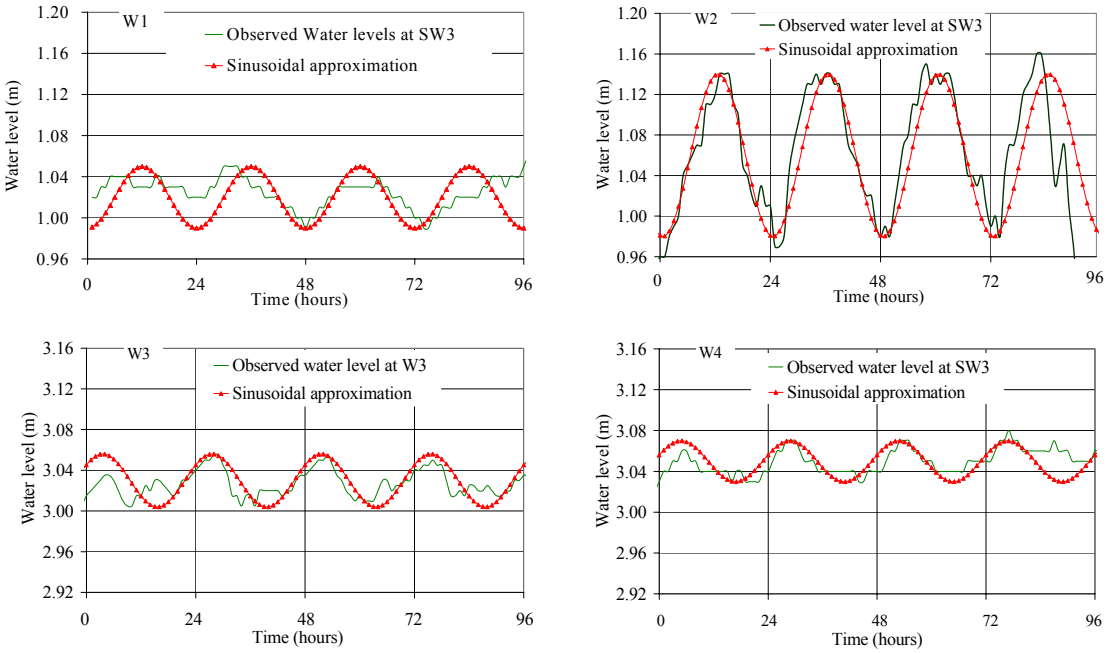

Fig. 4.2 Sinusoidal approximation for water level change

In groundwater aquifers, water flows downward in inland recharge areas and upward near the coast (Izuka and Gingerich, 1998). Therefore, a negative hydraulic gradient (head decreases with depth) must exist in recharge areas, and a positive hydraulic gradient (head increases with depth) must exist in discharge areas. Regional groundwater flows and/or the inland direction tidal water flow may change the vertical head gradient. Observation wells in this study are located relatively far from the coast, and all of them show substantial negative vertical head gradient (Fig. 3.4). The magnitude of the hydraulic

gradient in the shallow subsurface layer (0-20 m) is greater than in deep aquifers (20-50 m), which suggests the presence of regional groundwater flow and/or the tidal water flow. The average hydraulic gradient (May-July) in the shallow subsurface layer at W2 and W4 are about the same (1.7 m/10 m at W2 and 1.4 m/10 m at W4). However, hydraulic gradients in deeper aquifer depths (20-50 m) change significantly as the distance from the observation well to the coast is increased. A vertical hydraulic gradient of 0.04 m/10 m was estimated at the W2 and it increased by a factor of 10 (0.46 m/10 m) at the W4. This observation suggests that the effect of external hydraulic head, which is either regional groundwater flow or the tidal water flow or both, gradually decreases as the distance from the coast is increased.

Japanese cities such as Tokyo and Osaka have been developing and urbanizing rapidly during the last century, and groundwater has been used as an alternative water source to meet the excessive water demand. In Sendai, groundwater wells used for the domestic water supply are within the range of 10-30 m depth, and therefore, domestic groundwater use does not have an effect on the water level fluctuations at the deepest sub-wells (depth below 40 m). On the other hand, there are no records of excessive groundwater use for the industrial or irrigational activities. Therefore, it is reasonable to assume that the diurnal groundwater level fluctuations in SW3s are caused by the periodic rise and fall of the tide water stage in the ocean.

Hydrological time series frequently show strong periodicity (Serfes, 1991 and Kim et al., 2006). Therefore, time series analysis was conducted to examine the characteristics of tidal and water level fluctuations in the observation well itself and to understand the correlations between the tidal stage and water level fluctuations in observation wells. Auto-correlation analysis is important to distinguish periodicity from a general time series. When the correlation is calculated between a series and a lagged version of itself, it is called auto-correlation. A high correlation is likely to indicate periodicity in the corresponding time duration. When $\bar{x}$ is the mean of the series, the auto-correlation coefficient at lag k of a series $x_0, x_1, x_2, \ldots x_{n-1}$ can be defined as

$$\text{Auto}-\text{correlation}(k) = \frac{\sum_{i=0}^{n-1-k}\left(x_i - \bar{x}\right)\left(x_{i+k} - \bar{x}\right)}{\sum_{i=0}^{n-1}\left(x_i - \bar{x}\right)^2} \tag{4.22}$$

Tidal data were obtained from the Japanese Oceanographic Data Center (JODC) measured at Sendaiko monitoring station. Auto correlation functions of the hourly tidal fluctuation and water level records of SW3s in all observation wells for one week (08-14 October 2005) were presented in Fig. 4.3. A straight drop down of auto-correlation value

from 1 to 0 indicated that there are no correlated characteristics. However, similar and strong periodicities were reflected in the auto-correlation function of tides and water levels in W2, W3 and W4. Conversely, very low periodicity was detected at W1.

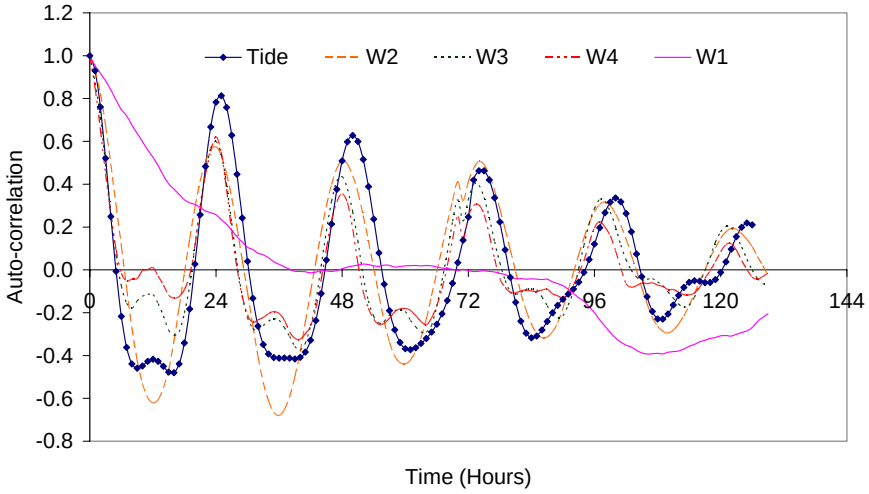

Fig. 4.3 Auto-correlation functions of tides and water levels.

Cross correlation analysis is a standard method of estimating the degree to which two series are correlated. In coastal aquifers, cross correlation analysis is important to understand how strong the tidal effect on water level fluctuations and the time delay to response for tides. When two series are x_i and y_i, where, i = 0, 1, 2,……,n-1, the cross correlation at lag k can be defined as;

$$\text{Cross correlation}(k) = \frac{\sum_{i=0}^{n-1-k}\left(x_i - \bar{x}\right)\left(y_{i+k} - \bar{y}\right)}{\sqrt{\sum_{i=0}^{n-1}\left(x_i - \bar{x}\right)^2}\sqrt{\sum_{i=0}^{n-1}\left(y_i - \bar{y}\right)^2}}$$

where $\bar{x}$ and $\bar{y}$ are the means of the corresponding series. In this study, several cross correlation analyses were performed to examine the relation between tidal fluctuation and water level changes in observation wells. Moreover, correlations of water level fluctuation between observation wells are also presented (Fig. 4.4 and Table 4.1). The maximum cross correlation coefficient of tides and water levels (0.74) was found in W2-SW3 after 6 hours. Similar to the auto-correlation function, cross correlation of water level with tides also displays a very low value at W1-SW3. Therefore, an explanation for the reason for the different behavior of W1 will be necessary for clear understanding. The Sendai harbor with many costal structures is located immediatly in front of W1 (Fig. 3.1b), and it reduced the strength of the tides. This might be a possible explanation for the low

performance at W1, while the other wells show good correlations with tide. Except W1, in general, as the distance of the well from the coast increased, the peak value of the cross-correlation decreased and the time lag increased. A similar trend is noted in temperature change as the distance from coast increased. Not only the initial temperature values, but also the magnitudes of seasonal temperature change, were subjected to attenuation as the distance from the coast increased. This behavior may confirm the definite influence of tides on aquifer thermal regime.

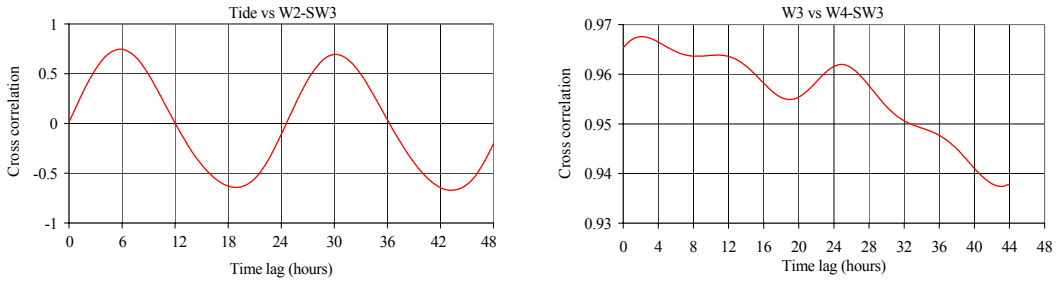

Fig. 4.4 Cross correlation functions.

Table 4.1 Results of cross correlation analysis

	Distance (m)	Time delay (hours)	Wave number (m^{-1})	Maximum Cross correlation
W3 Vs W4	1000	1.5	0.00039	0.97
W2 Vs W4	2300	4	0.00045	0.76
Tide Vs W2	3600	6	0.00044	0.74
Tide Vs W3	4900	8	0.00043	0.72
Tide Vs W4	5900	10.5	0.00047	0.43
Tide Vs W1	2800	1	-	0.1

Very high cross correlation coefficients were found among the water level fluctuations in each observation well itself when compare to the cross correlation coefficients of tides and water level fluctuations (Table 4.1). Furthermore, as the distance between wells increased, the correlation coefficient decreased. Groundwater levels in coastal aquifers are influenced not only by tides but also the recharge water from precipitation. Water level fluctuations in shallow subsurface layer (first and second sub-wells in all the well points) are more sensitive to the precipitated water. However, water level fluctuation in the deepest sub-wells also shows a reasonable increasing trend with rainfall (Fig. 4.5). Therefore, water level records in observation wells contain of two trends: sinusoidal fluctuation caused by the tides and an increasing or decreasing trend resulting from the recharge water from precipitation. When considering the cross

correlation analysis of the tidal stage and the groundwater level, the time series of tidal records do not respond to the water level change due to precipitation. This obviously causes the cross correlation value of tides and water level fluctuations to be lower than the cross correlations of water levels in observation wells.

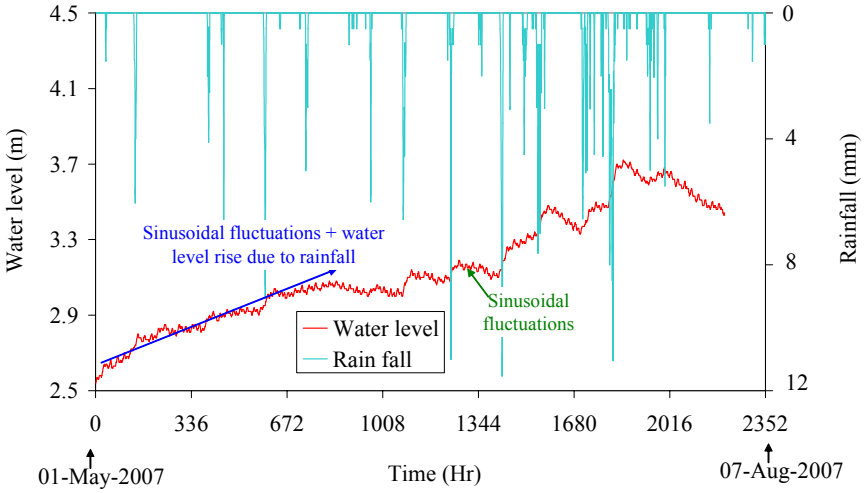

Fig. 4.5 Two trends of water level fluctuations in W4-SW3.

4.3 Temperature-depth profiles in observation wells

The seasonal temperature changes observed at all well points at different aquifer depths are shown in Fig. 4.6. According to the two-dimensional steady groundwater and heat flow analysis by Domenico and Palciauskas (1973), in the absence of significant vertical water flow, temperature gradient in subsurface layer is constant. The temperature depth profile is concave with infiltrating water flux in the recharge area, while the profile with upward water flux in the discharge is convex (Taniguchi et al., 2005). Temperature-depth profiles in this research can be discussed under two main categories: (a) seasonal temperature change at the shallow and bottom parts of the aquifer depths; and (b) deviations from the general geothermal gradient.

Discussing category (a), the groundwater temperatures in the bottom parts of the observation wells (40-50 m) considerably changed during the observation time, and it is noted that the magnitude of change in groundwater temperature decreased as the distance from coast increased (0.89 ^{0}C in W1 and 0.17 ^{0}C in W4). The temperature may have changed because (1) an increase in sea water temperature at the coastal boundary and its conduction and advection effects; (2) the heat source effect; (3) an increase in heat transfer from the ground surface due to changes in air temperature; and (4) the advection effect of recharge water from precipitation and surface water bodies such as rivers.

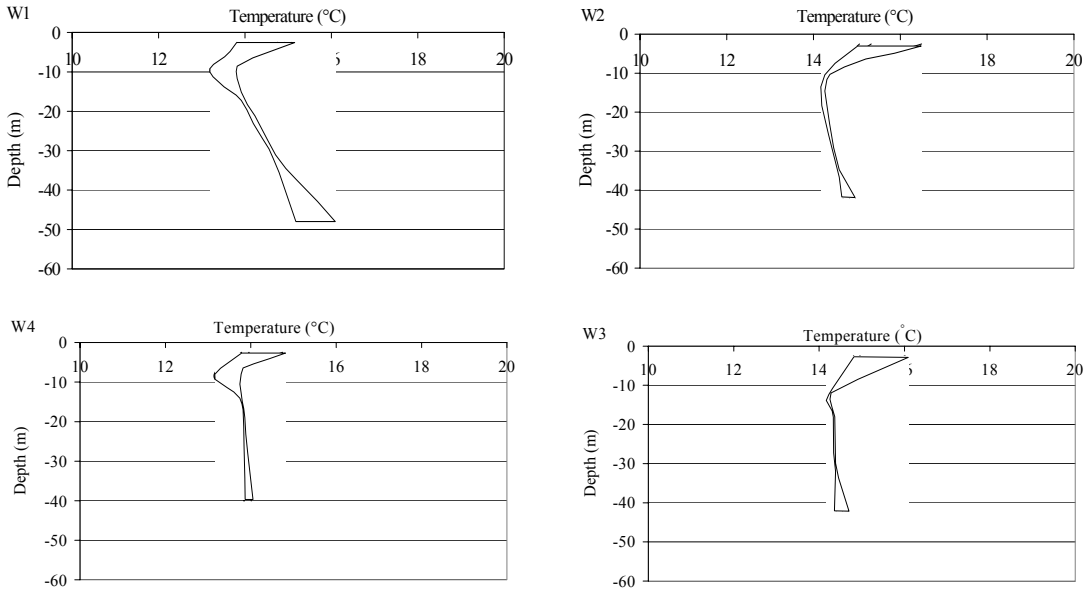

Fig. 4.6 Seasonal temperature change from May, 2007 to Feb, 2008.

Even though, Japan is located in one of the most active seismic and volcanic zones in the world, no evidence of volcanic activities has been reported in decades in the study area. The Sendai plain is located in a stable geological region: therefore, argument (2) can be rejected.

When considering the combined effects of possibilities (3) and (4), even though significant temperature fluctuations were experienced just below the water table (about 3 m from the ground surface), these fluctuations failed to continue below 15 m (Fig 4.6). Stallman (1965) proposed that heating and cooling of the land surface due to air temperature changes produces a temperature fluctuation on the ground surface and penetrates below the aquifer in various magnitudes at different depths by heat conduction and groundwater advection. The amplitude of temperature fluctuation attenuates with depth. Taniguchi (1994) followed this method to estimate the recharge rates in the Nara basin, Japan and observed the amplitude of groundwater temperature at shallow aquifer depths through seasonal changes. In his research, a maximum of 5.3 ^{0}C amplitude at 2 m depth was observed and there was insignificant change below depths of 15-20 m. In accordance with the past studies and observations of this research, it can be concluded that in the shallow aquifers, seasonal change in air temperature and the effects of surface water temperatures affect the subsurface temperature but do not continue below the depths of 15-20 m in the Sendai plain.

According to the observations of JODC, the average sea water temperature at 50 m depth has increased about 6.2 ^{0}C from May, to November 2007. Therefore, the most

reasonable explanation for the increase in water temperature below the depth 40 m is possibility (1).

For the case of temperature depth profiles' deviations from the general geothermal gradient (category b), Uchida and Hayashi (2005) observed very low (≤ 1.5 ^{0}C/100 m) general geothermal gradient in the Sendai plain for depths of 0-60 m. In this study, the concave shape of the temperature-depth profiles near to the ground surface (0-15 m) largely results from ground surface temperature change and infiltrating water flux in recharge area. However, the deviation from general geothermal gradient below the depth of 20 m includes not only groundwater recharge but also some other factors as well.

Annual mean air temperature in the Sendai plain has increased about 1.71 ^{0}C during the last 80 years. The magnitude of global warming is about 0.5 ^{0}C/100 years (Huang et al., 2000). Therefore, the increased air temperature in Sendai includes not only global warming, but also the effects of urbanization. Even though, these figures represent the change of air temperature, and not the ground surface temperature, surface temperature usually changes similarly to the air temperature. Signatures of the combined effects of global warming and urban heat island are preserved in subsurface thermal regime and have been used in many studies to understand the anthropogenic effects on an aquifer thermal regime (Ferguson and Woodbury, 2004; Bodri and Cermak, 1999). Taniguchi et al. (2005) estimate the urbanization effect on subsurface temperature in Tokyo, Osaka and Nagoya in Japan and suggest that the depth apart from the thermal gradient may show differences in the history of urbanization in the cities. Therefore, one possible reason for the deviation in the temperature depth profiles from the general thermal gradient might be the wide development and urbanization in last few decades on the Sendai plain.

The periodic rise and fall of the tide water stage in the ocean produces sinusoidal groundwater level fluctuations in adjacent inland aquifers. The effect is most noticeable when observation wells are close to the coast, and as the distance from the coast increases, tidal influence decreases. On the Sendai plain, evidence of tidal effects on groundwater level fluctuation was clearly noticeable at deep aquifer depths (sub-wells 3 in Fig. 3.4). Seawater temperature is different than the groundwater temperature and mixing of the fresh groundwater and seawater due to the tidal effect alters the aquifer thermal regime below certain depths. Therefore, the one other possible cause, which alters the temperature-depth profiles from geothermal gradient, might be the tidal effect. Therefore, the heat transport model developed in section 4.1.2 was used to incorporating the advection effects of the tidal water in temperature distribution in Sendai plain.

4.4 Model verification with field observations

To estimate the appropriate value for β from the Eq. (4.21), it is necessary to find the parameter *a* from the field observed water level data. Amplitudes of water level fluctuation in observation wells decreased with increasing distance from the coast. Fig. 4.7 shows the plots of ln (amplitude at *x*) versus *x* at water level observation wells (in the deepest sub-wells).

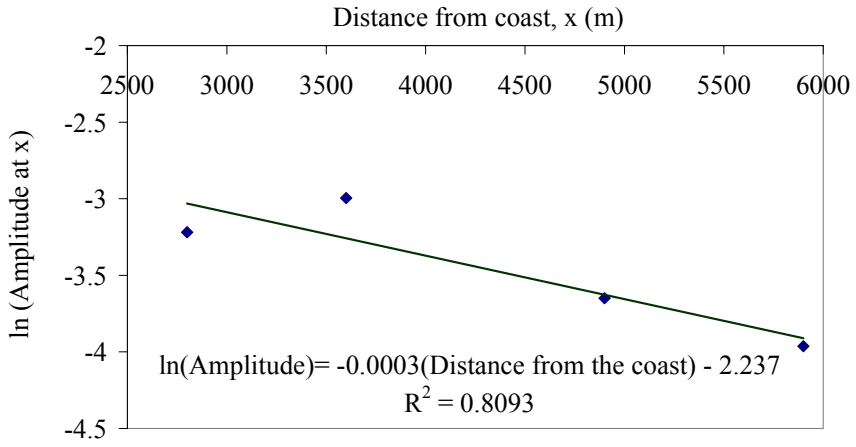

Fig. 4.7 Estimate *a* from water level amplitudes.

The gradient of the regression line (0.0003) obtained by the least-squares method gave the approximate value for the amplitude decay in the Sendai plain. The wave number calculated from the phase lags (0.00039-0.00047 in Table 4.1) also gives a reasonable match with the damping results. The coastal line was considered as the left hand side boundary (LHS) and W4, which is the most distant observation well, was taken as the right hand side (RHS) boundary. Therefore, *L* was estimated to be 5900 m. Monthly averaged sea water temperature from May to August at 50 m depth from sea surface was taken as the representative temperature for T_0 (19.5 ^{0}C). An appropriate value was estimated for T_L (14 ^{0}C) based on the observed 1-hr temperature records. These values were applied in Eq. (4.21) to find the unknown value of the temperature decay coefficient (β=-4.1).

The calculated value of β was substituted in Eqs. (4.18) and (4.19) to find the unknown parameters in Eq. (4.4). The accuracy of the estimated β value was verified by matching the simulated and observed temperature records (Fig. 4.8).

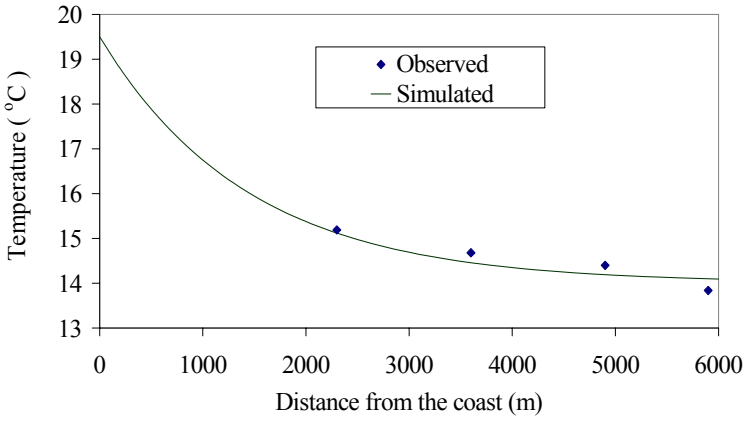

Fig.4.8 Verification of simulated results.

Simulated results showed good agreement with the observed temperature records. The residual temperature (RT), which is the difference between the observed temperature and the simulated temperature at an observation well, also was calculated. As can be seen from the Fig. 4.8, RT is low near to the coast (0.1 ^{0}C at W1) and it increases with the distance away from the coast (0.3 ^{0}C at W4). These results confirmed that tidal effects at the ocean significantly contribute to the temperature distribution at the deeper depth in coastal aquifers and the influence of tides decreases as the distance from the coast increases.

According to Eq. (4.21), the accuracy of the determined value β depends on the degree of accuracy to which *a* can be resolved from the field data. Water level records at the observation wells were measured automatically and the possible recording errors were minimal. The other factor which governs the accuracy of *a* was the distance to the observation well from the coast (*x*) which also can be measured with an accuracy of ± 100 m by the Global Positioning Systems (GPS). The maximum change of RT for 100 m change of *x* was about 0.035 ^{0}C in W1. Therefore, the error induced by calculating *a* was within the acceptable limit. Furthermore, simulated temperature records were sensitive to the recording errors of the temperatures at boundary conditions (T_0 and T_L). Increasing T_0 and T_L by 1 ^{0}C caused a maximum change of RT by 0.13 ^{0}C and 0.51 ^{0}C at W1. On the other hand, temperature change in sea water due to climate change or in fresh groundwater due to combined effects of climate change and urbanization may significantly affect the temperature balance in the transition zone, which will adversely affects coastal ecosystems. As an example for surface water bodies under changing climate, Battin et al. (2007) projected 20-40% of average decline in basin-wide spawning population with respect to 1.3-1.5 ^{0}C water temperature change. However, potential impacts of groundwater

temperature change have not been fully understand, and therefore, a methodology such as one presented in this study will be useful in integrated coastal ecosystem management programs.

4.5 Effect of hydro-geological properties on temperature distribution

The estimated value of β mainly depends on the wave number *a,* which is given by the aquifer parameters (*K*, θ and *D*) and the frequency of oscillation of tides (τ). In general, hydrogeologic parameters such as hydraulic conductivity and porosity vary significantly from site to site. Hydraulic conductivity ranges over many orders of magnitude (10^{0} to10^{-5} m/s) which cause a notable difference in temperature distribution by groundwater advection. When the hydraulic conductivity is high so that the temperature distribution by the ground water advection is dominant, β value is negatively small and the temperature distributes more gently through the porous medium (Fig. 4.9). On the other hand, when the hydraulic conductivity is low, it leads to a negatively high β value and has a significant effect on the temperature distribution within a short distance of the coast.

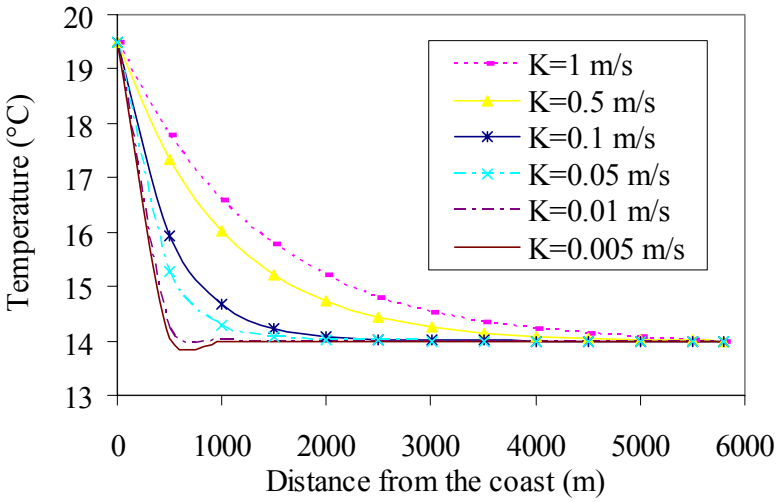

Fig. 4.9 Temperature distribution patterns with hydraulic conductivity

The other factor which governs the convective temperature distribution of the aquifer is the porosity. Porosity is the percentage of the total volume of soil that consists of pore space. The volume of void space through which a fluid can flow within a rock is often substantially less than suggested by its total porosity. Therefore, in groundwater hydrology, the term effective porosity is used which measures the volume of a soil or rock sample that consists of interconnected pore space available for fluid flow. In general effective porosity of porous medium changes over the range of 0.1 (clay and lime stone) to

0.35 (gravel and sand). To investigate the effect of effective porosity on the temperature distribution, the porosity was changed from 0.15 to 0.35. As depict in the Fig. 4.10, the temperature distribution is smoother when the effective porosity is low than when the porosity value is high. Under a specific hydraulic gradient, groundwater velocity is high so that the convective heat transfer is strong in the aquifers with small porosity values, and it is low in aquifers with high porosity values. However, as shown in the Fig. 4.9 and Fig. 4.10, a change in hydraulic conductivity has a more significant impact on temperature distribution than porosity.

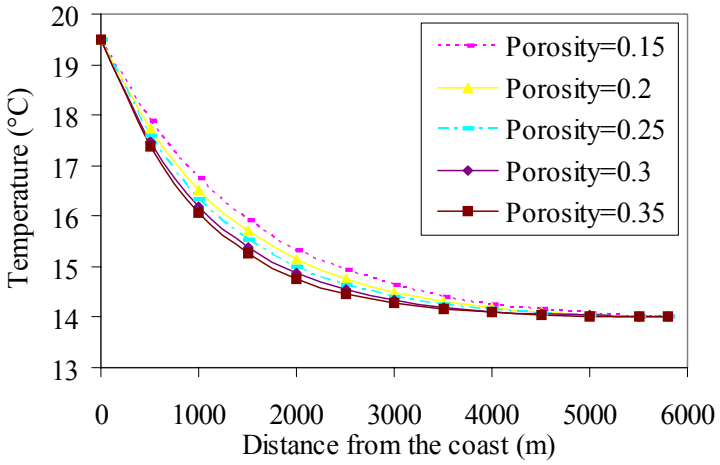

Fig. 4.10 Temperature distribution patterns with effective porosity

4.6 Probable effects of sea water and inland aquifer temperature change

Global warming inevitably increases the sea water temperature. The Intergovernmental Panel on Climate Change (IPCC) reveals that increases in sea temperature of 1-2 ^{o}C are expected by 2100 in response to enhanced atmospheric greenhouse gas concentrations (Bijlsma et al., 1995). On the other hand, combined effects of urbanization and climate change on groundwater recharge also cause significant changes in aquifer thermal regime. Higher temperatures, earlier snowmelt, and potential decreases in summer precipitation increase risk of drought. In addition, anthropogenic stresses, such as land use change and excessive groundwater pumping notably declines the groundwater table. Taniguchi (1995) estimated 2.35 ^{0}C of groundwater temperature change over the course of three decades due to excessive pumping in the Nara basin, Japan. Therefore, estimating the magnitude of temperature changes in the transition zone due to temperature change at the fresh water and sea water boundaries will be important for coastal environment management.

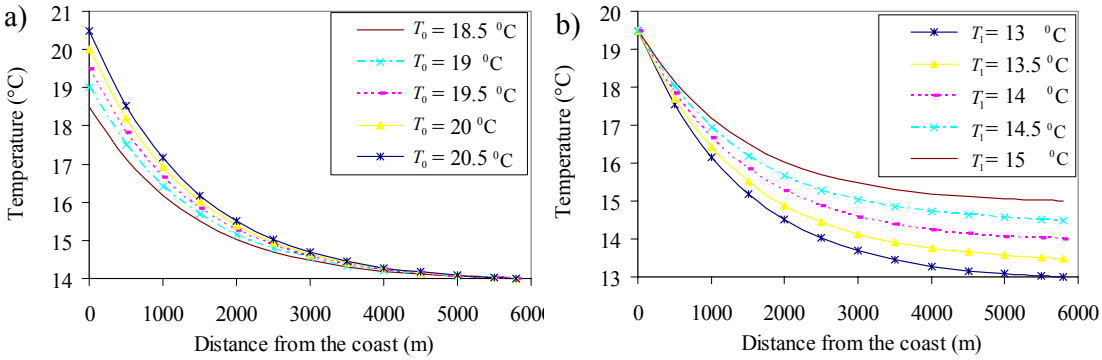

Fig. 4.11 Temperature change in transition zone due to temperature change at the boundaries; a) sea water and b) fresh water.

Fig. 4.11a represents the temperature distribution patterns for ± 1 ^{0}C change from present sea water temperature while the groundwater at the inland boundary remains constant. Fig. 4.11b shows the temperature distribution patterns for the same magnitude of temperature change at the inland fresh water boundary while the sea water temperature remains unchanged. When considering the potential effects of temperature change on coastal wetlands and the ponds, the temperature distribution within the range of the first 1000 m from the coast is most important. As depicted in Fig 4.11, sea water temperature change has a significant effect on groundwater temperature change nearer to the coast than the fresh water temperature change. This is because, within the transition zone, sea water has great influence near to the coastal boundary, while the fresh water effect is more robust near to the fresh water boundary. However, the combined effect of temperature change at the sea water and fresh water boundaries may significantly affect groundwater temperature change. For comparison, 1 ^{0}C temperature raise at the seaward margin (possibly due to global warming effects) and a 1 ^{0}C temperature fall at the inland boundary (due to the positive impact of reforestration as in Battin et al., 2007) will result in a 0.4 ^{0}C temperature raise at a distant 500 m away from the coast (area of coastal wetlands). Such estimations will be important for mitigating climate change impacts, where aquifer temperature increases due to sea water temperature rise would likely compensate by lowering inland boundary temperature under coastal environment management programs. Moreover, a 1 ^{0}C temperature rise at both boundaries will lead to a 1 ^{0}C temperature change within the entire zone. These figures may have significantly threaten the ecological balance of the coastal ecosystems.

4.7 Applicability of the developed methodology in general coastal aquifers

In terms of coastal ecosystem management perspectives under the adverse effects of urbanization and climate change, it will be important to propose a method to find the β value with different aquifer and tidal characteristics. Thus, Eq. (4.21) was considered with Eq. (4.10) in such a way that the β value can be determined based on specific site and tidal characteristics. A set of type curves were developed for a specific distance (L=2000m) as in Fig. 4.12. These type curves together with the proper observations at inland aquifer (T_L) and ocean (T_0) and appropriate hydrogeologic parameters (K, θ and D) will be important for accurate estimation of temperature distribution in coastal aquifers.

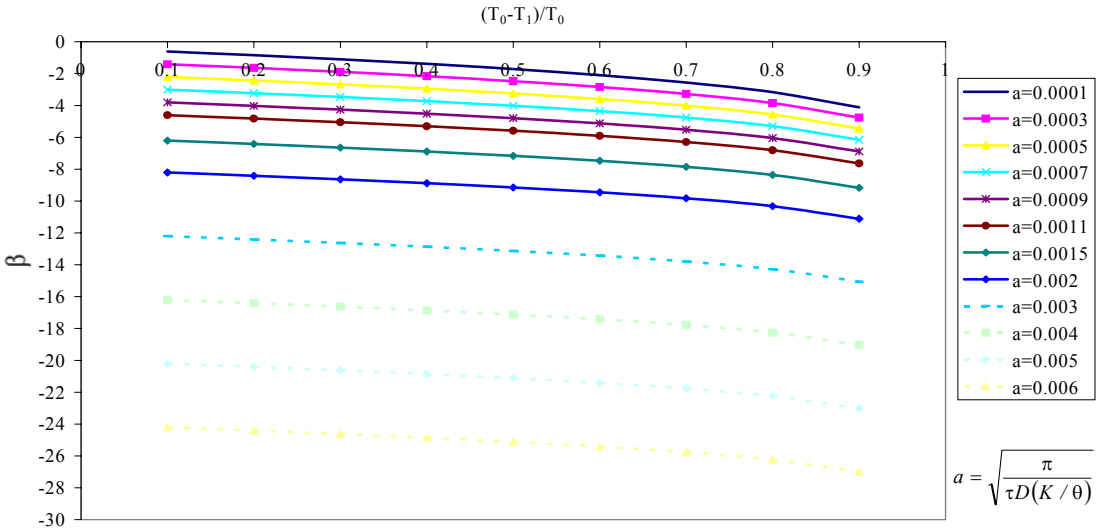

Fig. 4.12 Change in the temperature decay coefficient (β) with wave number (a)

As there are wide ranges of efforts to mitigate the anthropogenic effects on coastal environment, the method proposed in this study will be useful in terms of planning coastal ecosystem management programs. Even though, entire mitigation of climate impacts is extremely difficult or impossible, habitat restoration programs with proper forestall targets may offset the effects of climate change. Land-use practices, such as reforestation programs have the potential to decrease groundwater temperature in the aquifer by increasing shading (Battin et al. 2007). If the objective is to evaluate the long-term effects of urbanization and climate change on coastal environment or to monitor the success of habitat restoration programs in terms of temperature change, the installation of a minimum of one observation well will be adequate within the specified distance of this study (2000m). Approximate values of hydraulic conductivity (K), porosity (θ) and unconfined aquifer depth (D) can be determined from the excavated soil properties. Moreover, if the already installed observation wells are available, a new set of type curves can be

developed based on Eq. (4.21). In this case the value of L will be the horizontal distance to the most distant observation well from the coast and the observations of other wells can be used to verify the results.

4.8 Conclusions

Groundwater temperature change in coastal aquifers may have definite effects on fundamental ecological processes and the geographic distribution of aquatic species in groundwater dominated coastal wetlands, estuaries and ponds. This study was conducted to estimate the effect of seawater and groundwater temperature changes on coastal aquifers thermal regimes. A new analytical model and a set of type curves were developed to estimate the temperature distribution in the transition zone based on different aquifer and tidal characteristics.

The sensitivity analysis indicates that the model is highly sensitive for the hydraulic conductivity of the aquifer that directly relates with the heat transport by the groundwater advection. When the hydraulic conductivity of the porous medium is high (e.g. 1×10^{0} m/s), sea water flows in a grater distance from the coast, and the temperature distributes gently through the seawater and freshwater margins. However, if the hydraulic conductivity is low (e.g. 1×10^{-4} m/s), the tidal effect dissipates within a shorter distance from the coast and temperature falls very rapidly within a small distance.

The proposed model was applied in the Sendai plain where a good correlation was found between the tide and groundwater level fluctuations (maximum of 0.74). Significantly high correlation was obtained between the water level fluctuations at observation wells them self (maximum of 0.97). It was further observed that the tidal effect on groundwater level fluctuation and temperature distribution significantly decays as the distance from the coast increases. Verified results in the Sendai plain indicated that the individual effect of seawater temperature change has a profound effect on temperature change closer to the coast than a fresh groundwater temperature change. The combined effects of temperature change (possibly due to the effects of urbanization and climate change) at two boundaries within the range of $\pm1\ ^{0}$C will lead to a 0.4 to $1\ ^{0}$C temperature change in the vicinity of the coast (500 m away from the coast), where, in general, the coastal wetlands are located. These figures may be critical in terms of ecological balance.

The developed methodology is useful in areas with limited groundwater observation wells. It can be applied in coastal aquifers where the hydraulic conductivity ranges over many orders of magnitude. Furthermore, it will be important for coastal ecosystem management programs to evaluate the long-term effects of urbanization and climate change on the coastal environment.

CHAPTER 5

URBANIZATION AND CLIMATE CHANGE IMPACTS

Groundwater temperature is a key parameter regulating the ecological balance of groundwater-dominated ecosystems, such as wetlands, estuaries and ponds. Urbanization effects may adversely change the groundwater temperature (Taniguchi et al., 1999a; Taniguchi et al., 1999b; Reiter, 2007), which in turn affects for the fundamental ecological processes and the geographic distributions of aquatic species (Jones et al., 2006; Eaton and Scheller, 1996).

In recent studies, there have been several attempts to determine the combined effects of urbanization and past global warming on average deviations from steady state thermal profiles (Taniguchi, 2007; Majorowicz et al., 2006). However, it is difficult to discriminate between the effects of global climate change and heat loss from buildings in terms of possible causes for changes in the temperature profiles. Furthermore, little attention has been paid to the development of long-term groundwater temperature monitoring programs, especially in developing countries, because of the large initial investment and lack of data. Therefore, in this chapter, first, we aim to study the urbanization effect on local scale aquifer temperature change in the Sendai plain. For this objective, we will carefully analyze the convective effect of groundwater flow and the outcome of past ground surface warming that may have been caused by different levels of urbanization at the local scale and by global climate change to understand the impact of these factors on present aquifer temperature. In second, we will develop a set of type curves that can be used to test the accuracy of the estimates from the temperature–depth method. Considering the difficulty associates with obtaining enough observations to verify the estimates and the level of uncertainty in the temperature–depth profile method, these type curves are expected to be most useful in areas where limited hydrological data are available.

5.1 Evidences of urbanization and climate change impacts in the Sendai plain

Meteorological stations (Fig. 3.1a) that are operated by the Japanese Meteorological Agency (JMA) have the longest temperature records available for the region (since 1891 at Ishinomaki, Yamagata and Fukushima and since 1927 at Sendai and Morioka). These records indicate no significant trends until the middle of the 19th century. However, according to the records of the Sendai meteorological station, the annual mean temperature in the Sendai area has increased by about 1.8ºC from 1947 to 2007 with a rate

of 0.02ºC/year (Fig. 3.5). Sendai city experienced rapid development after the destruction of the Second World War, and became the economic center of the region. Fukushima and Yamagata cities, whose development took place during same time period and which have a similar level of urbanization as Sendai city, show similar magnitudes of air temperature change (0.017 and 0.018ºC/year, respectively) from 1947 to 2007. The areas of Morioka and Miyako are dominated by mountains and agricultural lands that exhibit a significantly low rate of temperature rise (0.011 and 0.005ºC/year, respectively) from 1947 to 2007. In contrast to temperature, annual precipitation in the Sendai plain shows no strong trend over the last 80 years (Fig. 3.5).

Some significant differences in land use types exist at the local scale surrounding the wells. When selecting the representative land use types, the predominant category in the 10, 000 m^2 surrounding the well was chosen. Wells W2, W3 and W4 are located in paddy field areas and have similar surface characteristics and land use histories. Well W1 is located in a residential area that is partially covered with home gardens and vegetation. However, the unpaved area surrounding W1 is significantly smaller than in the areas surrounding W2, W3 and W4. Well W5 is located at the city center, which is more urbanized than all other well locations (Fig. 3.2). All well locations are situated within seven kilometers of the city center and the Sendai meteorological station.

Background temperature in the aquifer is higher than the annual average air temperature, giving an upward heat flow from the interior of the earth. Under steady state heat conduction, this produces a linear geothermal gradient within homogeneous depth intervals. However, in all wells, there is clear evidence of a temperature profile inversion from the general geothermal gradient. The magnitude of ground surface warming, which was calculated as the difference between the observed subsurface temperature profile and the extrapolated steady state linear curve to the ground surface, ranges from spans 0.9–1.3ºC. The depth of departure from the general geothermal gradient is different in each well, which may indicate local variations in the magnitude of surface warming and groundwater recharge. Starting from the bottom of the temperature-depth (T–D) profile of each well, the first point that deviated from the general geothermal gradient by 0.1ºC was designated as the representative depth of departure from steady state heat conduction (Taniguchi, 2006). Well W5 shows the greatest depth of departure (60±1 m), followed by W1 (52±1 m). Wells W2, W3 and W4 exhibit similar depths of departure (38±1 m, 40±1 m and 42±1 m, respectively), reflecting their similar site conditions.

5.2 Analytical modeling

Temperature distribution in one-dimensional homogeneous porous media with constant incompressible fluid flow can be described as

$$\alpha\left(\partial^2 T/\partial z^2\right)-\beta\left(\partial T/\partial z\right)=\partial T/\partial t\,, \tag{5.1}$$

where T is temperature, z is depth from the ground surface, t is time, α (= $k/c\rho$) is the thermal diffusivity of the aquifer and $\beta = vc_0\rho_0/c\rho$, where v is the vertical groundwater flux (positive is downward), $c_0\rho_0$ is the heat capacity of the water and $c\rho$ is the heat capacity of the porous medium. Assuming that the heat capacity is constant and that the groundwater and aquifer are in thermal equilibrium, the initial boundary conditions for a linear increase in ground surface temperature can be written as

$$T_{(z,0)} = T_0 + az \tag{5.2}$$

$$T_{(0,t)} = T_0 + bt\,, \tag{5.3}$$

where T_0 is the ground surface temperature at $t = 0$, a is the general thermal gradient, and b is the rate of surface warming. Under the above initial boundary conditions, Carslaw and Jaeger (1959) obtained an analytical solution for the temperature distribution as a function of depth and time:

$$T = T_0 + a\left(z-\beta t\right)+\left\{\left(b+\beta a\right)/2\beta\right\}\times$$
$$\left[\left(z+\beta t\right)\exp\left(\beta z/\alpha\right)\mathrm{erfc}\left\{\left(z+\beta t\right)/2\left(\alpha t\right)^{1/2}\right\}+\left(\beta t-z\right)\mathrm{erfc}\left\{\left(z-\beta t\right)/2\left(\alpha t\right)^{1/2}\right\}\right]\,. \tag{5.4}$$

In the absence of convective heat flow, steady state heat conduction produces a linear T–D profile within homogeneous aquifer depth intervals. Deviations from the steady state can be caused by both transient GST change and groundwater recharge or discharge. According to the two–dimensional steady state groundwater and heat flow analysis of Domenico and Palciauskas (1973), the temperature depth profile is concave with infiltrating water flux in the recharge area, while the profile is convex with upward water flux in the discharge area. This phenomenon has been used in many studies to estimate subsurface groundwater flow (Ferguson et al., 2003; Taniguchi et al., 2003). With the presence of a cooling (Pollack and Huang, 1998) or warming trend (Huang et al., 2000) at the ground surface, the curvature of the T–D profile is altered accordingly, making it difficult to discriminate the individual effects of groundwater flow and diffusion of transient GST change. Nevertheless, the starting time of GST change (t in Eq. 5.3) must

be carefully selected, as it may have a significant impact on the curvature of the T–D profile that may mislead the estimation of groundwater flow (v).

5.3 Preliminary analysis for parameter calibrations

The undisturbed depths of the aquifer (e.g., below 60 m at W5) exhibit an approximately linear T–D profile. Extrapolation of this linear portion to the ground surface yields the intercept temperature (T_0) (Majorowicz et al., 2006). If thermal conductivity is assumed to be uniform over the representative depth interval, the general geothermal gradient (a) can be estimated from the gradient of the undisturbed portion of the T–D profile. Therefore, the parameters a and T_0 in Eq. 5.4 can be estimated with reasonable accuracy (±0.002ºC /m, ± 0.1ºC, respectively) from the estimated T–D profile in each observation well. A series of synthetic T–D profiles over different values of b, t and v can then be formulated and compared with the observed T–D profile in the Sendai plain for a preliminary approximation of the parameters in Eq. 4.

All parameter values of the porous medium ($\alpha = 5.8 \times 10^{-7}$ m^2 s^{-1}, $c = 930$ J kg^{-1} ºC^{-1}, and $\rho = 2500$ kg m^{-3}) were assigned based on values previously determined by Uchida and Hayashi (2005) in the Sendai plain. The specific heat and density of water were assumed to be 4.18×10^3 J kg^{-1} ºC^{-1} and 10^3 kg m^{-3}, respectively. The seasonal change in ground surface temperature has a strong influence on groundwater temperature just below the water table. However, the amplitude of temperature oscillation attenuates with depth (Stallman, 1965). In general, seasonal oscillations do not have a significant effect at depths below 15–20 m (Taniguchi, 1994). Long-term hourly temperature observations (from May, 2007 to February, 2008) in the Sendai plain, taken at different aquifer depths in W1–W4, show that seasonal GST change has no effect at depths below 12 m. Therefore, the T–D profiles below 12 m can be used for long–term analysis (Taniguchi et al., 2003).

Fig. 5.1a shows the temperature distribution patterns when t remains constant (60 years). If groundwater recharge is considered to be the sole parameter for groundwater temperature change ($v = 200$ and $b = 0$ curve in Fig. 5.1a), it fails to explain the observed temperature increase above a depth of 40 m, especially near the ground surface. This is because recharge water flow carries cool water down from the ground surface; as time passes, temperature at a particular depth gradually decreases. Therefore, there must have been some level of ground surface warming during the considered time period to account for the observed T–D profile. Another interesting observation is that, when comparing two recharge rates, the magnitude of the decrease in aquifer temperature due to cool water infiltration increases as the depth from the ground surface increases. In contrast, when b is increased with other parameters held constant (Fig. 5.1c), temperature change is greater

near the ground surface and decreases as depth increases. Therefore, when t is constrained to an appropriate value, these phenomena can be used for parameter calibration.

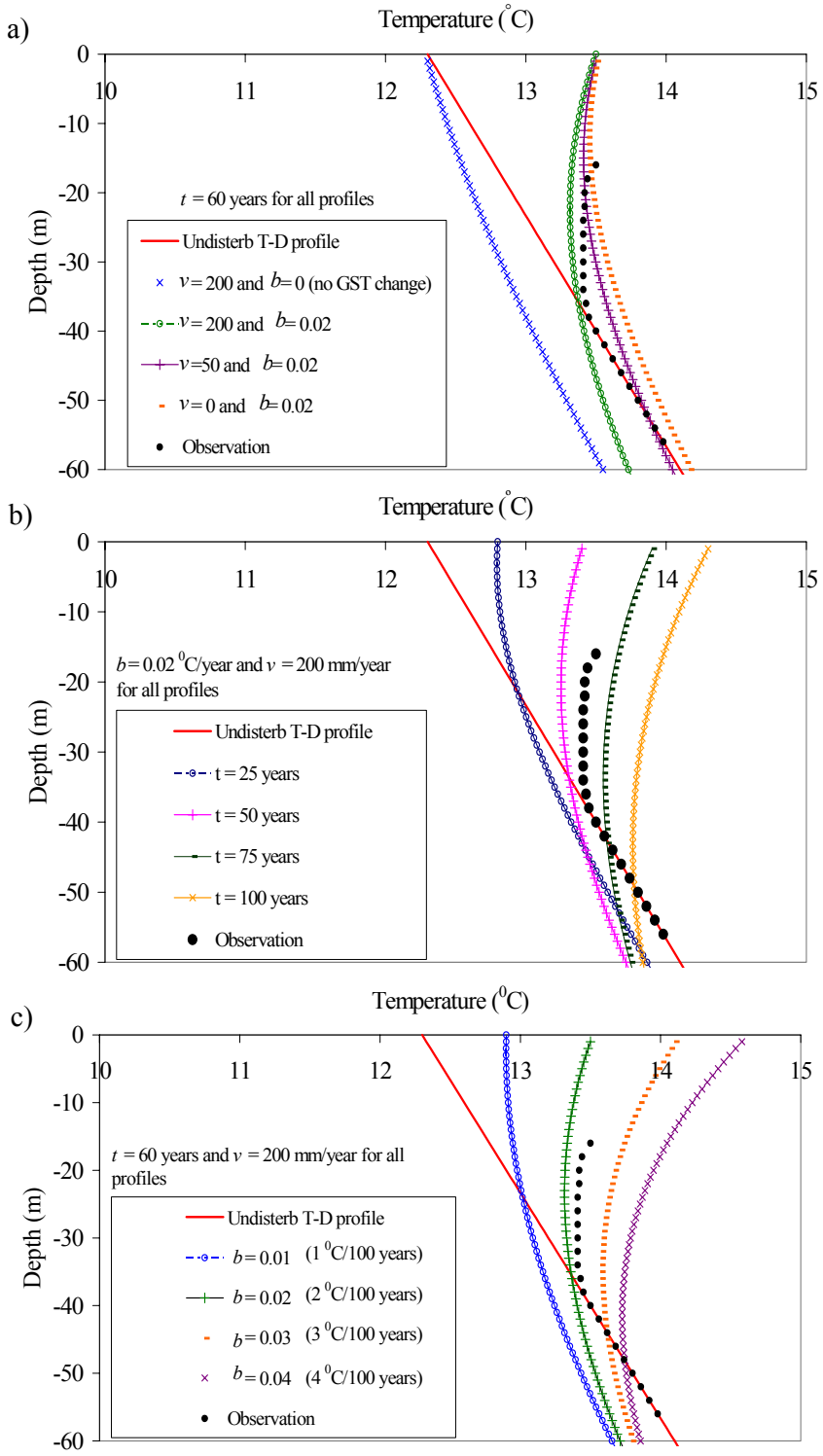

Fig. 5.1 Synthetic temperature–depth profiles

Fig. 5.1b) shows the T–D profile change over time when v and b are held constant. The groundwater recharge rate was selected based on other studies that have estimated groundwater recharge to range from 100–480 mm/year in different catchments in Japan (Taniguchi et al., 2003; Uchida and Hayashi, 2005; Taniguchi et al., 1999a). Several studies have found that, over the long term, SAT change primarily drives GST change (Baker and Ruschy, 1993; Putnam and Chapman, 1996; Majorowicz and Skinner, 1997). Many studies have considered this to be a direct relationship (Ferguson et al., 2003; Ferguson and Woodbury, 2005; Taniguchi et al., 1999a). However, this direct relationship between SAT and GST was questioned by Mann and Schmidt (2003), who examined the effect of seasonal snow cover change on GST change. In that study, SAT was found to explain only half of the variance in GST during the cold season. At the same time, SAT was determined to be the dominant parameter influencing GST during the warm season. In our study area, there are no records of permanent snow cover during the study period. Moreover, snow does not remain long enough to penetrate cold water to deeper aquifer depths. Therefore, the effect of snow cover change can be neglected for our long-term study. In the Sendai plain, SAT has increased at a rate of 0.02ºC/year during the last 60 years (Fig. 3.5). Therefore, the same magnitude of GST warming was assigned for the preliminary analysis. This parameter was later adjusted for local conditions based on the observed T–D profile at each observation well. The disturbed portion of the observed T–D profile in Fig. 5.1b) lies between the t = 50 and t = 75 years curves. The curves corresponding to t = 25 and t = 100 years can be rejected, even if v and b depart from their assigned values, due to the large differences in temperature (more than ± 1ºC) from the observed T–D profile. According to the records of the Sendai meteorological station, SAT shows almost no trend in the area from 1927 to 1947. Moreover, other meteorological stations in the region, such as Ishinomaki and Yamagata, also show stable patterns over 56 years (1891–1947). Therefore, in this analysis, t was set to 60 years (1947–2007).

The remaining two parameters, v and b, are critically important for the simulation of T–D profiles and their comparison with the observed records, because both parameters change the curvature of the T–D profile. Therefore, it is possible to have several combinations of v and b for an observed T–D profile. However, in addition to the curvature, other properties of the T–D profile and the observed water level records at different aquifer depths can be used as evidence to compare the differences between the T–D profiles of the observation wells and to select parameter values. According to Darcy's Law, a strong hydraulic gradient represents substantial water flow. Therefore, when a pre–calibrated value is available for the groundwater recharge (v) in the catchment (e.g., based on water budget technique) and if the aquifer is fairly homogeneous, different hydraulic gradients can be used to explain the diverse recharge rates and curvatures of the

T–D profiles in different observation wells. Moreover, the depth of departure from the general thermal gradient of the aquifer is also a useful indicator to estimate *b* within a range. If ground water recharge is reasonably similar, a greater depth of departure from a linear T-D relationship represents a greater degree of ground surface warming (*b*) at the local scale. These differences in *b* between the observation wells may be attributed to the degree of urbanization at each location. When these two criteria are considered, the curvature of the observed T–D profile can be matched with the simulated T–D profiles based on Eq. 5.4. As illustrated in Fig. 5.1a and c, GST warming has a profound effect in the shallow sub-surface layer during a given time period, while groundwater recharge has a significant effect on the curvature at deep aquifer depths. This phenomenon can be used as a final consideration to match the simulated T–D profile with the observed temperature records.

5.4 Model verification with field observations

A series of *b* and *v* parameters were considered to produce temperature profiles based on Equation 4 and matched with the observed T–D profiles in different locations. As previously described, T_0 and *a* were estimated from the linear portion of the T–D profile in each observation well. The parameter *t* was considered to be 60 years. Simulated results with constrained parameters are shown in Fig. 5.2 and Table 5.1.

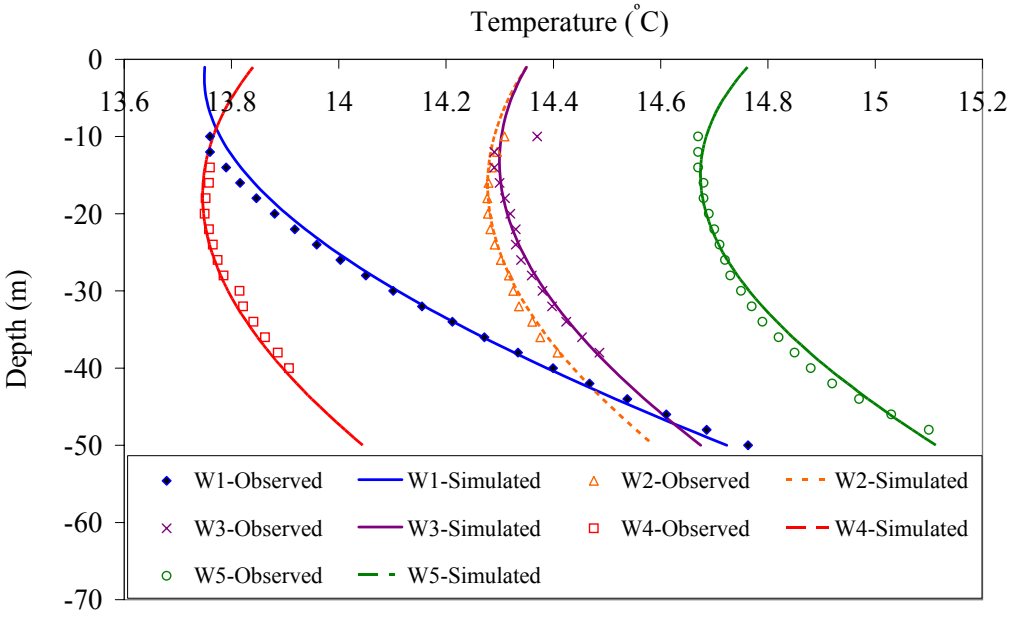

Fig. 5.2 Observed and simulated T-D profiles

Table 5.1 Physical observations and constrained parameters at different well locations.

Well	Land-use type	Time averaged hydraulic gradient (m/m)	Depth of departure from general geothermal gradient (m)	T_0 (^{O}C)	a (^{O}C/m)	v (mm/ year)	b (^{O}C/ year)
W1	Residential	0.077	52	12.60	0.047	105	0.0195
W2	Agricultural	0.169	38	13.45	0.030	215	0.0150
W3	Agricultural	-	40	13.45	0.029	170	0.0150
W4	Agricultural	0.148	42	12.85	0.029	180	0.0165
W5	Commercial	-	60	13.70	0.033	130	0.0210

Estimates of b and v are reasonably consistent with the level of urbanization, the observed hydraulic gradient and the depth of departure from the steady state profile at each location. The highest GST warming rate was found for W5, followed by W1. W2, W3 and W4 show similar warming rates, which are noticeably less than those of W5 and W1. These values closely match the observed depths of each observation well that deviate from the general geothermal gradient. In other words, large b values indicate higher levels of urbanization at a given location. W2, W3 and W4 are located in agricultural areas that are expected to have less GST warming than residential (W1) or urban commercial (W5) areas. Therefore, if it is assumed that the level of global warming is uniform over the region, then differences in representative b values may represent differences in the level of urbanization around each well location. Moreover, estimated recharge rates for W1, W2, and W4 agree well with their differences in observed hydraulic gradients. However, the estimated recharge rate for W5 is somewhat larger than that of W1, which shows some disagreement with their land–use types. There are two possible reasons for this behavior. First, the accuracy of the T–D profile method may not be adequate to distinguish small differences in recharge due to various uncertainties in parameter estimates. Second, the geology and land cover near an observation well may be different than the major land-use category surrounding the well. Nevertheless, the significant difference in magnitude (110 mm/year) between W1 and W2 may reasonably represent the influence of land cover type on groundwater recharge. Moreover, considering the level of uncertainty of various methods (Scanlon et al., 2002; Ferguson and Woodbury, 2005), recharge estimates from the T–D profile method will be tested with the range of recharge rates calculated from other techniques.

5.5 Model verification with groundwater recharge estimated by other techniques

In addition to the T–D profile technique; many other methods to estimate groundwater recharge exist, such as the water budget technique, Darcy's method and the water table fluctuation (WTF) method. However, all of these methods suffer from uncertainty in accurately estimating the aquifer parameters, such as hydraulic conductivity and specific yield. This may cause substantial errors in the resulting estimates (Healy and Cook, 2002). Scanlon et al. (2002) have suggested that errors in estimating groundwater recharge by Darcy's law can be one order of magnitude or more, while the water budget technique is somewhat more accurate. Ferguson and Woodbury (2005) have also observed that the accuracy of recharge estimates from T–D profiles is within one order of magnitude. Therefore, we estimated groundwater recharge using three methods to compare with the estimates obtained from the T–D profiles. The water budget technique is discussed in detail below along with the description to use it in general application.

5.5.1 *Water budget technique*

For a given region, precipitation and temperature (i.e., potential evapotranspiration) primarily govern annual mean evapotranspiration and runoff rates. In arid or semi–arid regions, potential evapotranspiration is greater than precipitation, which results in high evapotranspiration and less runoff. Similarly, if potential evaporation rates are fairly low, then for a given amount of precipitation, runoff is likely to exceed evapotranspiration. Furthermore, runoff and groundwater recharge are greatly influenced by soil type and land cover. Runoff in urban areas with sealed surfaces is grater than in areas with strong vegetation. The groundwater recharge rate is higher in watersheds that have soils with high infiltration rates (sands and gravels) than in watersheds with predominately silt and clay soils, which generally have low infiltration rates. Under these circumstances, the concept of water balance provides a framework for estimating groundwater recharge and corresponding temperature distributions at different sites and under different climatic conditions. The simple water budget for any catchment can be written as

$$P - ET = R + RO\,, \tag{5.5}$$

where P is precipitation, ET is evapotranspiration, R is groundwater recharge and RO is surface runoff.

Surface runoff estimation

Surface runoff occurs when the precipitation rate is higher than the infiltration rate. Soil and land cover types have a strong influence on the amount of surface runoff in a given area. Surface runoff in an urban area with sealed surfaces is greater than in areas with more vegetation. Soil types with well-drained capacity (sand and gravel) have high infiltration rates and therefore, less surface runoff. In contrast, clay soil has low infiltration rates and therefore, enhances the surface runoff.

The Soil Conservation Service Curve Number (SCS–CN) method developed by the United States Department of Agriculture (USDA) is a simple, widely used (Randhir and Hawes, 2009; Kipkorir et al., 2002; Steenhuis et al., 1995) and efficient method for determining runoff. The curve number (CN) is a particular value assigned to a specific watershed based on soil group, type of land cover, and degree of saturation. The surface runoff is directly estimated from the CN value, and the precipitation depth is estimated by reading the set of type–curves developed based on the empirical relationships (Eqs. 5.6 and 5.7). This method is not dependent upon the duration or intensity of rainfall; only the volume of rainfall is considered. According to the standard SCS–CN method, with precipitation P, surface runoff (RO) can be estimated as

$$RO = (P - 0.2S)^2 / (P + 0.8S), \tag{5.6}$$

where S is the potential maximum retention after runoff begins. The potential maximum retention is determined by the CN value and therefore varies with different soil groups and land cover types.

$$S = (1000 / CN) - 10, \tag{5.7}$$

where S, P and RO are measured in inches. CN differs depending on the hydraulic soil group, land cover type and antecedent moisture condition (AMC). The soil hydraulic groups are divided into four categories, A, B, C and D, in order from the greatest infiltration capacity to the least. Soils in category A have low runoff potential, and water is transmitted freely through the soil. Soils in categories B and C have moderately low and moderately high runoff potential, respectively. Soils in Category D are a strong barrier to water movement through the soil and have high runoff potential. Saturated hydraulic conductivity (SHC) of the least transmissive layer between the ground surface and the 50 centimeter range varies from among soil types A, B, C and D as follows: A > 4×10^{-5}, $4\times10^{-5} \le$ B < 1×10^{-5}, $1\times10^{-5} \le$ C < 1×10^{-6}, and D ≤ 1×10^{-6}. The AMC value represents the degree of saturation of a particular soil type: AMCI for dry conditions, AMCII for average

conditions and AMCIII for wet conditions. CN tables from the National Engineering Handbook (USDA, 1972) present the corresponding CN values for different land use categories such as agricultural, forest, urban and residential.

We used available GIS data and land use maps to classify the different land use groups. Soil hydraulic groups were identified based on a geological survey and previous borehole results. AMCII was selected to represent the moderate soil moisture conditions in the Sendai plain (Water Environmental Map No. 1, Geological Survey of Japan).

Evapotranspiration

Evapotranspiration is one of the primary processes of water transfer in the hydrological cycle. Therefore, accurate estimation of evapotranspiration is of great importance for groundwater recharge estimation. There are many well established methods to estimate potential evapotranspiration, such as the water budget, mass–transfer, combination, radiation and temperature based methods. The Penman Monteith (PM) equation is known to provide a very accurate estimate of potential evapotranspiration and is widely used to calculate the short-term evapotranspiration rate in agricultural water demand estimation. However, the wide range of data required for these methods makes it difficult to implement them in areas where limited meteorological information is available. Temperature based methods give reasonably accurate results (Tsutsumi et al., 2004) for annual water budget estimation based on mean monthly temperatures. Our study focuses on long–term anthropogenic effects on groundwater recharge and the associated thermal regimes; therefore, temperature based evapotranspiration estimation is expected to provide reasonably accurate annual recharge estimates. We chose the SCS Blaney Criddle method (Shuttleworth, 1992), a widely used temperature–based method. This method estimates potential evapotranspiration in terms of the measured temperature and daily percentage of annual daytime hours.

$$ET_0 = K_t\left(T \times p/100\right) \tag{5.8}$$

$$K_t = 0.0173T - 0.314\,, \tag{5.9}$$

where ET_0 is the monthly potential evapotranspiration (inches), T is the mean monthly temperature (ºF) and p is the daily percentage of annual daytime hours during the month. In water budget calculations, actual evaporation is the decisive parameter that, under natural conditions, is determined largely by vegetation, climatic conditions and soil conditions. The Bagrov relationship estimates actual evapotranspiration from precipitation and potential evaporation and is also modified by the storage properties of the evaporative

zones. Storage properties in a location are particularly influenced by land use and soil types. Forests and agricultural land have more storage capacity than sealed surfaces in urban areas, and the greater binding capacity of the soil enhances its storage capacity. Therefore, we used the effectivity parameters based on the Bagrov relationship (Glugla and Krahe, 1995; Glugla and Muller, 1997) to account for the effect of climatic conditions and land use types on actual evapotranspiration rates.

If the surface runoff and actual evapotranspiration in Eq. (5.5) are estimated using the proposed methods, the resulting recharge rate automatically accounts for the effects of land cover type and soil characteristics in a particular catchment. In the estimation of surface runoff, monthly rainfall is assumed to occur as a single storm event in the particular month (Ranjan et al., 2006). The entire catchment was divided into six land use categories with a 250 m × 250 m grid size based on the GIS and land use map data. Furthermore, three soil types were considered based on the available geological maps (Water Environmental Map No. 1, Geological Survey of Japan) and previous borehole results. In summary, 18 subcategories (Table 5.2) were considered.

Table 5.2. Land-use categories

Land use category		Area (km^2)
Forest	coarse gravel and sand	136
	fine sand and silt	2.1
	clay	0
Agricultural	coarse gravel and sand	45
	fine sand and silt	42.5
	clay	14.6
Rural	coarse gravel and sand	37.4
	fine sand and silt	14.2
	clay	0
Low density housing	coarse gravel and sand	42.7
	fine sand and silt	8.6
	clay	15.7
High density housing	coarse gravel and sand	24.6
	fine sand and silt	8.4
	clay	11.9
Industrial	coarse gravel and sand	0.25
	fine sand and silt	3.1
	clay	1.7

Various CN values from the National Engineering Handbook (USDA, 1972) were assigned to each land use category to estimate the surface runoff. Actual evapotranspiration was found to be 690 mm/year, which is consistent with the findings of Tsutsumi et al. (2004) (519–624 mm/year). Summations of the monthly averaged evapotranspiration and runoff values within the year were used in Eq. (5.5) to estimate the

annual recharge. The spatially averaged recharge rate was estimated to be 135 mm/year for the Sendai plain. Changing the CN values (runoff estimation) and effective parameters (evapotranspiration estimation) by ±1–10% of their assigned value in various combinations results in recharge rate estimates ranging from 105–190 mm/year. Even the consistency of the estimated recharge rate is doubtful, due to various uncertainties (Healy and Cook, 2002); this estimate can be used as a primary value to discuss variations in recharge among the different locations with the available hydraulic gradients.

5.5.2 Water level fluctuation method

This method implicitly assumes that rising water levels in the observation wells are due to recharge water. In addition to water level records over a considerable time span, a reliable estimation of specific yield is required. Then, the recharge is calculated as

$$v = S_y \left[\frac{\Delta h}{\Delta t} \right] \tag{5.10}$$

where v is groundwater recharge, S_y is specific yield, h is water level height, and t is time. However, water level fluctuations are not always indicative of groundwater recharge and may be caused by other factors, such as evapotranspiration and local groundwater pumping. Therefore, water level measurements over short time periods are more important for the accuracy of the result. Moreover, water level records at a shallow sub–surface depth with sharp increases are more suitable for the analysis, because wetting fronts tend to disperse over long distances at deeper aquifer depths (Healy and Cook, 2002). We used the water level records measured at 1–hour intervals in SW1s (Table 3.1), which best illustrate the groundwater rise and fall over short time periods in the shallow subsurface layer (Fig. 5.3).

The parameter Δh was estimated from the difference between the peak of the rise and the low point of the extrapolated antecedent recession curve at the time of the peak (more details in Healy and Cook, 2002). Water level records from W4 were not used for the analysis, as the screen interval of W4 is considerably deeper than that of W1 and W2 (Table 3.1). Specific yield was considered to be 0.04 based on the effective porosity (0.2) given for the study area (Water Environmental Map No. 1, Geological Survey of Japan). Estimated recharge rates range from 120–190 mm/year in W1 and W2. Increasing and decreasing the specific yield by 10% of its original value results in estimated recharge rates ranging from 110–210 mm/year.

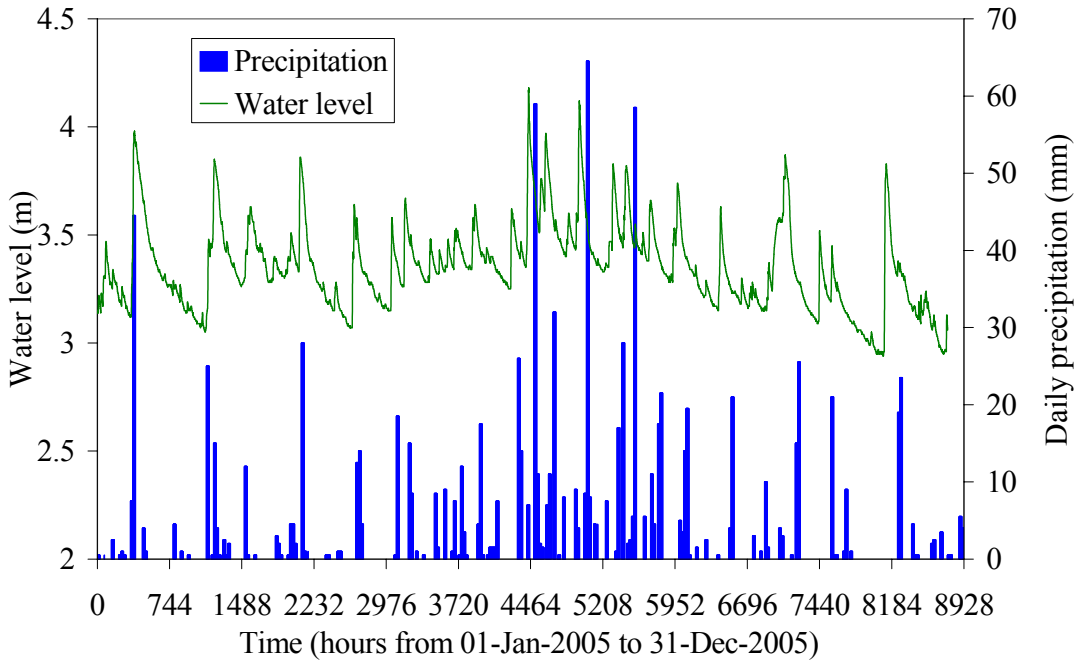

Fig. 5.3 Hourly water level records at W1–SW1

5.5.3. Darcy's law

The vertical recharge rate in the unsaturated zone can be expressed according to Darcy's law as

$$v = K_v\left[\frac{d(h+z)}{dz}\right] \tag{5.11}$$

where v is groundwater recharge, K_h is the appropriate vertical hydraulic conductivity, h is the water potential, and z is the height above the datum. The accuracy of recharge rates estimated using Darcy's law depends on the accuracy of the hydraulic conductivity and head-gradient measurements. In this study, hourly water levels at different aquifer depths were measured over three years and used to calculate the appropriate hydraulic head gradients. Sub–wells with different screen intervals and the sophisticated automated electronic technique of water level measurement guarantee the accuracy of the water head at a specific depth. However, uncertainty in the hydraulic conductivity estimate may have a significant impact on the calculated recharge rate.

Fig. 5.4a shows the monthly averaged water level gradients at different observation wells in May and July 2007. W2 and W4 have a higher hydraulic gradient (approximately two times higher) than W1. W2 and W4 are located in paddy field areas, while W1 is

located in a largely paved residential area. Therefore, W2 and W4 are expected to have higher hydraulic gradients and greater recharge rates than W1. However, recharge differences may be larger or smaller than hydraulic gradient differences, due to spatial variability in hydraulic conductivity. Using a vertical hydraulic conductivity of 4×10^{-8} ms^{-1} (2×10^{-4}–1×10^{-8} ms^{-1} in Uchida and Hayashi, 2005), the vertical hydraulic gradient needed to produce groundwater recharge of 135 mm/year (the estimate from the water budget technique) is about 0.107 m/m. This value is similar to the averaged hydraulic gradients in Fig. 5.4a. Therefore, estimated recharge rates from the observed hydraulic gradients range from 100-210 mm/year.

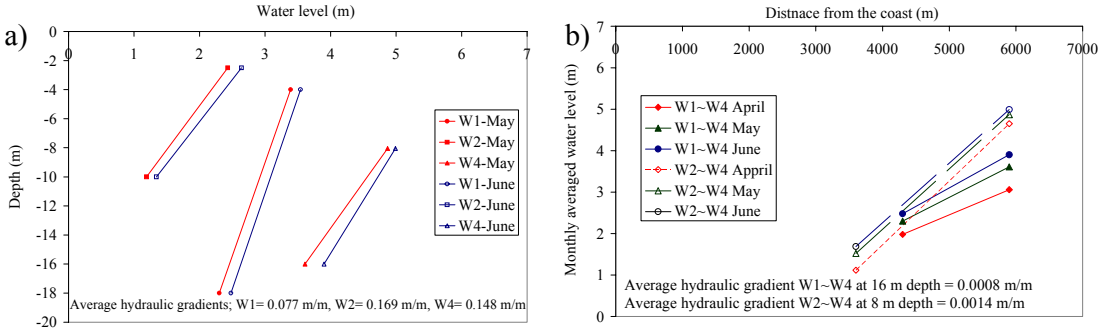

Fig. 5.4 Vertical and horizontal water level gradients

In addition to recharge rates, hydraulic gradients provide an important indication of the multidimensional groundwater flow in the area. In accordance with the findings of Lu and Ge (1996), Reiter (2001) and Bense and Beltrami (2007), horizontal water flow in a semi–confining aquifer can significantly affect the vertical temperature distribution in the basin. Therefore, the adequacy of a one-dimensional heat transport model must to be confirmed (e.g. Ferguson et al., 2003). However, the Sendai plain is experiencing transient surface temperature change, which in turn, alters the curvature of the T–D profile. Therefore, theoretical derivations by Lu and Ge (1996) and Reiter (2001), which are based on a steady state assumption, may not be applicable. In these circumstances, physical observations such as hydraulic gradients can be used as a surrogate to verify the applicability of a one-dimensional temperature distribution model. As shown in Fig. 5.4b, the averaged vertical hydraulic gradient is notably (120 times) higher than the averaged horizontal hydraulic gradient. Assuming anisotropy (horizontal to vertical hydraulic conductivity) of one order of magnitude, this still indicates greater vertical than horizontal water flow. Lu and Ge (1996) have proposed a dimensionless parameter that depends on the horizontal and vertical water velocities and temperature gradients. When this dimensionless parameter is less than 0.01, the relative error introduced by neglecting horizontal flow is less than 1%. In the present study, the averaged vertical temperature

gradient was higher by one order of magnitude than the averaged horizontal temperature gradient (Fig. 3.3), giving the dimensionless parameter a value less than 0.01. Even though, this value is not comparable with a transient boundary condition at the ground surface, differences of orders of magnitude between the horizontal and vertical hydraulic gradients and temperature gradients may confirm the adequacy of a one–dimensional heat transport equation in the Sendai plain.

Estimated groundwater recharge rates from T–D profiles (105–215 mm/year) are perfectly match with estimates from three other techniques (the water budget method, Darcy's method and the WLF method), which produced the groundwater recharge estimates in a consistent range (105–210 mm/year). Moreover, the constrained parameters of groundwater recharge and the rate of surface warming at different observation wells are consistent with the land use type and level of urbanization experienced in the past around each site. Therefore, we can assume that the constrained parameters reasonably match with the site conditions in the Sendai plain.

5.6 Past urbanization and climate change impacts on aquifer thermal regimes

Many studies indicate that in the second half of the 20th century, urban heat island and deforestation effects dominated the factors influencing steady state temperature distribution in aquifer thermal regime. Our study has also found clear evidence of SAT and GST warming over 60 years in the Sendai plain. SAT in the Sendai plain has increased at a rate of 0.020ºC/year (2ºC per hundred years). Observed T–D profiles indicate that GST has increased by 0.015–0.021ºC/year. However, separation of the individual effects of climate change and urbanization on GST warming is a subjective exercise. Hansen and Lebendeff (1987) analyzed global trends in air temperature change and found a 0.005–0.007ºC/year warming rate during the period of 1880–1985. Huang et al. (2000) also found similar results by investigating present-day T–D profiles in more than 600 boreholes throughout the world; these authors estimated approximately 0.5ºC of global warming over the 20th century. Following the above findings, Taniguchi (2006) assumed 0.006ºC/year of global warming to separate the effects of global warming and urbanization on surface warming in Bangkok, Thailand. In our study area, there is a clear difference in SAT warming between urban and rural areas. While highly urbanized areas, such as Sendai, exhibit a significant warming rate (0.02ºC/year), rural areas, like Miyako (Fig. 3.1b) and Fukaura (40° 38' 42"N, 139° 55' 54"E), show notably low warming trends (0.005 and 0.004ºC/year, respectively). If the urban heat island and global warming effects are considered to be the dominant factors of influencing aquifer temperature, then in the absence of major changes in land use, SAT warming in a rural area can be attributed to

global warming. Therefore, in accordance with past studies (Hansen and Lebendeff, 1987; Huang et al., 2000; Taniguchi, 2006) and long-term measurements from rural meteorological stations (e.g. Miyako and Fukaura), we assumed a 0.004ºC/year rate of global warming in the study area. If this value is assumed to be spatially uniform over the region, a 0.016ºC/year urban heat island effect is obtained for the Sendai area (difference between SAT warming and global warming).

5.7 Uncertainties of the estimations

Proper understanding of the past effects of urbanization and global warming on present aquifer temperature distributions are important in order to predict future changes in the aquifer thermal regime due to climate change. This study examined a combination of parameters among several possibilities in a preliminary analysis. When depth of departure from the steady state profile was used as the indicator with a reliable range of possible groundwater recharge and GST warming rates, the theoretically derived time (t=60 years) since the transient changes began was consistent with the time that the Sendai plain began to experience significant SAT warming. However, compared with the broad time scales that have been used to find signatures of past climate change from borehole records (e.g., five centuries in Huang et al., 2000), we analyzed a time history of only 1.2 centuries. This is mostly because of our poor knowledge about past climate change due to the absence of meteorological observations over the centuries. While some research has reported evidence of surface cooling (Pollack and Huang, 1998), other studies (Hansen and Lebendeff, 1987) have concluded that considerable global warming occurred in the past. Huang et al. (2000) have estimated a continuous GST warming trend over five centuries, with the largest temperature rise in the 20th century. Therefore, it is possible that the aquifer T–D profiles have been influenced to different degrees by climatic trends occurring before the observational period of this study. In addition to the influence of historical climate trends, the transient time period considered in this study may be subjected to variations at the very local scale surrounding the observation wells. However, land use maps and the Sendai city office data reveal that development throughout the area started around the same time in the middle of the 20th century. Nevertheless, all the observation wells are located within less than seven kilometers of the city center. Therefore, the timing of variations in GST that we selected in this study based upon our preliminary theoretical analysis and climatic observations may be appropriate for the all observation wells in the basin.

According to the constrained parameters in Table 5.1, rates of SAT and GST warming surrounding observation wells are slightly different. W1–W4 showed somewhat

lower GST warming rates than SAT changes, while W5 showed a somewhat higher warming rate. GST does not necessarily track SAT trends (Beltrami and Kellman, 2003, Schmidt et al., 2001) and can vary with site conditions such as albedo, vegetation, and other factors (Mann and Schmidt, 2003). Therefore, these differences may be attributed to the level of urbanization experienced at different locations.

5.8 Applicability of developed methodology in other catchments

From the perspective of ecosystem management under the influence of adverse anthropogenic effects, it will be important to propose a methodology to estimate long-term groundwater temperature changes under different site (soil and land cover types) and climatic (temperature and precipitation) conditions. As demonstrated in this study, reliable estimates of the timing of variation in GST can be made from historical climatic records, and the accuracy of the estimates can be checked against the observed T–D profiles (depth of departure from the general geothermal gradient), giving reasonable indications of the level of urbanization at the local scale. However, the remaining parameter of Equation 5.4, β (in terms of v), is critical for the accuracy of the results (Majorowicz et al., 2006). Therefore, the T–D profile method should not be used alone to estimate groundwater recharge (Ferguson and Woodbury, 2005). In such a case, the water balance method can be applied to test the accuracy of the estimated recharge rates.

The concept of an Aridity Index has been widely used in hydrological applications to account for spatial variations in temperature and precipitation in arid, semi–arid and humid regions (Arora, 2002; Trabucco et al., 2008). This index represents the degree of dryness of the climate at a given location. Among the variety of indexes that have been proposed (e.g. Budyko, 1958; Pike, 1964), we selected the modified version proposed by E. de Martonne in 1925 due to its simple data requirements (Oliver and Fairbridge, 1987). The aridity index (AI) is defined as

$$\mathrm{AI} = P / (T + 10) \tag{5.12}$$

where T and P are the mean annual temperature (ºC) and precipitation (mm), respectively, at a particular location. A set of type curves (Fig. 5.5) were developed based on Eq. (5.5) that give the relationship between the β value and AI for different soil types. Surface runoff and actual evapotranspiration were estimated using the methodology described in section 5.5.1. Several assumptions were made to simplify the solution for practical applications. For runoff estimation, monthly rainfall is considered to be uniformly distributed over the year and is assumed to occur in a single storm event in each month.

Similarly, for evapotranspiration estimation, mean monthly temperature is considered to be uniform over the year. Furthermore, based on the general pattern of changing percentage of monthly sunshine hours with latitude, the average daily percentage of annual daytime hours (p in Eq. 5.8) was used.

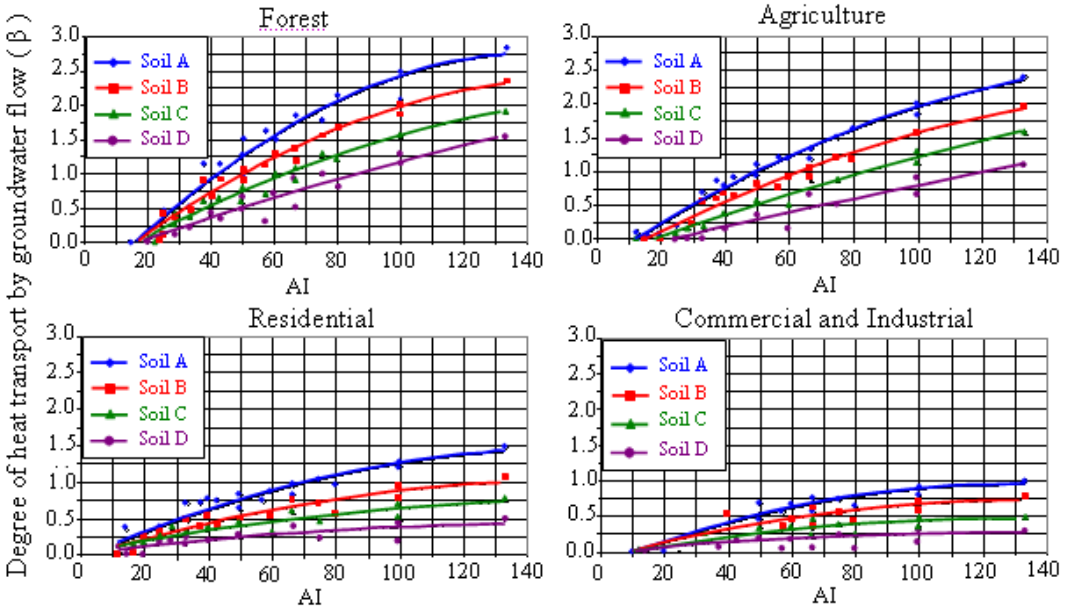

Fig.5.5 Degree of convective heat transport based on Aridity index

Table 5.3 Criteria for the selection of representative soil types (Source: USDA, 1972)

Soil property	Soil A	Soil B	Soil C	Soil D
Saturated hydraulic conductivity of the least transmissive layer	$>4.0\times10^{-5}$ m/s	$\leq4.0\times10^{-5}$ to $>1.0\times10^{-5}$ m/s	$\leq1.0\times10^{-5}$ to $>1.0\times10^{-6}$ m/s	$\leq1.0\times10^{-6}$ m/s
	and	and	and	and
Depth to water impermeable layer	0.5 to 1.0 m	0.5 to 1.0 m	0.5 to 1.0 m	< 0.5 m
	and	and	and	and
Depth to high water table	0.6 to 1.0 m	0.6 to 1.0 m	0.6 to 1.0 m	< 0.6 m

As AI is increases (more precipitation for a given temperature), actual evapotranspiration reaches the potential evapotranspiration (Bagrov relation). Moreover, for a given retention value, the rate of increasing surface runoff is greater with increasing precipitation (Equation 6). Therefore, when AI is high (particularly when AI > 60), even though more water enters the aquifer, the rate of water loss (due to evapotranspiration and runoff) from the system is greater than the rate of water entering the system. A similar phenomenon was observed in the Sendai plain under predicted future increases in precipitation and temperature. As a result, the rate of increasing groundwater recharge

decreases, and the shape of the relationship between β and AI is convex for all land use types.

In general, surface runoff is lower and groundwater recharge is higher in non-sealed areas, such as forested and agricultural areas; therefore, the β value is lower for a given AI value in sealed areas, such as commercial and industrial lands. Thus, if the other parameters (precipitation, rate of surface warming and thermal properties) are similar, the curvature of the T–D profile must be greater in non-sealed areas than in sealed areas. When considering the effect of different soil types (Table 5.3) for a given land use type, surface runoff is low and groundwater infiltration is high for the well drained soils (Soil types A and B), and therefore, the β value for a given AI is greatest for soil type A and lowest for soil type D in all land-use categories. This means that for the same land cover type, ground surface temperature, aquifer thermal properties and equal depth, the groundwater temperature will be higher in clay soils than in gravel or sandy soils.

The accuracy of the developed type curves was tested against the observed T–D profiles in the Sendai plain. W1 was excluded due to its lack of consistency with the examined land-use type. The hydraulic conductivity of the Sendai plain was considered to be homogeneous and less than 1×10^{-6} ms^{-1} (Soil type D), which produces an acceptable groundwater recharge range based on the observed hydraulic gradients, as estimated by other techniques. Table 5.4 shows the percentage error between the observed values and those obtained from the type curves at the observation wells.

Table 5.4 Percentage errors of the observed and developed β values

Well number	Land use type	β Observed (m/year)	β from type curves (m/year)	Percentage of error (%)
2	Agricultural	0.39	0.35	11
3	Agricultural	0.31	0.35	13
4	Agricultural	0.32	0.35	9
5	Commercial	0.23	0.28	14

The AI was calculated to be 55 in the Sendai plain, based on an average annual precipitation of 1254 mm and an annual mean air temperature of 12.6ºC. When selecting the representative soil and the land use types, the predominant category in the 10, 000 m^2 surrounding the well point was chosen. The percentage error for estimating the β value from the developed type curves is below 15%, which confirms the applicability of the proposed methodology for general use. However, care must be taken when selecting the appropriate land–use type and hydraulic conductivity, otherwise, the method may over- or under-estimate the true recharge value. Therefore, we do not recommend the use of these

type curves alone. However, this method can be used to evaluate the accuracy of estimates from the T–D profile method.

5.9 Conclusions

Temperature changes inevitably impact fundamental ecological processes and the geographic distribution of aquatic species in coastal ecosystems. In the Sendai plain, the magnitude of aquifer temperature change at the ground surface, as evaluated from subsurface temperatures at five observation wells, spans 0.9–1.3ºC. Clear evidence was found for the influence of ground surface temperature change in the deeper aquifer depths, up to 38–60 m, at which aquifer temperature departs from a steady state T–D profile. A series of synthetic T–D profiles were produced and compared with the observed data to distinguish the individual effects of each parameter influencing temperature distribution at the local scale. Spatial variation in hydraulic gradients estimated using water level records at different aquifer depths and depth of departure from a steady state T–D profile proved to be very useful for determining reliable vales of groundwater recharge and rate of surface warming. Estimated groundwater recharge rates from T–D profiles (105–215 mm/year) were further verified against estimates from three other techniques (the water budget method, Darcy's method and the WLF method), which produced the groundwater recharge estimates in a consistent range (105–210 mm/year). Moreover, the constrained parameters of groundwater recharge and the rate of surface warming at different observation wells are consistent with the land use type and level of urbanization experienced in the past around each site. When a global warming rate of 0.004ºC/year was selected based on meteorological records from rural areas in the region, the urbanization effect was estimated to account for about 75% of the aquifer temperature change (0.7–1.0ºC) in the Sendai plain.

We also developed a set of type curves that can be used generally to estimate temperature distribution patterns for different soil and land cover types. This method was applied to account for variations in temperature and precipitation in different countries. Four soil types and four land use types were selected to represent the variations in site characteristics. The percentage error in estimating the β value using the developed type curves range from 9–14% in the Sendai plain. Therefore, considering the higher degree of uncertainty inherent in recharge estimation using T–D profiles and other techniques, these type curves can be used to test the accuracy of the estimates in general applications. This study on aquifer thermal regimes will help managers to maintain or achieve the ecological balance of groundwater ecosystems, and the methodology that we developed will assist planners and decision–makers in the environmental management programs.

CHAPTER 6

FUTURE PREDICTIONS OF CLIMATE CHANGE IMPACTS

6.1 Different scenarios and their assumptions

Assessing the anticipated impacts of climate change requires predicting the future behavior of the global climate system. The Intergovernmental Panel on Climate Change (IPCC) Fourth Assessment Report (AR4) gives a set of Global Climate Models (GCMs) (e.g., HADCM3 from the United Kingdom, MRI from Japan, and GFDL from USA) with a well standardized group of scenarios (e.g., A2, A1B, and B1) for climate impact studies. However, each GCM incorporates slightly different assumptions and model structures that give different results for each model. Moreover, each GCM has a different grid resolution, which generates specific results for each model. Therefore, it is preferable to consider a range of models and scenarios instead of relying on a single forecast (Salathe, 2005).

A set of scenarios assists in the understanding of possible future developments of complex systems. The assessment of climate change dictates a global perspective and a very long time horizon that covers periods of at least a century. As the prediction of future anthropogenic green house gas (GHG) emissions is impossible, alternative GHG emissions scenarios become a major tool for the analysis of potential long-range developments of the socio-economic system and corresponding emission sources. The quantitative inputs for each scenario include regionalized measures of population, economic development and energy efficiency, the availability of various forms of energy, agricultural production and local pollution controls that can be summarized as follows (Alley et al., 2007).

6.1.1 A1FI, A1T and A1B

The A1 storyline and scenario family describes a future world of very rapid economic growth, global population that peaks in mid-century and declines thereafter, and the rapid introduction of new and more efficient technologies. Major underlying themes are convergence among regions, capacity-building, and increased cultural and social interactions, with a substantial reduction in regional differences in per capita income. The A1 scenario family develops into three groups that describe alternative directions of technological change in the energy system. The three A1 groups are distinguished by their technological emphasis: fossil intensive (A1FI), non-fossil energy sources (A1T), or a balance across all sources (A1B; where balanced is defined as not relying too heavily on

one particular energy source, on the assumption that similar improvement rates apply to all energy supply and end use technologies).

6.1.2 A2

The A2 storyline and scenario family describes a very heterogeneous world. The underlying theme is self-reliance and preservation of local identities. Fertility patterns across regions converge very slowly, which results in continuously increasing population. Economic development is primarily regionally oriented and per capita economic growth and technological change more fragmented and slower than other storylines.

6.1.3 B1

The B1 storyline and scenario family describes a convergent world with the same global population that peaks in mid-century and declines thereafter, as in the A1 storyline, but with rapid change in economic structures toward a service and information economy, with reductions in material intensity and the introduction of clean and resource-efficient technologies. The emphasis is on global solutions to economic, social and environmental sustainability, including improved equity, but without additional climate initiatives.

6.1.3 B2

The B2 storyline and scenario family describes a world in which the emphasis is on local solutions to economic, social and environmental sustainability. It is a world with continuously increasing global population, at a rate lower than A2, intermediate levels of economic development, and less rapid and more diverse technological change than in the B1 and A1 storylines. While the scenario is also oriented towards environmental protection and social equity, it focuses on local and regional levels.

6.2 Differences among general circulation models

The simulations of several models and emission scenarios provide uncertainty in the range of potential climate changes in the future. For this study, a set of results presented for the IPCC AR4 was considered. Projected data from 1927–2000 for the 20C3M scenario were considered as a baseline climate. Year 1927 was selected as the base due to climate data availability in the Sendai metrological station. For future climates, results of 2000–2100 from A2, A1B and B2 scenarios were considered. Specifically, results from 5 models, (Table 6.1) which provide 5 and 15 simulations for the 20^{th} and 21^{st} centuries, respectively

Table 6.1 GCMs from different organizations and their resolutions

Model	Organization	Resolution of the grid box containing the Sendai plain (km^2)
HADCM3	UK Metrological Office, UK	90465
MIROC	National Institute for Environmental Studies, Japan	75400
CCSM3	National Centre for Atmospheric Research, USA	19070
CSIRO	Australia's Commonwealth Scientific and Industrial Research Organization, Australia	34410
ECHAM5	Max-Plank-Institute for Meteorology, Germany	34410

(5 for each emission scenario), were used. For the comparisons of different model performances for present day climate and future trends, time series of monthly mean temperature and precipitation from the representative grid box of each model, containing the target station in the Sendai metrological station (38.26°N and 140.90°E), were extracted. Fig. 6.1a) shows the linear trends of different GCM scenarios with a comparison of observed trend over 73 years (1927-1999). The findings from Hansen and Lebendeff (1987), and Huang et al. (2000) suggested that global averaged warming in 20th century ranges from 0.5-0.7 °C/century. Of the five GCMs analyzed, three of them (HADCM3, ECHAM5, and CSIRO) simulate warming trend in 20th century (black color boxes in Fig. 6.1a) for the grid box containing the Sendai plain. CCSM3 model simulate very little trend while MIROC exhibits slight negative trend. Even though, the temperature trend is less dependent on grid resolution, GCMs usually unable to capture the local effects of urban heat island of the size of Sendai city. This may explain the mark of significantly higher warming rate in the Sendai plain than the simulations from five GCMs (Observed warming rate is over two times higher than the HADCM3 model, which simulates the highest warming rate among five GCMs). According to the warming trends in the future, HADCM3 model predicts the highest warming rate in the end of 21st century. However, in accordance with the IPCC AR4, magnitude of global warming in later part of the 21st century expects to be significantly higher than the 20th century. Thus, it is reasonable to assume that the simulations from HADCM3 may not over predict the future but a possibility and therefore, can be used as a potential impact predictor for the future studies in the Sendai plain.

Even though, there are some significant geographical variations of climate change, particularly with respect to precipitation, globally mean precipitation is projected to increase in future. According to IPCC AR4, high latitudes countries (e.g. Japan) likely

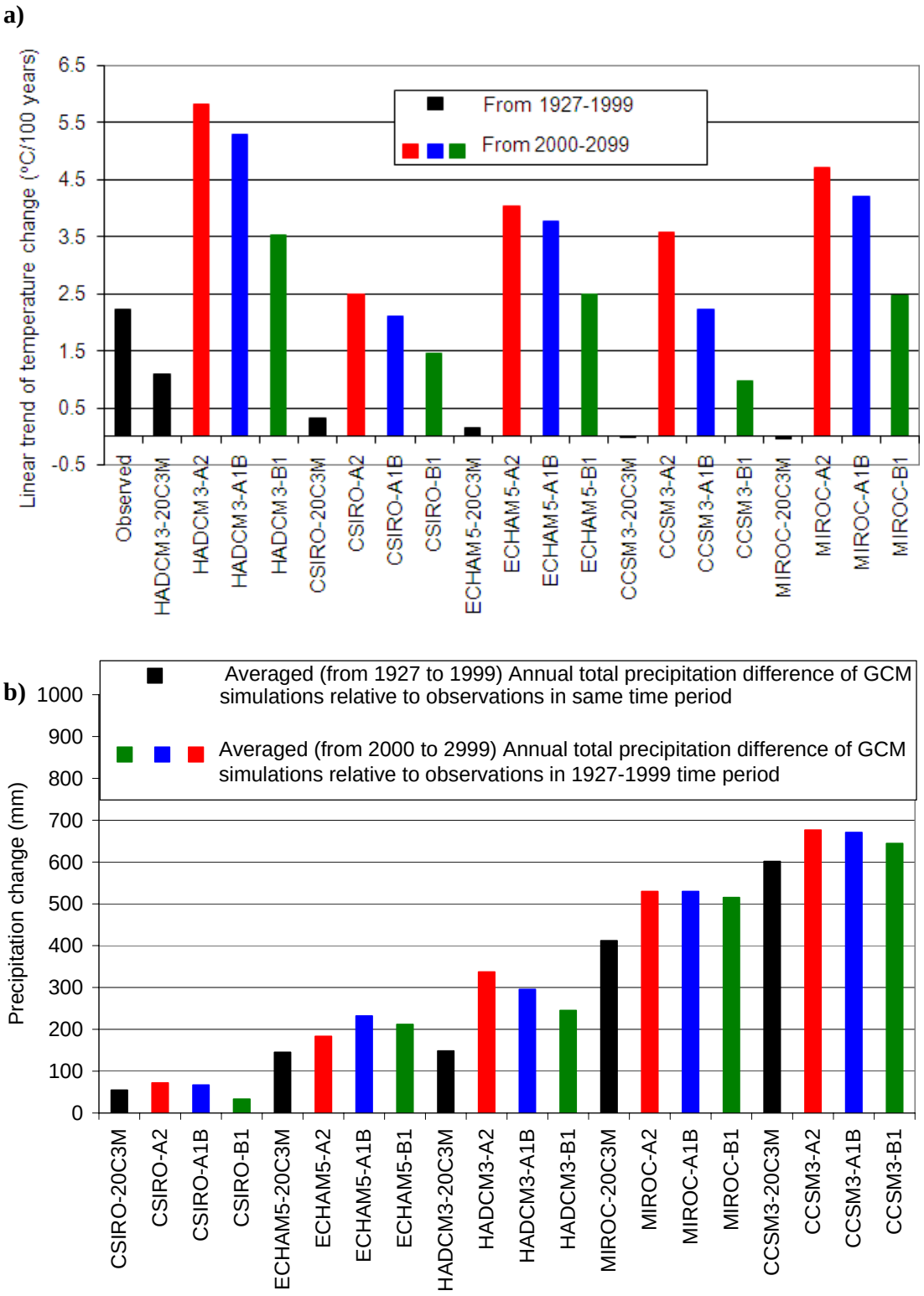

Fig. 6.1 Comparisons of observed climatic parameters with the different GCM scenarios; a) linear trend of temperature change and b) averaged annual total precipitation change relative to the observations during 1927-1999.

experience high precipitation events. As depicts in Fig. 6.1b, all GCMs predict potential of increasing precipitation in the 21st century in different magnitudes. HADCM3, MIROC and CCSM3 models simulate significant precipitation change, which predict over 300 mm of annual total precipitations rise in 21st century relative to the observations in 20th century. When comparing GCM simulations with observed precipitation in same time horizon (1927-1999 in black color in Fig. 6.1b), CSIRO and HADCM3 exhibit comparatively smaller biases (55mm and 149mm, respectively) while CCSM3 shows the strongest wet bias (601 mm).

6.3 Downscaling methodology

Reliable assessment of anticipated climate change impacts eventually requires fine resolution projection (~10 km^2) of climate parameter at the local scale, which cannot be resolved by current GCMs. Model predictions with such high resolutions are computationally demanding and not likely to become widely available in the near future. For example, HADCM3 model has very coarse resolution, which in spatial scale, approximately equal to 90465 km^2 of the grid box containing the Sendai plain. Even though, some models like MIROC3_2-HI and CCSM3 recently produce model predictions with comparatively higher resolution (12185 km^2 and 19070 km^2 resolutions reference to the Sendai plain, respectively), they are still far behind to be used for site specific assessments. As a result, GCMs cannot explicitly account for the physical-geographic characteristics of the fine scale structure (e.g. inland water bodies, coastal lines, mountain ranges, and land use) that significantly govern the local climate. However, GCMs show a good performance in simulating large scale circulation and climatic features that affect regional climates (Salathe et al., 2007). This obstacle can be overcome by relating the coarse resolution GCM output to the heterogeneous local climate (Fig. 6.2).

Over the decades, both dynamic (Solman and Nunez, 1999) and statistical methods (Wilby and Wigley, 2000; Widmann et al., 2003; Zhang, 2005) have been introduced; but the statistical methods are frequently used to downscale GCM projections to finer scales. All the statistical downscaling techniques translate the large-scale GCM data into a high resolution distribution based on empirical relationships. The transfer function method was used to link the statistical relationship between GCM output (predictors) and local climatic variables (predictands). Most commonly used predictors include airflow indices, wind strength and direction, mean sea-level pressure, and relative humidity (Solman and Nunez, 1999; Wilby and Wigley, 2000). In this method, predictors must have the ability to incorporate not only the local climatic variations but also the effects of climate change. Among the parameters of concern in this research, the sea level pressure has significant

influence on local precipitation. Thus, Widmann et al. (2003) found that direct use of GCM precipitation as a predictor gives good agreement for Pacific Northwest precipitation, and Zhang (2005) successfully used this method to assess the climate change impacts on water resources, soil erosion, and crop production in Oklahoma, USA. Similarly, the large–scale surface air temperature is a robust predictor for local temperature (Salathe and Mote, 2007). However, the transfer function method is based on the assumption that the probability distribution of the present climate will fully continue to the future.

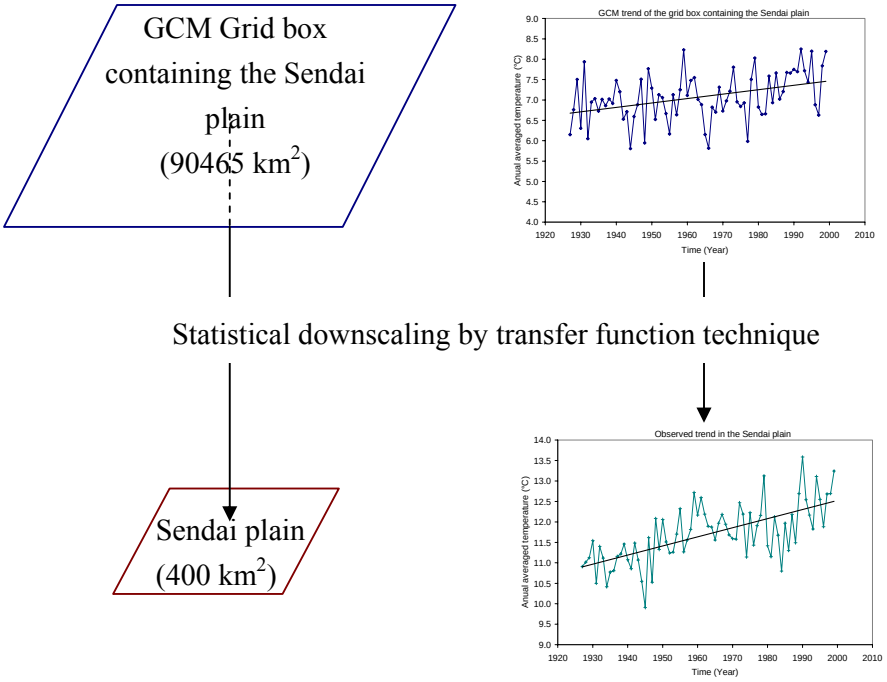

Fig. 6.2 Schematic representation of transfer downscaling technique

The regression relationships required for statistical downscaling (transfer functions) are calibrated using parallel time series of GCM output and local scale observations for the period of 1967–2006 for the corresponding variables. As an example, for each calendar month, the ranked observational monthly precipitations were plotted with the ranked GCM projected precipitation (quartile plot), and linear and non–linear functions were fitted to each plot to obtain the appropriate transfer functions for each month (Wood et al., 2004). The transfer functions were determined in such a way that the determination coefficient (r^2) of the corresponding regression is always larger than 0.9. These transfer functions were then used to downscale the 1947–1966 GCM data to the Sendai plain and later verified with the observed precipitation. For climate prediction,

these transfer functions were further used to downscale the 2060–2099 GCM monthly precipitation. Likewise, the GCM projected monthly temperatures were downscaled in the same manner as for precipitation.

6.4 Downscaling results in the Sendai plain

The determination coefficient (r^2) of the linear and nonlinear regressions was considered for the selection of the appropriate transfer functions. Nonlinear regression always gives better agreement (minimum r^2 of 0.92 for ECHAM5 A1B precipitation in December and maximum r^2 of 0.99 for HADCM3 B1 temperature in January) than the linear regression. However, the r^2 of linear regression also gives good values as close as those from nonlinear regression (above 0.8). Therefore, both linear and nonlinear functions were used in such a way that the r^2 of the corresponding transfer function was always above 0.9.
The ability to represent the local climate in the Sendai plain of each model were assessed by comparing the bias in the long–term monthly mean precipitation and temperature relative to the observed data. The seasonal performance of a particular model depends on its capability to correctly capture the regional metrology and topography. Thus, the seasonal cycle of each model was also compared with the local climate.

6.4.1 Temperature

There is a consistent bias in some models relative to observed temperature, while some models show under and overpredictions. The HADCM3 model shows the strongest bias among the selected models that greatly underpredict (≈ 7 °C in winter) the local temperature. The ECHAM5 model overpredicts throughout the year (≈ 2 °C), except in August, where the GCM slightly underpredicts. The CCSM3 model exhibits a warm bias during winter (≈ 0.5 °C) and a cold during summer (≈ 1.0 °C). The downscaled temperature values for HADCM3 A2 scenario were plotted with observed temperature in Fig. 6.3a for all months of the year, illustrating how well the selected transfer functions reproduce the temperature values at the Sendai station.

According to Fig. 6.3b, which depicts the verification of the derived transfer functions from 1927–1966, downscaled temperatures indicate slight overprediction and underprediction for August and April, respectively. However, in general, the derived transfer functions show good applicability for all months. In a similar manner, all other model scenarios provide good agreement with the verified results.

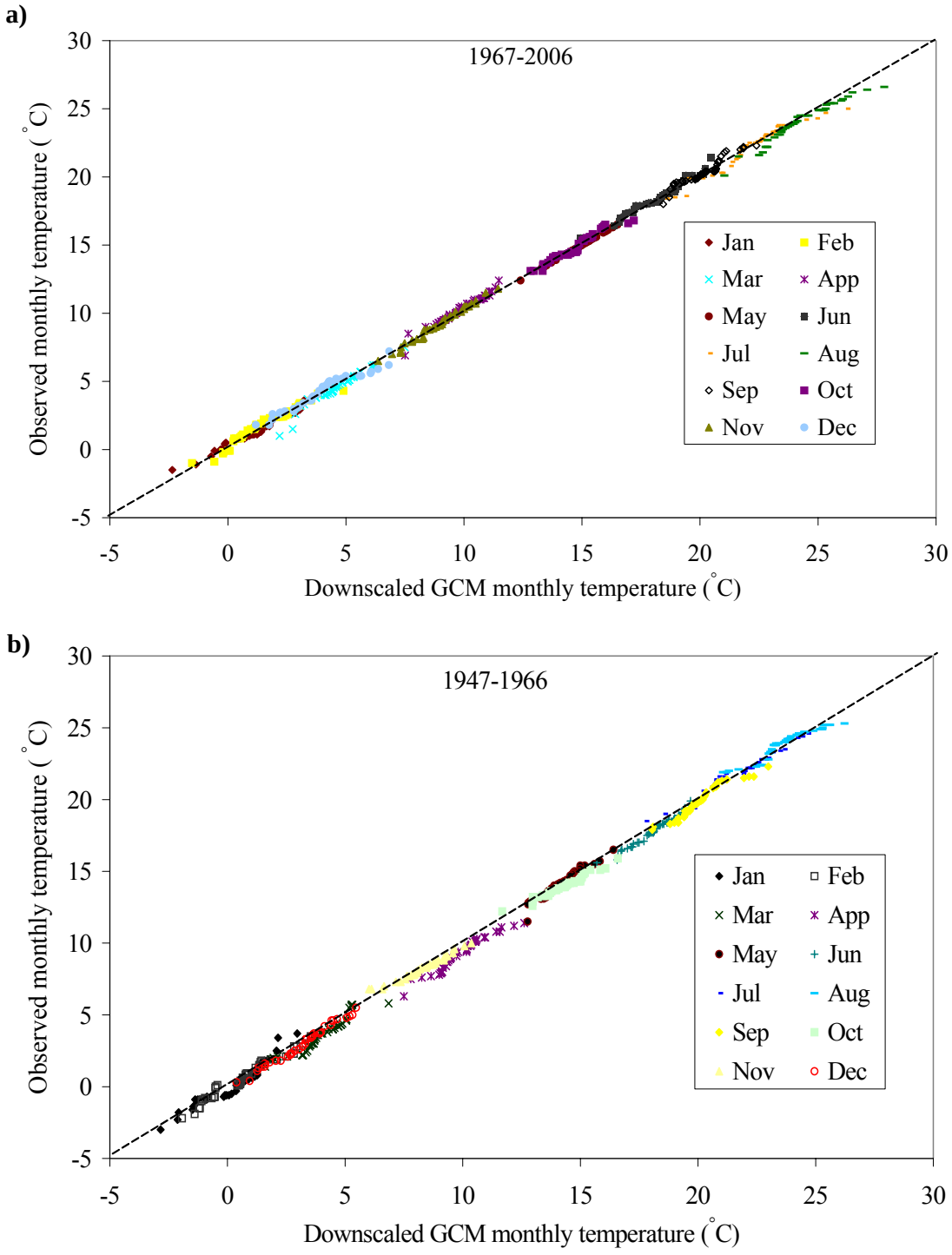

Fig. 6.3 Quartile plots of observed vs. downscaled temperature for HADCM3 A2; a) transfer functions calibration, and b) transfer functions verification.

In fact, there are marked differences among the scenarios in general. For all the models, the A2 scenario gives the highest temperature rise in 2060–2099 time period followed by the A1B and B2 scenarios. Among the models, HADCM3 shows the highest temperature increase from the time period of 1967–2006 to 2060–2099 (3.9 °C for A2 scenario), and ECHAM5 (2.6 °C for A2 scenario) illustrate the lowest temperature rises. When compared with the present trend of surface warming in the Sendai plain during last 60 years (0.02 °C/year), the CSIRO B1 scenario shows the most similar rate of surface warming in the future (0.0192 °C/year) than the other model scenarios. All other model scenarios provide higher rates of surface warming (above 0.02 °C/year), except the CCSM3 B1, which gives the minimum rate of air temperature rise in the future (0.0117 °C/year).

Moreover, comparing the present (1967–2006) and future (2060–2099) climates, there are significant differences in seasonal air temperature change among the GCMs. HADCM3, MIROC, and CCSM3 (for all scenarios) are projected to cause substantially higher warming in summer (July–August) than in winter (January–February). Among them, HADCM3 A2 produces the highest temperature difference (about 2.7 °C in Fig. 6.4; here, warming is 5.9 °C and 3.2 °C in summer and winter, respectively, Fig. 6.5) than the MIROC A2 scenario (about 1.3 °C; here, warming is 4.1 °C and 2.8 °C in summer and winter, respectively) or the CCSM3 A2 scenario (about 2.2 °C; here, warming is 5.7 °C and 3.5 °C in summer and winter, respectively). In contrast to the three models above, ECHAM5 A1B (Fig. 6.4) predicts more warming in winter than in the summer (about 1.0 °C difference; here, warming is 3.6 °C and 2.6 °C in winter and summer, respectively). Therefore, HADCM3 MIROC, and CCSM3 models stand in contrast to the common assumption that winter warming exceeds summer warming, and ECHAM5 agrees with it. CSIRO model scenarios depict reasonably similar magnitude of warming in summer and winter (A1B warming is 2.8 °C and 2.7 °C in winter and summer, respectively). However, these trends indeed would increase the evapotranspiration demand and cause dramatic effects on groundwater recharge and temperature distribution in the Sendai plain.

6.4.2 Precipitation

In contrast to temperature, there is no consistent precipitation bias among the considered GCMs relative to the observations at the Sendai metrological station. In some months, GCMs are projected to be overpredicting (e.g., HADCM3 throughout the year except September and October), and in some months they are underpredicting (e.g., ECHAM5 from July to November). Fig 6.6 shows the downscaled GCM data of the HADCM3 A2 scenario for the calibrated and verified transfer functions.

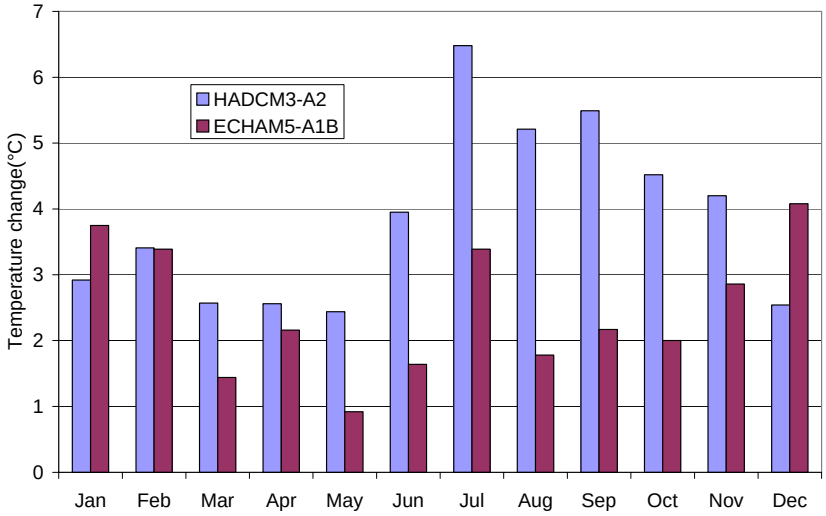

Fig. 6.4 Seasonal variation of warming during 2060-2099 relative to 1968-2007

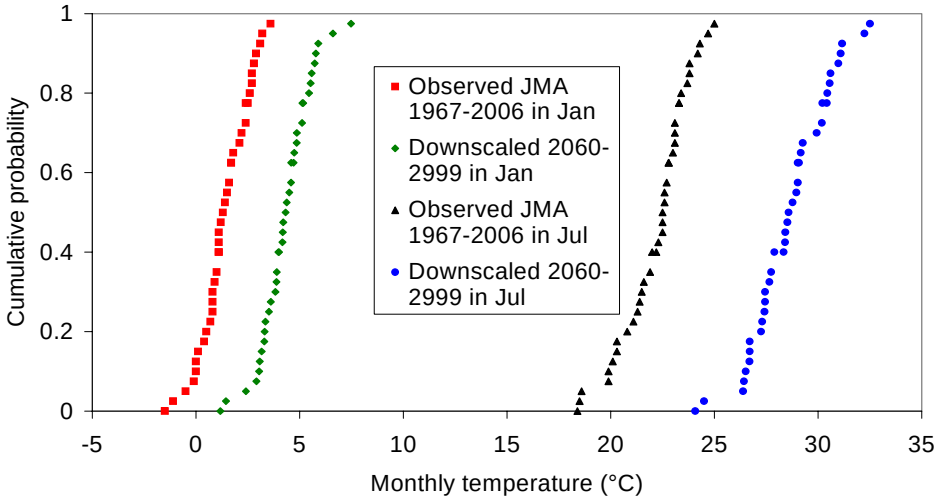

Fig. 6.5 Cumulative probability distribution of temperature in summer (July) and winter (Jan) during present (1968-2007) and future climates (2060-2099)

Unlike temperature, sea level patterns govern the local variability in precipitation (Salathe et al., 2007; Wilby and Wigley, 2000; Widmann et al., 2003). Therefore, fitting a linear or a simple nonlinear transfer function for precipitation is more difficult than for the temperature. Thus, compared with the temperature, downscaling results for precipitation show less agreement with the observed records. Verified results during 1927–1966 indicate several significantly deviated points from the 1:1 line, suggesting a poor match for August and September, while the other months show reasonably good agreement for the predictions. However, in general all the model scenarios show comparatively good results for precipitation that can be used for long–term impact predictions.

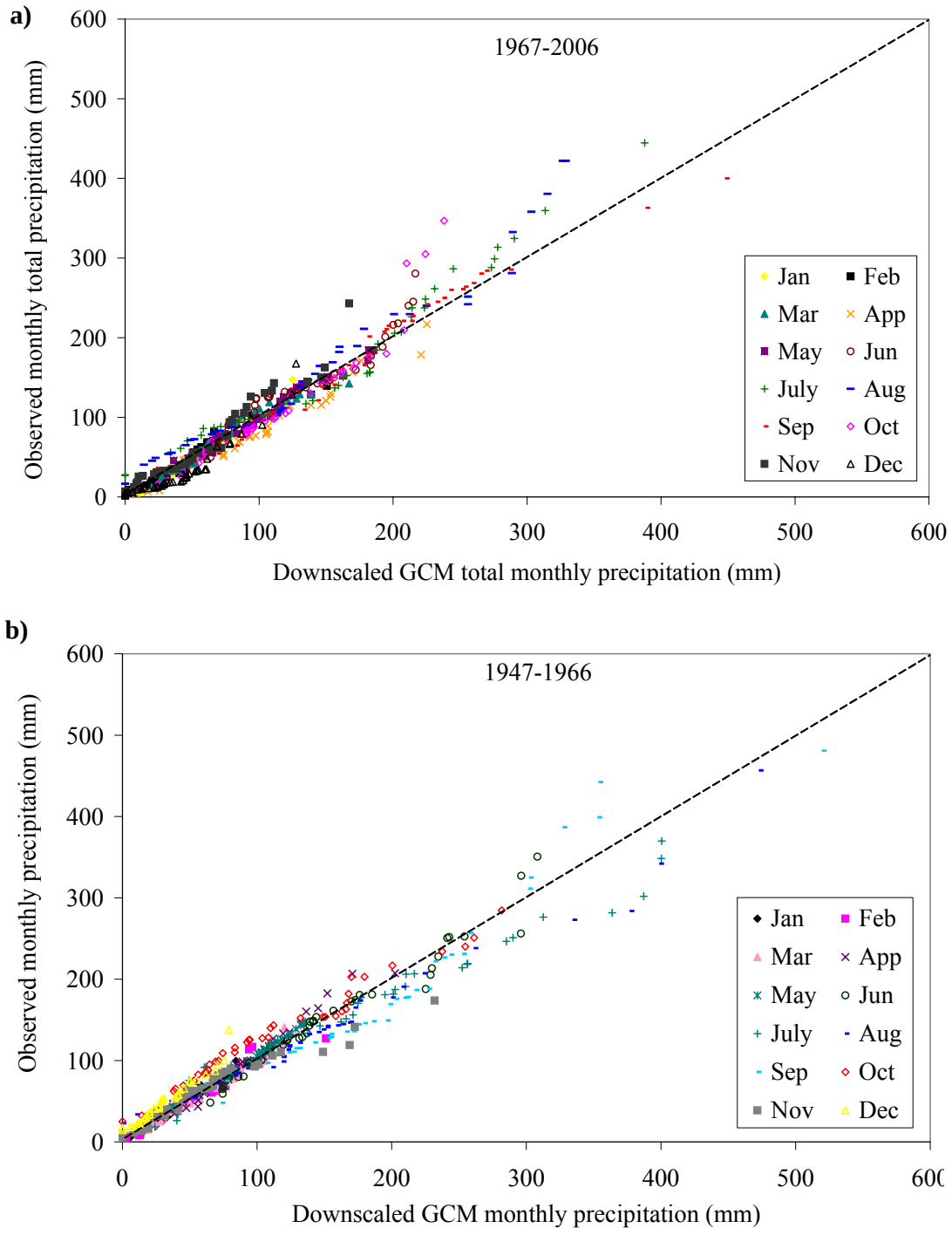

Fig. 6.6 Quartile plots of observed vs. downscaled precipitation for HADCM3 A2; a) transfer functions calibration, and b) transfer functions verification.

Except CSIRO B1, all other GCM scenarios exhibit an increased trend of precipitation for the 2060–2099 time period than the annual average of the past 40 years

(1967–2006). As usual, the HADCM3 A2 scenario produces the highest annual precipitation rise (345 mm; about 28% change from past 40 years' average), and the CSIRO B1 scenario gives the minimum precipitation change, which predicts 9 mm/year reduction relative to present climate. The ECHAM5 model shows a moderate wet condition, where its B1 scenario produces the highest of 203 mm precipitation increase (about 17% change from past 40 years' average) compared to the A2 and A1B scenarios.

Seasonally, HADCM3 and ECHAM5 scenarios are projected to cause higher precipitation in summer (average of July–August) than the spring (average of April–June). Among all the model scenarios, HADCM3 A2 produces the largest precipitation change difference between the seasons (about 74 mm as in Fig. 6.7; here, the change is 94 mm and 20 mm in summer and spring, respectively). The cumulative probability distributions in Fig. 6.7 depict the clear difference in the precipitation change in the 2060–2099 time period compared to the present climate (1967–2006) and also the shift between the two seasons.

In contrast to HADCM3 and ECHAM5 models, MIROC, and CCSM3 model scenarios predict higher precipitation in spring than the summer. Among them, CCSM3 A1B produces the largest precipitation change difference between the seasons (about 32 mm; here, the change is 29 mm and -3 mm in spring and summer, respectively). Quite opposite to all the models, CSIRO model scenarios are projected precipitation reductions in both summer and the spring, where the highest decline is predicted to occur in the summer for B1 scenario (41 mm as in Fig. 6.8).

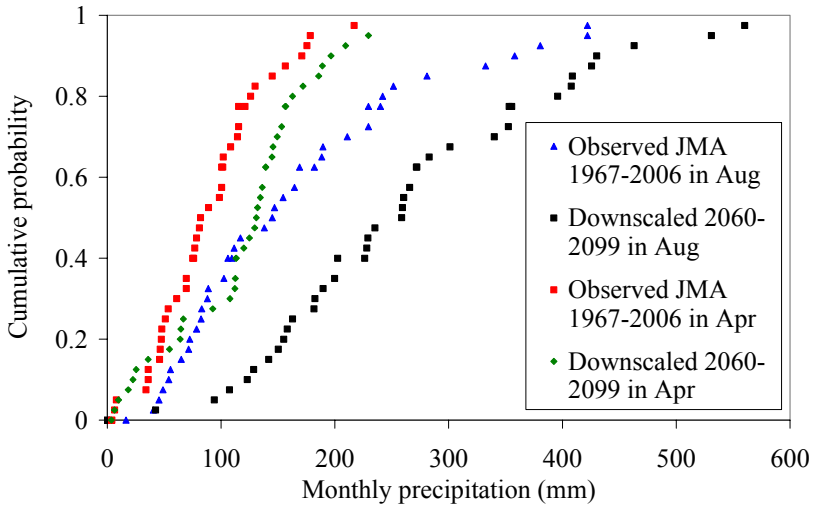

Fig. 6.7 Cumulative probability distribution of precipitation in summer (Aug) and spring (Apr) during present (1968-2007) and future climates (2060-2099)

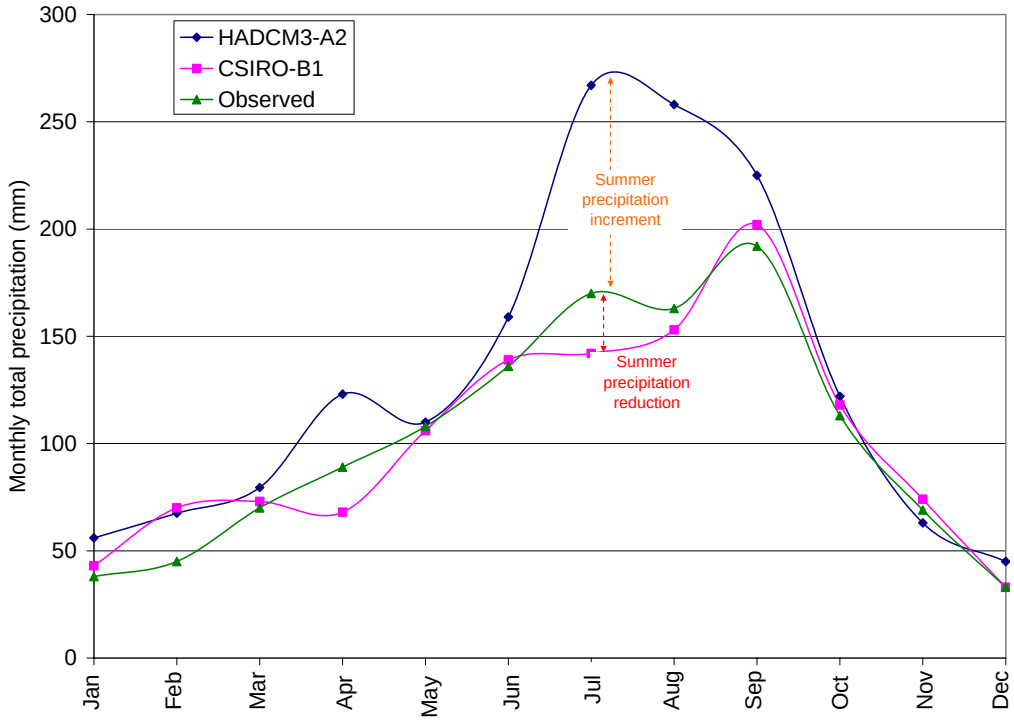

Fig. 6.8 Seasonal precipitation change by two different scenarios

6.5 Climate change impacts

6.5.1 Groundwater recharge and aquifer temperature

In the Sendai plain, the background temperature in the aquifer is higher than the annual average air temperature. Therefore, recharge water flow caries the cool water from the top of the ground surface and produces a concave shape for the temperature–depth profile. Thus, when the surface air temperature increases over time, the maximum temperature change is experienced near the ground surface of the aquifer, and the temperature decreases as the depth from the ground surface increases. The water table usually occurs in a range of 3–7.5 m from the ground surface, which is shallow near to the coast and comparatively deep when the distance from the coast increases (3 m in W2 and 7.5 m in W4 as depicts in Fig. 5.4). Therefore, the aquifer temperature change at 8 m below the ground surface was considered as the representative depth for the comparison of the impacts from different scenarios.

To account for the climate change effects on hydrology in the Sendai plain, we substituted the projected precipitation and temperature (as the evapotranspiration) into the water budget technique (Equation 5.5) and estimated the possible variations of groundwater recharge for each model scenario (Table 6.2).

Table 6.2 Comparison of aquifer temperature changes in 2080 using different scenarios

Model	Scenario	Climate change		Hydrology change	
		Precipitation [$P_{2060–2099} - P_{1967–2006}$] (mm/year)	Air temperature [$T_{2060–2099} - T_{1967–2006}$] (°C)	Recharge (mm/year)	Annual average aquifer temperature change at 8 m depth from ground surface [$T_{2080}–T_{2006}$] (°C)
HADCM3	A2	345	3.90	116 (-19*)	3.2
	A1B	209	3.80	100 (-35*)	3.1
	B1	87	2.50	133 (-1.5*)	2.0
MIROC	A2	217	4.71	103 (-32*)	4.0
	A1B	236	4.26	115 (-20*)	3.6
	B1	144	2.87	142 (7*)	2.3
ECHAM5	A2	188	2.6	150 (15*)	2.0
	A1B	198	2.50	165 (30*)	2.0
	B1	203	2.00	182 (47*)	1.5
CCSM3	A2	144	3.68	96 (-39*)	3.1
	A1B	169	2.68	143 (8*)	2.2
	B1	28	2.34	117 (-18*)	1.8
CSIRO	A2	38	2.65	108 (-27*)	2.1
	A1B	68	2.12	155 (20*)	1.7
	B1	-9	1.83	165 (30*)	1.5
If the present surface warming trend continue in the future		–	2.0	135 (0*)	1.4

* Groundwater recharges reduction relative to 2007 estimation.

The estimated recharge values by the water budget technique and temperature–depth profiles span practically the same range. Therefore, the percentage of spatially averaged groundwater recharge change from 2006 to 2080 estimated by the water budget technique was multiplied by the 2006 recharge rate in each observation well to obtain an approximate recharge change in those well locations (e.g., recharge of $W1_{t=2080}$ = recharge of W1 from temperature–depth $profiles_{t=2006}$ × [recharge from the water budget

technique$_{2080}$ / recharge from the water budget technique$_{2006}$]). Moreover, averages of the mean annual temperature during three time periods (1947–1966, 1967–2006 and 2060–2099) were used to estimate the linear rate of SAT warming in each scenario. In this case, GST change was assumed to follow a trend similar to SAT changes, an assumption that has been found to be acceptable for a long-term analysis (Huang et al., 2000). The magnitude of the difference between the future SAT warming trend and the present SAT warming rate (0.02ºC/year) of each scenario was added to the constrained value of parameter *b* at each observation well to estimate a new corresponding GST warming rate considering the effect of future climate change at the local scale. The combined effects of groundwater recharge variation (β) and ground surface temperature change (*b*) were applied in Equation (5.4) to estimate the potential impacts on aquifer temperature change.

Table 6.2 shows the potential range of groundwater temperature change under each scenario. These results were further compared with another possible groundwater temperature change scenario, which assumes that the same magnitude of surface temperature warming in the past (from 1947 to 2006) will be continued in the future. In this case, only the change in temperature was considered, while the recharge rates at each well were held constant.

In climate impact prediction, it is preferable to consider a set of scenarios that produce a range of possibilities instead of relying on single forecast (Salathe, 2005). According to the statistical downscaling, future precipitation will increase by different magnitudes under all scenarios. The estimated recharge rates (Table 6.2), which incorporate both precipitation and temperature changes, exhibit a decreasing trend (1–29% reductions from the original values using the water budget technique) for some scenarios of HADCM3, MIROC and CCSM3 models and project a increasing trend (5–35% increments from the original values using the water budget technique) for some scenarios CSIRO of and ECHAM5 models in the future. It is noted that the additional evapotranspiration due to a higher degree of temperature rise (1.8–4.7 ºC) has a stronger effect on a greater recharge rate than extra precipitation. Fifteen scenarios in this study give a potential range of aquifer temperature change in the future (1.5–4.0 ºC). The results from the B1 scenario are close to those predicted if the present trend of GST warming continues in the future (1.4 ºC). Above scenarios also show that the depth of departure from a steady state profile increases by different amounts, demonstrating the possibility of future climate change impacts at deeper aquifer depths. The depth of departure increases as GST warming rate (*b*) increases. However, in the Sendai plain, the average groundwater temperature is higher than the annual averaged SAT. Therefore, the opposite mechanism occurs when downward water flux slows the time rate of depth departure from a steady state. As an example, even though the rate of GST change of HADCM3 A2 scenario is

higher than the CCSM3 A2 scenario (3.6 and 3.4 °C/century, respectively), owing to its higher groundwater recharge reduction in the future (20 mm/year than HADCM3 A2), CCSM3 A2 scenario gives larger depths of departure than the HADCM3 A2 scenario (Fig. 6.9). These results confirm that at a given time, GST change has a profound effect on the shallow sub-surface layer, while variation in groundwater recharge may have a greater effect at deeper aquifer depths.

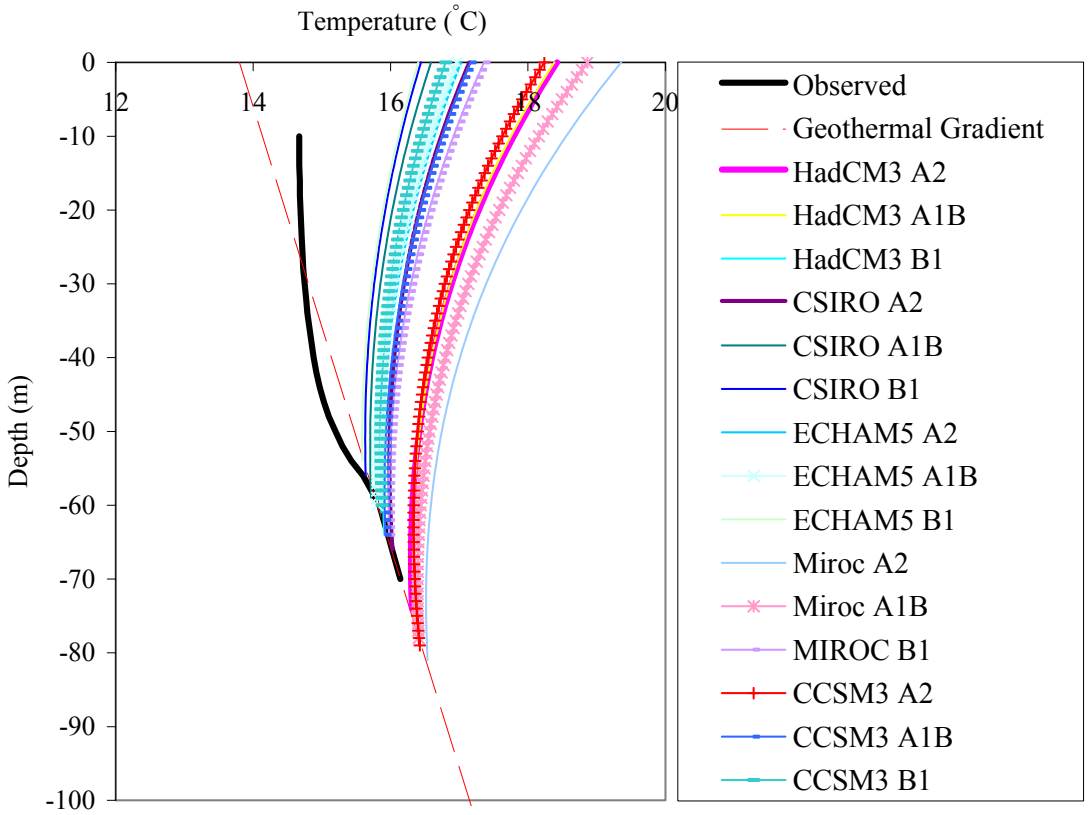

Fig. 6.9 Aquifer temperature change for different scenarios

6.5.2 Aquatic ecology

Water temperature can adversely affect aquatic species by altering the timing of migration, and rate of maturation, by increasing the susceptibility to diseases, and causing direct mortality (Lee and Bell, 1999; Oie and Olsen, 1993). To investigate possible interactions between the impacts of climate change and habitat, we evaluated the change of habitat suitability of three species; Sweetfish, Carp, and Pale-chub. Habitat suitability for the selected species in Japan, as formulated by Kojiri et al. (1997), was used (Fig. 6.10).

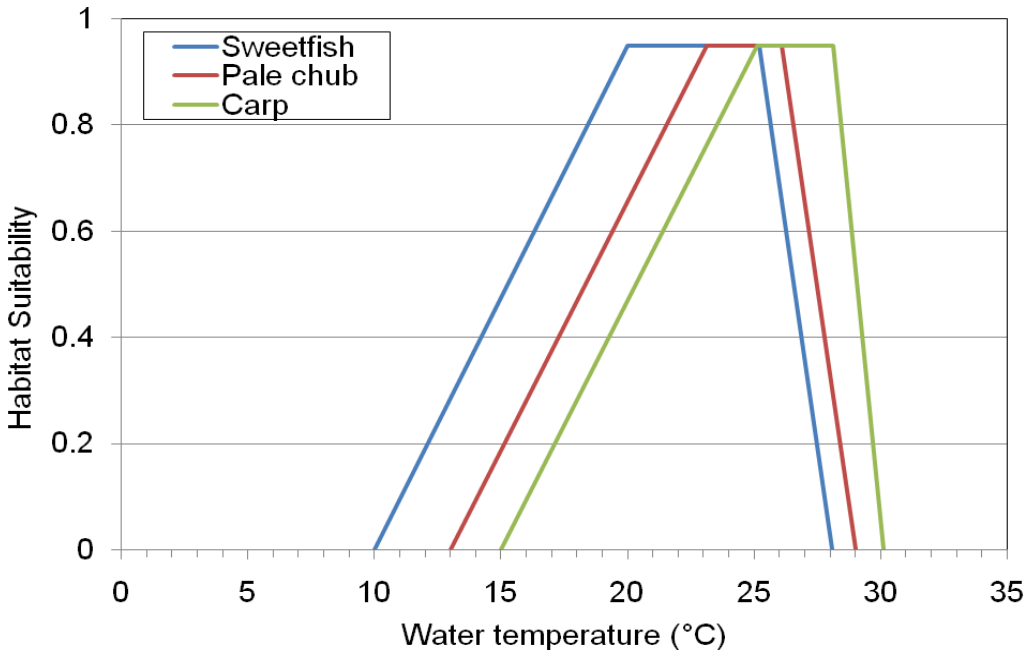

Fig. 6.10 Habitat suitability against water temperature (source: Kojiri et al., 1997)

Fig. 6.11 shows the simulated suitability of the selected fish species for the highest and lowest impact scenarios in terms of changing aquifer temperature in the Sendai plain (MIROC-A2 and ECHAM5-B1, respectively as in Table 6.2). The inhabiting suitability of sweetfish and pale chub which are favorable to relatively mild warm water exhibit strong differences for MIROC-A2 scenario (Fig. 6.11a and c) between the two study periods when a decrease of suitability occurs during July and August in the period of 2060 to 2099. Such an effect would seriously affect sweetfish and pale chub by shortening their inhabiting periods, eventually resulting to decrease the productivity of particular species and forcing them to migrate in higher latitude areas. The suitability for fish that require warm water, such as carp is slightly increased under MIROC-A2 scenario due to the global warming (Fig. 6.11e). ECHAM5-B1 scenario shows overall positive impact for all selected species (Fig. 6.11b, d and f) except for sweet fish which exhibits slight reduction of suitability in August in future. However, considering the fact that inhabiting suitability of selected species increase during summer (Jun, July and August), HADCM3, MIROC and CCSM3 scenarios which are projected to cause substantial higher warming in summer than in winter, would exert strong pressure on species like sweetfish and pale chub which are favorable to relatively mild warm water. Nevertheless, ECHAM5 model scenarios which predict average aquifer warming and more seasonal warming in winter than in summer may create little favorable inhabiting situations for the aquatic ecology in future.

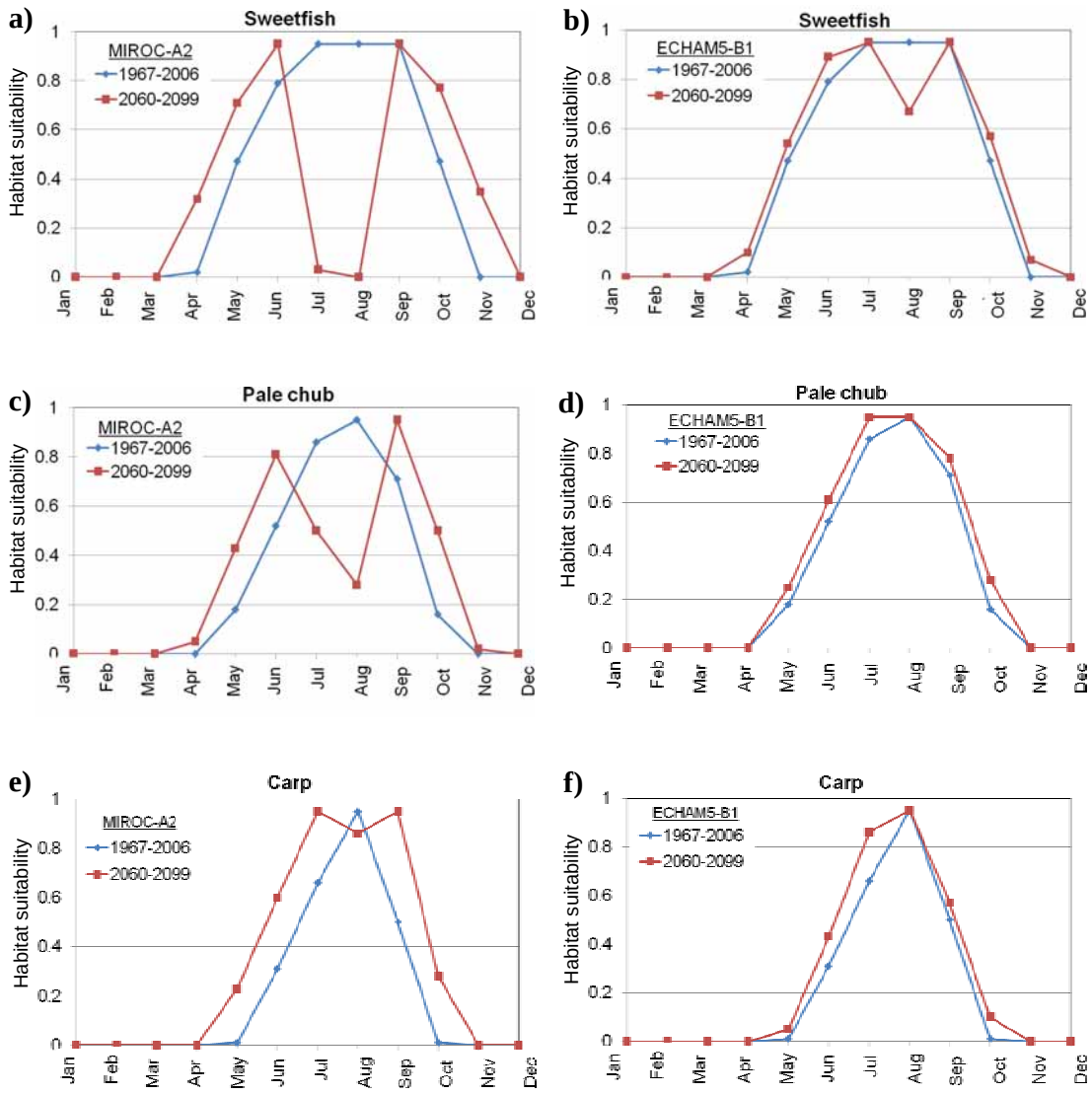

Fig. 6.11 Seasonal inhabitant suitability under changing climate

6.6 Constrains and limitations of the study

Proper understanding of the past effects of urbanization and global warming on present aquifer temperature distributions are important in order to predict future changes in the aquifer thermal regime due to climate change. This study examined a combination of parameters among several possibilities in a preliminary analysis. When depth of departure from the steady state profile was used as the indicator with a reliable range of possible groundwater recharge and GST warming rates, the theoretically derived time (t=60 years) since the transient changes began was consistent with the time that the Sendai plain began to experience significant SAT warming. However, compared with the broad time scales

that have been used to find signatures of past climate change from borehole records (e.g., five centuries in Huang et al., 2000), we analyzed a time history of only 1.2 centuries. This is mostly because of our poor knowledge about past climate change due to the absence of meteorological observations over the centuries. While some research has reported evidence of surface cooling (Pollack and Huang, 1998), other studies (Hansen and Lebendeff, 1987) have concluded that considerable global warming occurred in the past. Huang et al. (2000) have estimated a continuous GST warming trend over five centuries, with the largest temperature rise in the 20th century. Therefore, it is possible that the aquifer T–D profiles have been influenced to different degrees by climatic trends occurring before the observational period of this study. In addition to the influence of historical climate trends, the transient time period considered in this study may be subjected to variations at the very local scale surrounding the observation wells. However, land use maps and the Sendai city office data reveal that development throughout the area started around the same time in the middle of the 20th century. Nevertheless, all the observation wells are located within less than seven kilometers of the city center. Therefore, the timing of variations in GST that we selected in this study based upon our preliminary theoretical analysis and climatic observations may be appropriate for the all observation wells in the basin.

According to the constrained parameters in Table 5.1, rates of SAT and GST warming surrounding observation wells are slightly different. W1–W4 showed somewhat lower GST warming rates than SAT changes, while W5 showed a somewhat higher warming rate. GST does not necessarily track SAT trends (Beltrami and Kellman, 2003, Schmidt et al., 2001) and can vary with site conditions such as albedo, vegetation, and other factors (Mann and Schmidt, 2003). Therefore, these differences may be attributed to the level of urbanization experienced at different locations. However, for the long-term climate impact predictions, we assumed GST to increase at the same rate as SAT. Even though past urbanization effects were considered on present aquifer temperature change, we did not simulate the potential land-use changes that may occur in the future. In other words, we explicitly assumed that present site conditions will be preserved in the future. Therefore, as long as climate change is considered as the sole cause of SAT change, it is reasonable to assume a similar magnitude of GST change (Huang et al., 2000) from present values for a long-term analysis.

In the Sendai plain, past urbanization and climate change effects have altered the aquifer temperature by 0.9–1.3 $^{\circ}$C (the difference between the steady state linear curve extrapolated to the ground surface and the present observed values). The greatest change has occurred near the ground surface, as groundwater recharge decreases the effect as depth increases. If the climate change effect on GST change is assumed to be 0.004ºC/year,

the urbanization effect has been the dominant cause of aquifer temperature change during the past 60 years, altering aquifer temperatures by 0.7–1.0ºC. However, with respect to 15 scenarios' predictions of climate change in the Sendai plain, aquifer temperature will increase by 1.5–4.0ºC, which is notably higher than the urbanization effect experienced in the past. This strongly supports our hypothesis that climate change may be dominant cause of aquifer temperature change in the future in the Sendai plain. The estimated range of aquifer temperature change in this study is comparable with those founded in other studies, such as Ferguson and Woodbury (2004), which found a 2.5ºC increase in aquifer temperature during first 50 years out of a 3.5ºC total temperature change during 100 years of simulated time due to the urban heat island effect.

The transfer function method used in our study is based on the assumption that the probability distribution of the present climate will continue in the future. According to the comparison of downscaled temperature and precipitation with past climate data, the transfer functions that we developed are reasonably applicable for a long-term analysis. However, climate change may intensify in the future (IPCC AR4, 2007), resulting in different probability distributions than those of past climate change. Moreover, different GCMs incorporate slightly different assumptions and model structures, which produce different predictions. Therefore, it is preferable to consider a range of models and scenarios. In this study, we considered fifteen scenarios that span the impact within an applicable range. However, an analysis of more GCMs would produce a resilient range of impact with higher confidence.

6.7 Applicability of the study

GCMs output with various downscaling techniques link the global scale climate features to the local scale and make a flat-form for climate change studies. However, the downscaling of GCM outputs to the local scale requires extensive modeling, and therefore, it may not be advisable to select all available scenarios for impact predictions. On the other hand, different model structures with various grid resolutions produce different result for the same area of interest, which makes the use of single model with few scenarios realistically critical for climate impact studies. Moreover, owing to their various degree of model bias, magnitude of the climate parameter change in the future at the GCM grid scale did not necessarily indicate the same order of magnitude in downscaled results. As an example, according to Fig. 6.1a, HADCM3 A2 scenario possessed the highest warming rate in 21st century (6.2 °C/century) at the GCM grid scale, while MIROC A2 scenario gives the third highest warming rate (4.7 °C/century). However, according to downscaled temperature (Table 6.2), MIROC A2 model is projected to warm the surface

air temperature by 4.7 °C, which is 0.8 °C higher than the prediction from the HADCM A2 scenario. This is because, HADCM3 model produces the closest warming rate to the observations during 1927- 1999 (1.1 °C/century), while MIROC gives the highest model bias (2.3 °C/century). Therefore, when the statistical relationship is developed based on the past observations, degree of temperature change at the GCM grid scale is accordingly modified to suite with the existing model bias. Model bias may arise from various effects, and may not necessarily indicate that the model cannot correctly capture the large-scale climate change signals (Salathe et al. 2007). Therefore, a general index, which accounts the combined effects of model bias and the magnitude of climate parameter change in the future, would be very useful to select the appropriate model scenarios for the impact predictions.

For the temperature, it is noted that the higher degree of temperature change at the GCM grid scale produces high SAT warming rate for downscaled temperatures. Moreover, with respect to the observed warming rate in 1927-1999, positively larger model bias results for smaller warming rate at the local scale in future. Therefore, following index was proposed and the generated values were compared with the downscaled warming rates in the future in the Sendai plain (Fig.6.12a).

$$\text{Tem. Index} = \frac{\text{GCM warming rate}_{2000\text{-}2099} - \text{Warming bias}_{1900\text{-}1999}}{\text{Observed warming rate}_{1900\text{-}1999}} \qquad (6.1)$$

Similar to the temperature, when the magnitude of precipitation change at the GCM grid scale is large, it produces significant precipitation variation at the local scale. Moreover, with respect to the observed annual precipitation averaged during 1927-1999, positively larger model bias results for smaller precipitation at the local scale in future. Therefore, precipitation index was developed as a percentage of observed annual precipitation averaged during 1927-1999 time period (Equation 6.2). Furthermore, generated values were compared with the downscaled precipitation change during 2000-2099 relative to 1927-1999 time period observations at the local scale (Fig.6.12b).

$$\text{Pre. Index} = \frac{\left\{\begin{array}{c}\text{GCM precipitation change during 2000-2099} \\ \text{relative to observations during 1900-1999}\end{array} - \begin{array}{c}\text{Precipitation} \\ \text{bias}_{1900\text{-}1999}\end{array}\right\} \times 100\ \%}{\text{Average of observed annual precipitation during 1900-1999}}$$

The climate impact studies, such as flood simulation or land slide hazard predictions may require GCMs with higher precipitation change in the future (e.g. HADCM3 model as in Fig. 6.1). On the other hand, researches concerning the ecological balance of the eco-systems and water resources management perspectives would involve

a)

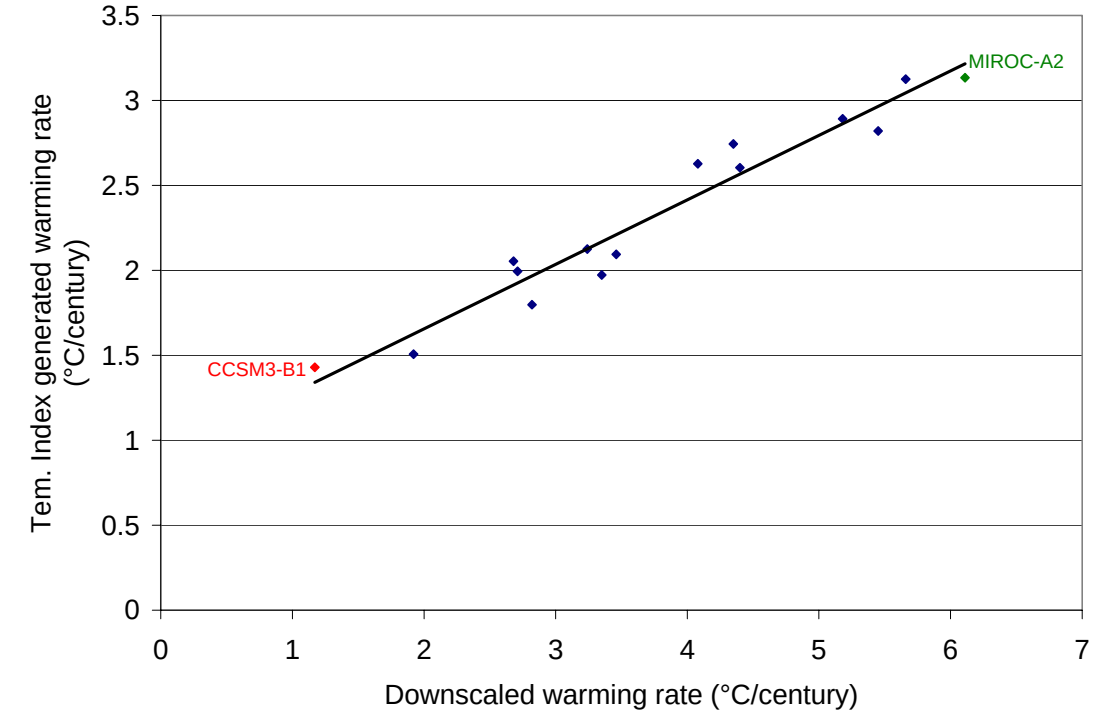

b)

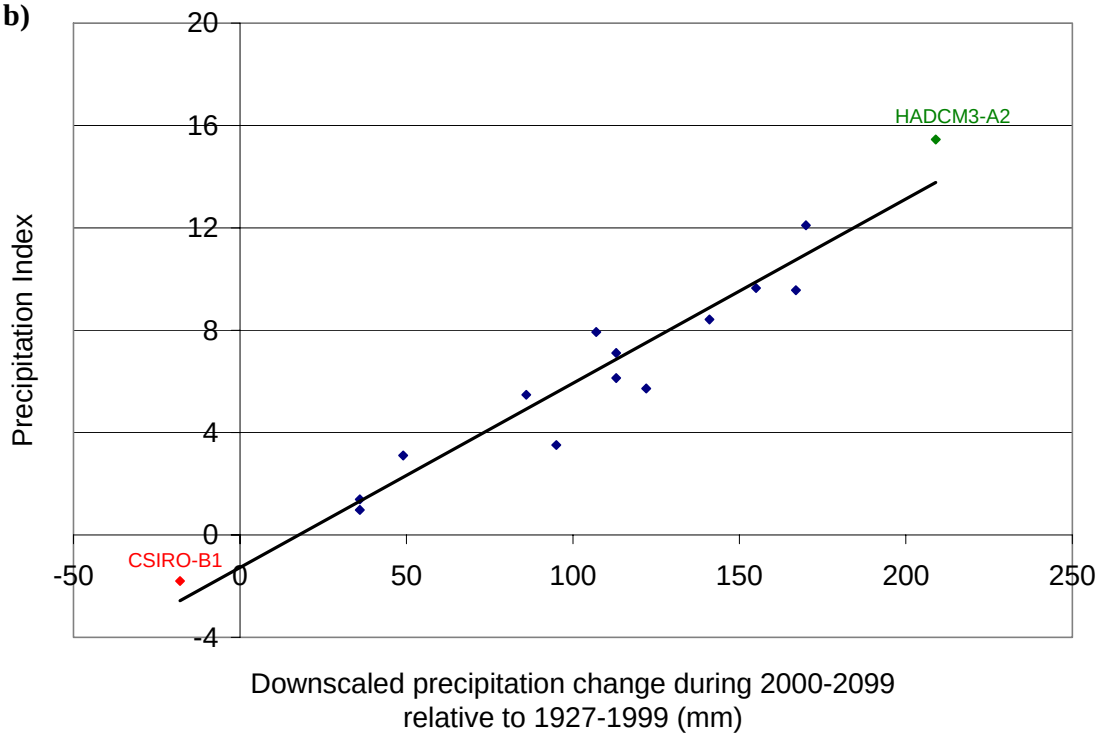

Fig. 6.12 Temperature and precipitation indexes for GCMs selection

the GCMs with higher degrees of air temperature change and decreasing trends of precipitation variations in the future (e.g. MIROC and CSIRO models, respectively). Therefore, considering the difficulty of GCMs to maintain the similar magnitudes of climate parameters change at the GCM grid scale while downscaling, the proposed indexes will be useful to select the appropriate GCMs for various climate impact studies.

Metrological observations as presented in our study confirmed that the magnitude of surface air temperature change in the urban area is significantly higher than in rural surroundings. This is because, in an urban environment, urban heat island effect dominates the causes of influencing the surface air temperature and associate ecosystem. When aquifer temperature is concerned, magnitude of deviation from steady state temperature-depth profile is strongly depending on the degree of urbanization at the local scale. Therefore, a relationship was examined between the level of urbanization and the surface air temperature change with respect to aquifer temperature change.

The level of urbanization is determined based on particular land-use types surrounding 5 km^2 areas from the observation well. Study area was divided to 250 × 250 m grid space and particular land-use types were selected based on available land-use map in year 2005. Different degrees of urbanizations were assigned for various land-use types as in Table 6.3.

Table 6.3 Level of urbanization for different land-use types

Land-use type	Level of urbanization (%)
Forest	0
Agricultural	20
Rural area	40
Low density housing area	60
High density housing and commercial area	80
Industrial area	100

The aquifer temperature change at 8 m depth below the ground surface was considered as a common parameter to examine the relationship between level of urbanization, aquifer temperature change, and surface air temperature change in the study area. At first, change of aquifer temperature from steady state T-D profiles (Fig. 5.1) was estimated from the observed T-D profiles and they were plot against to the level of urbanization at particular well locations as determined in Table 6.3. Moreover, aquifer temperature change with respect to the ground surface warming was simulated based on Equation 5.4. These two plots were brought together to examine the relationship between the level of urbanization and ground surface temperature change (Fig 6.13).

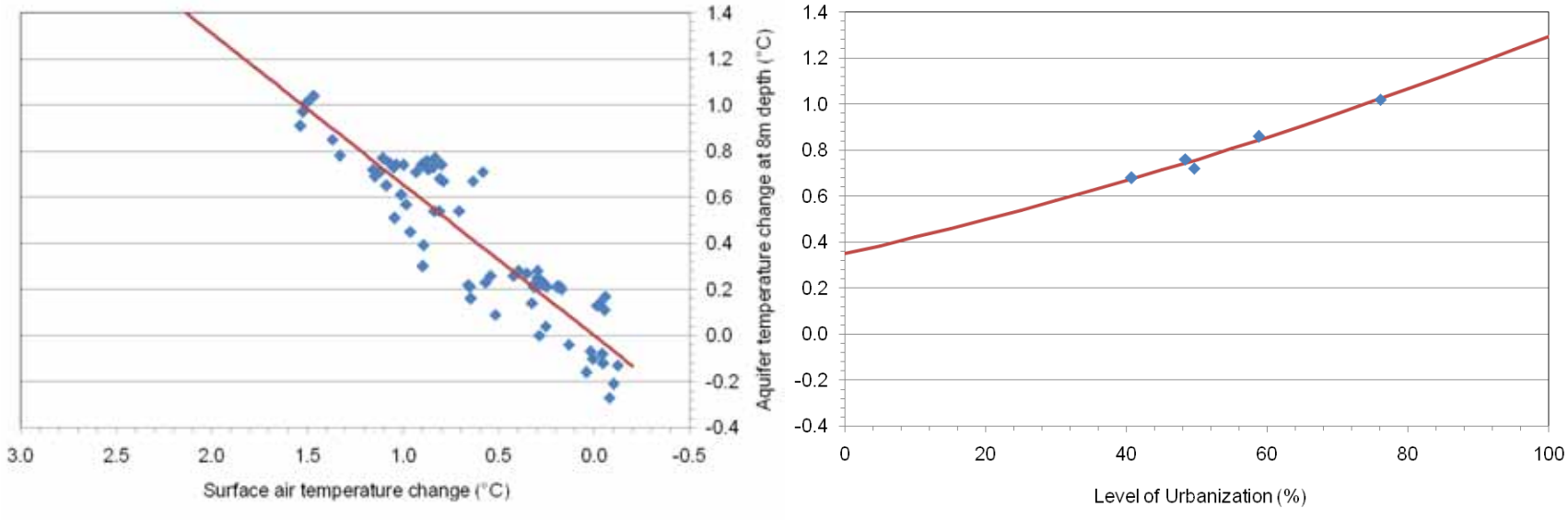

Fig. 6.13 Relationship between urbanization level and surface air temperature change with respect to the aquifer temperature change as a common parameter

The relationship between the level of urbanization and aquifer temperature change shows slight concave shape due to the variations of convective heat transport for the different level of urbanizations. In general, surface runoff is lower and groundwater recharge is higher in non-sealed areas, such as forested and agricultural areas (level of urbanization 0-40% in Fig. 6.13). Therefore, the cooling effect by the groundwater recharge is greater in low urbanized areas than in high urbanized areas, which eventually decelerates the effect of ground surface warming on aquifer thermal regime. In well urbanized areas, above cooling effect is small and aquifer temperature change is higher for same magnitude of ground surface warming. This phenomenon produces concave shape to the relationship between the level of urbanization and aquifer temperature change. However, when groundwater recharge is constant, ground surface warming is directly proportional to aquifer temperature change at a particular depth. Therefore, simulations were made for different recharge values and a linear relationship was developed for aquifer temperature and ground surface temperature (Fig. 6.13).

As there is wide concern on curbing green house gas induced global warming, in an urban environment, a relationship as developed in Fig. 6.13 will be important for the decision makers to understand the degree of temperature that can be decreased by compensating a feasible level of urbanized area. As an example, by reducing 20% of urbanizing level in the Sendai area (from 100% to 80%), it will be able to lower the surface air temperature by 0.4 °C, which is approximately equal to the magnitude of climate change effect to increase the surface air temperature in 20^{th} century (e.g. warming trend in Fukaura is 0.4 °C/100 years). Therefore, given the increasing certainty that climate change is accelerating, developed methodology through this study will guide the decision makers for making more resilient decisions to cope with its adverse impacts.

6.8 Conclusions

For the purpose of estimating potential global climate changes at the local scale, GCM outputs were statistically downscaled to the Sendai plain. There are significant differences among the GCM simulations and the scenarios themselves within a specific model due to the assumptions made and various spatial resolutions. Therefore, a set of GCMs and scenarios were considered that best reflect the possible climate change in a range. Five GCMs were analyzed, and their differences were discussed based on the model bias and the magnitude of climate parameter change in the future (2000-2099) relative to base time period (1927-1999). The transfer function method was used to develop the empirical relationship between large scale GCMs and local scale climate. GCM precipitation and temperature were selected as the sole predictors for the bias correction of the local climate.

Observed records of 1967–2006 were considered as the base for estimating the transfer functions, and they were verified with the observations of 1947–1966. The transfer functions developed for both precipitation and temperature show reasonably good agreement with the verified results. Among them, temperature downscaling exhibits better performance than precipitation. The verified transfer functions were then used to downscale the GCM data from 2060–2099.

For the temperature downscaling, the A2 scenario gives consistently stronger effects than the other scenarios for all selected GCMs. The A1B scenario exhibit moderate changes, while B1 have the lowest temperature rise in the 2060–2099 time period. Comparing the model performances, HADCM3 predicted the highest increase in ground surface air temperature (3.9 °C). Except CSIRO B1 scenario, the 2060–2099 precipitation also was projected to increase in all model scenarios. However, the A2 scenario does not always produce the highest precipitation change, as it does with temperature. The HADCM3 A2 scenario produces the highest annual precipitation rise (345 mm; about 28% change from past 40 year's average), and the CSIRO B1 scenario gives the negative precipitation change, which makes 9 mm/year reduction compared to the present climate.

Furthermore, the potential changes in the precipitation and temperature for each model scenario were applied to the water budget technique to estimate the possible recharge variations in the future. In general, HADCM3, MIROC and CCSM3 models are projected reductions of recharge, while ECHAM5 and CSIRO models are predicted to enhance the groundwater recharge in the future in the Sendai plain. When all model scenarios are considered groundwater recharge predictions will span in a range of 96-182 mm/year. Moreover, recharge variation together with the potential rate of surface warming, were substituted into the heat transport equation to estimate the changes in convective and conductive heat transportation in the subsurface layer in the Sendai plain. When considering the all GCM scenarios, the groundwater temperature at 8 m depth from the ground surface (the representative depth for the comparison) could possibly increase within the range of 1.5–4.0 °C by 2080 compared to the observations in 2007. If it is assumed that the present trend of surface warming (the rate of surface warming during last 80 years) and annual averaged precipitation remain unchanged, the groundwater temperature will likely increase by 1.4 °C (averaged in all well points) by the year 2080. However, according to the IPCC AR4, the magnitude of global warming in later part of the 21st century is expected to be higher than in 20th century, and therefore, groundwater temperature may increase within the range obtained from GCM scenarios. The ecological significance of the estimated impacts was evaluated in reference to three aquatic species. Inhabitant suitability of sweetfish, pale chub and carp were estimated with the effect of warming aquifer in 2060-2099 time periods. In general, HADCM3, MIROC and CCSM3

scenarios would exert strong pressure on species like sweetfish and pale chub which are favorable to relatively mild warm water. In contrast, ECHAM5 model scenarios may create little favorable inhabiting situations for the aquatic ecology in future.

Moreover, considering the difficulty of incorporating many GCMs for impact studies, two indexes were developed for precipitation and temperature, which choose the scenarios that have the ability to produce extremes climatic parameter change in the future. The proposed methodology will guide the researches to select the most suitable model scenarios in their studies, which indeed will reduce the extensive works of downscaling many scenarios for climate impact studies. Furthermore, a relationship between level of urbanization and ground surface air temperature change was developed by considering the aquifer temperature as a common parameter. According to that, by reducing 20% of urbanizing level in the Sendai area (from 100% to 80%), it will be able to lower the surface air temperature by 0.4 °C, which is approximately equal to the magnitude of climate change effect to increase the surface air temperature in 20^{th} century in Japan. Therefore, given the increasing certainty that climate change is accelerating, developed methodology through this study will guide the decision makers for making more resilient decisions to cope with its adverse impacts.

CHAPTER 7

SUMMERY, CONCLUSIONS AND RECOMMENDATIONS

7.1 Summery

The motivation of this research was to estimate the climate change impacts on aquifer thermal regimes in the Sendai plain. Continuous field measurements of groundwater temperature and aquifer water level fluctuations were made to understand the significant factors that influence the aquifer thermal regimes. In addition to the climate change and urbanization pressures, tidal effect is identified as a potential factor altering the aquifer temperature in coastal areas. Strong evidences were found to relate the tidal fluctuations with the deep aquifer water level variations and temperature distributions in the Sendai plain. Based on the above observations and preliminary analysis, new analytical solution and a set of type curves were developed to estimate the degree of temperature distribution in coastal aquifers under different tidal and aquifer characteristics.

In the shallow subsurface layers, urbanization and climate change effects are identified as the dominant causes of influencing the temperature distribution. An analytical model was applied to understand the different degrees of past urbanization and global warming impacts that have altered the aquifer temperature distribution in the Sendai plain. The estimated parameters of the analytical model were tested with the climatic and hydrological observations. Furthermore, a set of type curves were developed by combining the water budget technique and analytical model for heat transport in the subsurface layers, which can be used to test the accuracy of the groundwater recharge estimations from the temperature-depth profiles.

Moreover, output from five GCMs were spatially downscaled to Sendai metrological station to account the future climate change impacts. The long-term trends of temperature and precipitation changes were used to estimate the magnitude of ground surface temperature and groundwater recharge changes at the local scale in the Sendai plain. Based on above estimations, potential range of aquifer warming was estimated, which may guide the decision makers making more resilient decisions to mitigate the climate change impacts. Finally, two climatic indexes for temperature and precipitation were developed to identify the GCM scenarios that may have the most critical impacts at the local scales. The proposed indexes may be helpful for researchers to select the most suitable GCM in climate impact studies.

7.2 Conclusions

This study was conducted to estimate the climate change impacts on aquifer thermal regimes. Long-term measurements of aquifer temperature and groundwater level records suggest that the urbanization and climate change effects are more dominant in shallow subsurface layers, while tidal fluctuation has profound influence in deep aquifer depths. Time series analysis of tidal stage with the water level fluctuations in the inland aquifer found the maximum correlation coefficient of 0.74, suggesting reasonably good relationship between tide and water levels in the Sendai plain deep aquifer depths. Significantly high correlation was obtained between the water level fluctuations of observation wells them self (max of 0.97). In general, as the distance of the well from the coast increased, the peak value of the cross-correlation decreased and the time lag increased. A similar trend is noted in temperature change as the distance from coast increased. Not only the initial temperature values, but also the magnitudes of seasonal temperature change, were subjected to attenuation as the distance from the coast increased (0.89 °C and 0.17 °C at the nearest and the most distant observation points from the coast, respectively).

Based on the above findings, a new analytical model was developed to estimate the temperature distribution in the transition zone based on different aquifer and tidal characteristics. The sensitivity analysis indicates that the model is highly sensitive for the hydraulic conductivity of the aquifer that directly relates with the heat transport by the groundwater advection. When the hydraulic conductivity of the porous medium is high (e.g. 1×10^{0} m/s), sea water flows in a grater distance from the coast, and the temperature distributes gently through the seawater and freshwater margins. However, if the hydraulic conductivity is low (e.g. 1×10^{-4} m/s), the tidal effect dissipates within a shorter distance from the coast and temperature falls very rapidly within a small distance.

The proposed model was applied in the Sendai plain where a good correlation was found between the tide and groundwater level fluctuations. Verified results in the Sendai plain indicated that the individual effect of seawater temperature change has a profound effect on temperature change closer to the coast than a fresh groundwater temperature change. The combined effects of temperature change (possibly due to the effects of urbanization and climate change) at two boundaries within the range of $\pm1\ ^{0}$C will lead to a 0.4 to 1 ^{0}C temperature change in the vicinity of the coast (500 m away from the coast), where, in general, the coastal wetlands are located. These figures may be critical in terms of coastal ecological balance.

As there are wide ranges of efforts to mitigate the anthropogenic effects on coastal environments, the proposed method in this study will be useful in terms of planning and

monitoring the progress of coastal ecosystem programs. As an example, land-use practices, such as reforestation programs have the potential to decrease groundwater temperature in the aquifer by increasing shading. Therefore, estimations through the developed methodology in this study will be important for mitigating climate change impacts, where aquifer temperature increases due to sea water temperature rise would likely compensate by lowering inland temperature with the effect of reforestation program.

In the shallow subsurface layers, temperature distribution was examined considering the past effects of urbanization and global warming. In the Sendai plain, the magnitude of aquifer temperature change at the ground surface, as evaluated from subsurface temperatures at five observation wells, spans 0.9–1.3ºC. Clear evidence was found for the influence of ground surface temperature change in the deeper aquifer depths, up to 38–60 m, at which aquifer temperature departs from a steady state T–D profile. A series of synthetic T–D profiles were produced and compared with the observed data to distinguish the individual effects of each parameter influencing temperature distribution at the local scale. Spatial variation in hydraulic gradients estimated using water level records at different aquifer depths and depth of departure from a steady state T–D profile proved to be very useful for determining reliable vales of groundwater recharge and rate of surface warming. Estimated groundwater recharge rates from T–D profiles (105–215 mm/year) were further verified against estimates from three other techniques (the water budget method, Darcy's method and the WLF method), which produced the groundwater recharge estimates in a consistent range (105–210 mm/year). Moreover, the constrained parameters of groundwater recharge and the rate of surface warming at different observation wells are consistent with the land use type and level of urbanization experienced in the past around each site. When a global warming rate of 0.004ºC/year was selected based on meteorological records from rural areas in the region, the urbanization effect was estimated to account for about 75% of the aquifer temperature change (0.7–1.0ºC) in the Sendai plain.

We also developed a set of type curves that can be used in general application to estimate temperature distribution patterns for different soil and land cover types. This method can be applied to account for variations in temperature and precipitation in different countries. Four soil types and four land use types were selected to represent the variations in site characteristics. The percentage error using the developed type curves range from 9–14% in the Sendai plain. Therefore, considering the higher degree of uncertainty inherent in recharge estimation using T–D profiles and other techniques, these type curves can be used to test the accuracy of the estimates in general applications.

Moreover, we tested a hypothesis that treated climate change and urbanization as significant and equally important causes of potential changes in aquifer thermal regimes.

For the purpose of estimating potential global climate changes at the local scale, GCM outputs were statistically downscaled to the Sendai plain. There are significant differences among the GCM simulations and the scenarios themselves within a specific model due to the assumptions made and various spatial resolutions. Therefore, five GCMs were analyzed, and their differences were discussed based on the model bias and the magnitude of climate parameter change in the future (2000-2099) relative to base time period (1927-1999). The transfer function method was used to develop the empirical relationship between large scale GCMs and local scale climate. GCM precipitation and temperature were selected as the sole predictors for the bias correction of the local climate. Observed records of 1967–2006 were considered as the base for estimating the transfer functions, and they were verified with the observations of 1947–1966. The transfer functions developed for both precipitation and temperature show reasonably good agreement with the verified results. The verified transfer functions were then used to downscale the GCM data from 2060–2099.

For the temperature downscaling, the A2 scenario gives consistently stronger effects than the other scenarios for all selected GCMs. The A1B scenario exhibit moderate changes, while B1 have the lowest temperature rise in the 2060–2099 time period. Comparing the model performances, HADCM3 predicted the highest increase in ground surface air temperature (3.9 °C). Except CSIRO B1 scenario, the 2060–2099 precipitation also was projected to increase in all model scenarios. However, the A2 scenario does not always produce the highest precipitation change, as it does with temperature. The HADCM3 A2 scenario produces the highest annual precipitation rise (345 mm; about 28% change from past 40 year's average), and the CSIRO B1 scenario gives the negative precipitation change, which makes 9 mm/year reduction compared to the present climate.

Furthermore, the potential changes in the precipitation and temperature from each model scenario were applied to the water budget technique to estimate the possible recharge variations in the future. In general, HADCM3, MIROC and CCSM3 models are projected reductions of recharge, while ECHAM5 and CSIRO models are predicted to enhance the groundwater recharge in the future in the Sendai plain. When all model scenarios are considered groundwater recharge predictions will span in a range of 96-182 mm/year. Moreover, recharge variation together with the potential rate of surface warming, were substituted into the heat transport equation to estimate the changes in convective and conductive heat transportation in the subsurface layer in the Sendai plain. When considering the all GCM scenarios, the groundwater temperature at 8 m depth from the ground surface (the representative depth for the comparison) could possibly increase within the range of 1.5–4.0 °C by 2080 compared to the observations in 2007. If it is assumed that the present trend of surface warming (the rate of surface warming during last

80 years) and annual averaged precipitation remain unchanged, the groundwater temperature will likely increase by 1.4 °C (averaged in all well points) by the year 2080. The ecological significance of the estimated impacts was evaluated in reference to three aquatic species. Inhabitant suitability of sweetfish, pale chub and carp were estimated with the effect of warming aquifer in 2060-2099 time periods. In general, HADCM3, MIROC and CCSM3 scenarios would exert strong pressure on species like sweetfish and pale chub which are favorable to relatively mild warm water. In contrast, ECHAM5 model scenarios may create little favorable inhabiting situations for the aquatic ecology in future.

Moreover, considering the difficulty of incorporating many GCMs for impact studies, two indexes were developed for precipitation and temperature, which choose the scenarios that have the ability to produce extremes climatic parameter change in the future. The proposed methodology will guide the researches to select the most suitable model scenarios in their studies, which indeed will reduce the extensive works of downscaling many scenarios for climate impact studies. Furthermore, a relationship between level of urbanization and ground surface air temperature change was developed by considering the aquifer temperature as a common parameter. According to that, by reducing 20% of urbanizing level in the Sendai area (from 100% to 80%), it will be able to lower the surface air temperature by 0.4 °C, which is approximately equal to the magnitude of climate change effect to increase the surface air temperature in 20th century in Japan.

According to the IPCC AR4, the magnitude of global warming in later part of the 21st century is expected to be higher than in 20th century, and therefore, groundwater temperature may increase within the range obtained from GCM scenarios. Moreover, according to Alley et al. (2007), approximately 20-30% of animal species are likely to be at increased risk of extinction if increases in global average temperature exceed 1.5-2.5 °C. Therefore, predicted potential range of aquifer temperature change (1.5–4.0 °C by 2080) will be significant for the ecological balance of the ecosystem in the Sendai plain. Findings of this research will inform the policy makers for building resilient decisions for the mitigation measures. In such situation, developed methodologies of this study will be useful for the coastal ecosystem management programs to cope with the adverse effects of changing climate in the future.

7.3 Recommendations

Future researches for evaluating climate change and land-use impacts on aquifer temperature would incorporate following recommendations for more advance output of their studies.

- This study did not consider the possible effects of land use change that are likely in the future on the recharge and ground surface temperature changes. Therefore, consideration of the combine effects of urbanization and climate change may important and even be more dramatic from the ecological point of view.

- Due to the limitations of the analytical solution, uniform and steady rates of groundwater recharge and ground surface warming were assumed to simulate the temperature distribution in the shallow subsurface layers. These limitations can be overcome by applying numerical model, such as VS2DH (model for simulation of energy transport in variably saturated porous media from USGS), which facilitate to input annual variations of groundwater recharge and ground surface warming over long-term periods.

- Compared with the broad time scales that have been used to find signatures of past climate change from borehole records (e.g., five centuries in Huang et al., 2000), we analyzed a time history of only 1.2 centuries. This is mostly because of our poor knowledge about past climate change due to the absence of meteorological observations over the centuries. Therefore, performing the parameter calibration with the climatic observations over wide-range of time histories is highly recommended.

References

1. Alley R., Berntsen T., Bindoff N.L., Chen Z., Chidthaisong A., Friedlingstein P., Gregory J., Hegerl G., Heimann M., Hewitson B., Hoskins B., Joos F., Jouzel J., Kattsov V., Lohmann U., Manning M., Matsuno T., Molina M., Nicholls N., Overpeck J., et al. 2007. Climate change 2007: The physical science basis. Summary for policymakers. Intergovernmental Panel on Climate Change, Geneva, CH.

2. Allison G.B., Cook P.G., Barnett S.R., Walker G.R., Jolly I.D., and Hughes M.W., 1990. Land clearance and river Stalinization in the Western Murray basin, Australia. Journal of Hydrology, 119: 1-20.

3. Arora V.K., 2002. The use of the aridity index to assess climate change effect on annual runoff. Journal of Hydrology, 265: 164–177.

4. Baker D.G. and Ruschy D.L., 1993. The recent warming in eastern Minnesota shown by ground temperatures. Geophys. Res. Lett., 20: 371–374.

5. Bates B.C., Kundzewicz Z.W., Wu S. and Palutikof J.P. Eds., 2008. Climate Change and Water. Technical Paper of the Intergovernmental Panel on Climate Change, IPCC Secretariat, Geneva, 210 pp.

6. Battin J., Wiley M.W., Ruckelshaus M.H., Palmer R.N., Korb E. and Bartz K.K., 2007. Projected impact of climate change on salmon habitat restoration. Proceedings of the National Academy of Sciences 104 (16), 6720-6725.

7. Beltrami H, 2001. On the relationship between ground temperature histories and metrological records: a report on the Pomquet station. Global and Planetary Changes, 29: 327-347.

8. Beltrami H. and Kellman L., 2003. An examination of short- and long-term air–ground temperature coupling. Global and Planetary Change, 38: 291–303.

9. Bense V. and Beltrami H., 2007. Impact of horizontal groundwater flow and localized deforestation on the development of shallow temperature anomalies. Journal of Geophysical Research, 112, F04015 (doi:10.1029/2006JF000703).

10. Bijlsma L., Ehler C.N., Klein et al., 1995. Coastal zones and small islands. In: Watson, R.T., Zinyowera, M.C., and Moss, R.H. (eds) Climate change 1995 -Impacts, adaptations and mitigations of climate change: scientic-technical analyses: the second assessment report of the Intergovernmental Panel on Climate Change. Cambridge University Press, New York.

11. Bodri L., Cermak V., 1999. Climate changes of the last millennium inferred from borehole temperatures: regional patterens of climate changes in the Czech Republic-Part III. Global and Planetary Change 21: 225-235.

12. Bond-Lamberty B., Wang C. and Gower S.T., 2005. Spatiotemporal measurement and modeling of stand-level boreal forest soil temperatures. Agric. For. Meteorol., 131: 27– 40.

13. Bredehoeft J.D. and Papadopulos I.S., 1965. Rates of vertical groundwater movement estimated from the earth's thermal profile. Water Resources Research, 1: 325-328.

14. Brougere S., Dassargues A. and Hallet V., 2004. Migration of contaminant trough the unsaturated zone overlying the Hesbaye chalky aquifer in Belgium: a field investigation. J. Contam. Hydrol. 72: 135-164.

15. Budyko M.I., 1958. The Heat Balance of the Earth's Surface, trs. Nina A. Stepanova, US Department of Commerce, Washington, D.D., 259 p.

16. Carslaw H.S. and Jaeger J.C., 1959. Conduction of heat in solids, second ed. Oxford university press, New York.

17. Cartwright K., 1971. Redistribution of geothermal heat by a shallow aquifer. Geol. Soc. America Bull., 82: 3197-3200.

18. Cartwright K., 1974. Tracing shallow groundwater systems by soil temperatures. Water Resour. Res., 10: 847-855.

19. Chen Z., Grasby S.E., Osadetz K.G., 2002. Predicting average annual groundwater levels from climate variables: an empirical model. Journal of Hydrology, 2002:102-117.

20. Domenico P.A., and Palciauskas V.V., 1973. Theoretical analysis of forced convective heat transfer in regional ground-water flow. Geological Society of America Bulletin, 84: 3803-3814.

21. Eaton J.G., and Scheller R.M., 1996. Effects of climate warming on fish thermal habitat in streams of the United States. Limnol. Oceanogr., 4 l: 1109-1115.

22. Eckhardt K. and Uibrich U., 2003. Potential impacts of climate change on groundwater recharge and streamflow in a central European low mountain range. Journal of Hydrology, 284: 244–252.

23. Ferguson G., Woodbury A.D., and Matile G.L.D., 2003. Estimating deep recharge rates beneath an interlobate moraine using temperature logs. Ground Water, 41: 640–646.

24. Ferguson G. and Woodbury A.D., 2004. Subsurface heat flow in an urban environment. Journal of Geophysical Research, 109 (B2), B02402 (doi:10.1029/2003JB002715).

25. Ferguson G. and Woodbury A.D., 2005. The effects of climatic variability on estimates of recharge from temperature profiles. Ground Water, 43: 837-842.

26. Geological Survey of Japan AIST, 2004. Water Environmental Map No. 1 Sendai Plain, Geological Survey of Japan AIST.

27. Gitay H., Brown S., Easterling W. and Jallow B., 2001. Ecosystems and their goods and services. Climate change 2001: Impacts adaptation, and vulnerability, In: J.J McCarthy, O.F. Canziani, N.A. Leary, D.J. Dokken, K.S. White (Editors.). Contribution of Working Group II to the Third Assessment Report of the Intergovernmental Panel on Climate Change. Cambridge University Press, Cambridge, UK.

28. Glugla G. and Krahe P., 1995. Abflußbildung in urbanen Gebieten (Runoff formation in urban areas). Document series, Hydrologie/Wasserwirtschaft 14, Ruhr University of Bochum, pp.140-160.

29. Glugla, G., and Müller, E., 1997. Grundwasserneubildung als Komponente der Abflussbildung (New groundwater formation as a component of runoff formation), in:

Leibundgut C., S. Demuth (Eds.), Grundwasserneubildung (New groundwater formation). Freiburger Schriften zur Hydrologie, Band 5, pp. 23-35.

30. Gunawardhana L.N. and Kazama S., 2009. Tidal effects on aquifer thermal regime: An analytical solution for coastal ecosystem management. Journal of Hydrology, 377: 377-390.

31. Hansen J. and Lebedeff S., 1987. Global trends of measured surface air temperature. J. Geophys. Res., 92: 13345–13372.

32. Healy R.W. and Cook P.G., 2002. Using groundwater levels to estimate recharge. Hydrogeology Journal, 10: 91–109.

33. Huang S., Pollack H.N. and Shen P.Y., 2000. Temperature trends over the past five centuries reconstructed from borehole temperatures. Nature, 403: 756–758.

34. Izuka S.K. and Gingerich S.B., 1998. Ground water in the southern Lihue Basin, Kauai, Hawaii. US Geological Survey Water- Resources Investigations Report 98–4031, pp.71

35. Jacob C.E., 1950. Flow of ground water, chap. 5 in Rouse, Hunter (ed.), Engineering hydraulics: New York, John Wiley and Sons, p. 321-385.

36. Jones M.L., Shuter B.J., Zhao Y., and Stockwell J.D., 2006. Forecasting effects of climate change on Great Lakes fisheries: models that link habitat supply to population dynamics can help. Can. J. Fish. Aquat. Sci., 63: 457–468.

37. Kim K.Y., Seong H., Kim T., Park K.H., Woo N.C., Park Y.S., Koh G.W. and Park W.B., 2006. Tidal effects on variations of fresh-saltwater interface and groundwater flow in a multilayered coastal aquifer on a volcanic island (Jeju Island, Korea). J. Hydrol., 330: 525-542.

38. Kipkorir E.C., Raes D. and Massawe B., 2002. Seasonal water production functions and yield response factors for maize and onion in Perkerra, Kenya. Agricultural Water Management, 56: 229–240.

39. Kojiri, T., 1997. Impact analysis on water resources system due to global warming through classified input patterns and grid-typed run-off model. In: Proceedings of XXV Congress of IAHR, vol. I, pp. 377-384.

40. Lean J., Bunton C., Nobre C. and Rowntree P., 1996. The simulated impact of Amazonian deforestation on climate using measured ABRACOS vegetation characteristics, in Amazonian Deforestation and Climate, edited by J. Gash, C. Nobre, J. Roberts, and R. Victoria, pp. 549– 576, John Wiley, New York.

41. Lee C.E. and Bell M.A., 1999. Causes and consequences of recent freshwater invasions by saltwater animals. Trends in Ecology and Evolution, 14: 284-288.

42. Lu N. and Ge S., 1996. Effect of horizontal heat and fluid flow on the vertical temperature distribution in a semiconfining layer. Water Resources Research, 32: 1449-1453.

43. Majorowicz J., Grasby S.E., Ferguson G., Safanda J. and Skinner W., 2006. Paleoclimatic reconstructions in western Canada from borehole temperature logs: surface air temperature forcing and groundwater flow. Climate of the Past, 2: 1–10.

44. Majorowicz J.A. and Skinner W.R., 1997. Potential causes of differences between ground and surface air temperature warming across different ecozones in Alberta, Canada. Global and Planetary Change, 15: 79–91.

45. Mann M.E., Schmidt G.A., 2003. Ground vs. surface air temperature trends: Implications for borehole surface temperature reconstructions. Geophysical Research Letters, 30 (12), doi:10.1029/2003GL017170.

46. Mansure A.J. and Reiter M., 1979. A vertical groundwater movement correction for heat flow. J. Geophys. Res., 84: 3490-3496.

47. Nielsen P., 1990. Tidal dynamics of the water table in beaches. Water Resour. Res. 26: 2127-2134.

48. Nitoiu D. and Beltrami H., 2005. Subsurface thermal effects of land use changes. Journal of Geophysical Research, 110, F01005, (doi:10.1029/2004JF000151).

49. Oie G. and Olsen Y., 1993. Influence of rapid changes in salinity and temperature on the mobility of the rotifer Brachionus plicatilis. Hydrobiologia 255/256: 81-86.

50. Oltra R. and Todolf R., 1997. Effects of temperature, salinity and food level on the life history traits of the marine rotifer Synchaeta cecilia valenrina, n. subsp. Journal of Plankton Research, 19: 693-702.

51. Pike J.G., 1964. The estimation of annual runoff from meteorological data in a tropical climate. Journal of Hydrology, 2: 116–123.

52. Pollack H.N., and Huang S., 1998. Underground temperatures reveal changing climate. Geotimes., 43: 16–19.

53. Putnam S. N. and Chapman D. S., 1996. A geothermal climate change observatory: first year results from Emigrant Pass in Northwest Utah. J. Geophys. Res., 101: 21 877–21 890.

54. Randhir T.O. and Hawes A.G., 2009. Watershed land use and aquatic ecosystem response: Ecohydrologic approach to conservation policy. Journal of Hydrology, 364: 182–199.

55. Ranjan S.P., Kazama S. and Sawamoto M., 2006. Effects of climate and land use changes on groundwater resources in coastal aquifers. Journal of Environmental Management, 80: 25–35.

56. Reiter M., 2001. Using precision temperature logs to estimate horizontal and vertical flow components. Water Resources Research, 37: 663-674.

57. Reiter M., 2006. Vadose zone temperature measurements at a site in the northern Albuquerque Basin indicate ground-surface warming due to urbanization. Environ. Eng. Geosci., 12: 353–360.

58. Reiter M., 2007. Variability of recent ground surface temperature changes in the Albuquerque basin, central New Mexico. Journal of Geophysical Research, 112, D24S07 (doi:10.1029/2006JD008215).

59. Rosenberg N.J., Epstein D.J., Davidwang, Vail L., Srinivasan R. and. Arnold J.G., 1999. Possible impacts of global warming on the hydrology of the Ogallala aquifer region**.** Climatic Change, 42**:** 677–692.

60. Sakura Y., 1993. Groundwater flow estimated from temperatures in the Yonezawa basin, northeast Japan. Tracers in Hydrology, 215: 161-171.

61. Salathe E.P. Jr. and Mote W.P., 2007. Review of scenario selection and downscaling methods for the assessment of climate change impacts on hydrology in the United States Pacific Northwest. International Journal of Climatology, 27: 1611–1621.

62. Salathe E.P. Jr., 2005. Downscaling simulations of future global climate with application to hydrologic modelling. International Journal of Climatology, 25: 419–436.

63. Sampat P., 2001. Uncovering groundwater pollution. In *The state of the world 2001,* ed. L. R. Brown; C. Flavin; and H. French. London: W. W. Norton & Company.

64. Scanlon B.R., Healy R.W. and Cook P.G., 2002. Choosing appropriate techniques for quantifying groundwater recharge. Hydrogeology Journal, 10: 18–39.

65. Schmidt W.L., Gosnold W.D. and Enz J.W., 2001. A decade of air–ground temperature exchange from Fargo, North Dakota. Global and Planetary Change, 29: 311–325.

66. Serfes M.E., 1991. Determining the Mean Hydraulic Gradient of Ground Water Affected by Tidal Fluctuations. Ground water, 29: 549-555.

67. Shuttleworth W.J., 1992. Evaporation. In: D.R. Maidment (Editor). Handbook of Hydrology. McGraw-Hill, New York, NY, pp. 4.1-4.53.

68. Solman S.A. and Nunez M.N., 1999. Local estimates of global climate change: A statistical downscaling approach, Int. J. Climatol., 19: 835-861.

69. Stallman R.W., 1963. Computation of ground-water velocity from temperature data. In: R. Bentall (Editor). Method of collecting and interpreting Ground-Water Data. Water Supply Paper 1544-H. Washington, DC: USGS, 36-46.

70. Stallman R.W., 1965. Steady one-dimensional fluid flow in a semi-infinite porous medium with sinusoidal surface temperature. Journal of Geophysical Research, 70: 2821-2827.

71. Steenhuis T.S., Winchell M., Rossing J., Zollweg J.A. and Walter M.F., 1995. SCS runoff equation revised for variable source runoff areas. Journal of Irrigation and Drainange Engineering, ASCE 121/3: 234–238.

72. Suzuki S., 1960. Percolation measurements based on heat flow through soil with special reference to paddy fields. Journal of Geophysical Research, 65: 2883-2885.

73. Taniguchi M, Shimada J, Tanaka T, Kayane I, Sakura Y, Shimano Y, Siakwan D and Kawashima S., 1999. Disturbances of temperature–depth profiles due to surface climate change and subsurface water flow: An effect of linear increase in surface temperature caused by global warming and urbanization in the Tokyo metropolitan area, Japan. Water Recourses Research, 35: 1507–1517.

74. Taniguchi M., Shimano Y. and Kayane I., 1989. Groundwater flow analysis using the temperature in the upland areas at the western foot of Aso Volcanoes. J. Japane. Assoc. Hydrolo. Scienc., 19: 171-179.

75. Taniguchi M., Turner J.V. and Smith A.J., 2003. Evaluations of groundwater discharge rates from subsurface temperature in Cockburn Sound, Western Australia. Biogeochemistry, 66: 111-124.

76. Taniguchi M., Uemura T. and Sakura Y., 2005. Effects of urbanization and groundwater flow on subsurface temperature in three megacities in Japan. Journal of Geophysics and Engineering, 2: 320-325.

77. Taniguchi M., 1993. Evaluation of vertical groundwater fluxes and thermal properties of aquifers based on transient temperature-depth profiles. Water Resour. Res. 29, 2021-2026.

78. Taniguchi M., 1994. Estimated recharge rates from groundwater temperatures in the Nara basin, Japan. Hydrogeology Journal**,** 2: 7–14.

79. Taniguchi M., 1995. Analysing the long term reduction in groundwater temperature due to pumping. Hydrological Sciences Journal, 40: 407-422.

80. Taniguchi M., 2002. Tidal effects on submarine groundwater discharge into the ocean. Geophys. Res. Lett, 29: 1561–1564.

81. Taniguchi M., 2006. Anthropogenic effects on subsurface temperature in Bangkok. Climate of the Past Discussions, 2: 831-846.

82. Taniguchi M., 2007. Combined effects of urbanization and global warming on subsurface temperatures in four Asian cities. Vadose Zone J., 6: 591–596.

83. Trabucco A., Zomer R.J., Bossio D.A., Straaten O.V. and Verchot L.V., 2008. Climate change mitigation through afforestation/reforestation: A global analysis of hydrologic impacts with four case studies. Agriculture, Ecosystems and Environment, 126: 81–97.

84. Tsutsumi A., Jinno K. and Berndtsson R., 2004. Surface and subsurface water balance estimation by the groundwater recharge model and a 3-D two-phase flow model. Hydrological Sciences Journal, 49: 205–226.

85. Uchida Y. and Hayashi T., 2005. Effects of hydrogeological and climate change on the subsurface thermal regime in the Sendai Plain. Physics of the Earth and Planetary Interiors, 152: 292–304.

86. US Department of Agriculture, Soil Conservation Service, 1972. Hydrology, Nattional Engineering Handbook, Section 4. US Government Printing Office, Washington, DC, pp 10.1-10.24.

87. Wilby R.L. and Wigley T.M.L., 2000. Precipitation predictors for downscaling: observed and general circulation model relationships. Int. J. Climatol., 20: 641-661.

88. Widmann M., Bretherton C.S. and Salathe E.P. 2003. Statistical precipitation downscaling over the Northwestern United States using numerically simulated precipitation as a predictor, J. Climate, 16: 799-816.

89. Wood A.W., Leung R., Sridhar V. and Lettenmaier D.P., 2004. Hydrologic implications of dynamical and statistical approaches to downscaling climate model outputs. Climatic change, 62: 189–216.

90. Zhang X.C., 2005. Spatial downscaling of global climate model output for site-specific assessment of crop production and soil erosion. Agriculture and Forest Meteorology, 135: 215-229.

91. Ziagos J.P. and Blackwell D.D., 1981. A model for the effect of horizontal fluid flow in a thin aquifer on temperature-depth profiles. Geothermal Resource Council Transactions, 5: 221-223.

92. Ziagos J.P. and Blackwell D.D., 1986. A model for the effect of horizontal fluid flow in geothermal systems. J. Volcanol. Geothermal Res., 27: 371-397.